1 Paleoclimate Variability in the Mediterranean Region

Fatima Abrantes[a,b], Antje (Helga Luise) Voelker[a,b], Francisco Javier Sierro[c], Filipa Naughton[a,b], Teresa Rodrigues[a,b], Isabel Cacho[d], Daniel Ariztegui[e], David Brayshaw[f], Marie-Alexandrine Sicre[g], Luis Batista[a]

[a]Laboratório Nacional de Energia e Geologia—LNEG, Unidade de Geologia Marinha, Amadora, Portugal, [b]Centro de Investigação Marinha e Ambiental —CIMAR, Porto, Portugal, [c]Department of Geology, University of Salamanca, Salamanca, Spain, [d]GRC Geociències Marines, Department Estrat. Paleont. i Geoc. Marines Facultat de Geologia, Universitat de Barcelona, Barcelona, Spain, [e]Section of Earth and Environmental Sciences, University of Geneva, Geneva, Switzerland, [f]National Centre for Atmospheric Sciences, Department of Meteorology, University of Reading, Reading, UK, [g]CNRS, Laboratoire des Sciences du Climat et de l'Environnement, Gif-sur-Yvette, France

1.1 Introduction to Paleoclimatic Reconstruction Methods

The climatic system as we know it today is complex; variability is caused both by external forces and by internal processes. A look at the global record of ice volume for the past 65 million years (My) (Figure 1.1; Zachos et al., 2001) gives us the idea that Earth's history has been marked by climatic variation of an abrupt rather than of a gradual nature. Major climatic variations can be detected at four different timescales (Figure 1.2; Ruddiman, 2001):

1. Tectonic (>0.5 My) is caused by changes in atmospheric and oceanic circulation in response to changes in the relative position of continents and oceans and the opening and closing of gateways (i.e., plate tectonics). On this scale, the effects on the biological evolution and biogeochemical cycles are of particular importance.
2. Orbital (20–400 thousand years (ky)) is originated by variations in the earth's position relative to the sun—i.e., variations in orbital parameters, eccentricity, obliquity, and precession (Berger and Loutre, 1992; Imbrie and Imbrie, 1979). This scale is recorded back to 34 My, mainly through expansions and retractions of the global ice volume that occur with periodicities of 400, 100, 40, and 19–23 ky.
3. Millennial (a few thousand years) corresponds to climatic variations generated by interactions between slowly evolving components of the climatic system (e.g., the ocean and the cryosphere) resulting, for example, in the instability of the oceanic thermohaline circulation (Ganopolski and Rahmstorf, 2001). The effects of such changes over the land surface are generally mediated by changes in the atmospheric circulation.

The Climate of the Mediterranean Region. DOI: 10.1016/B978-0-12-416042-2.00001-X

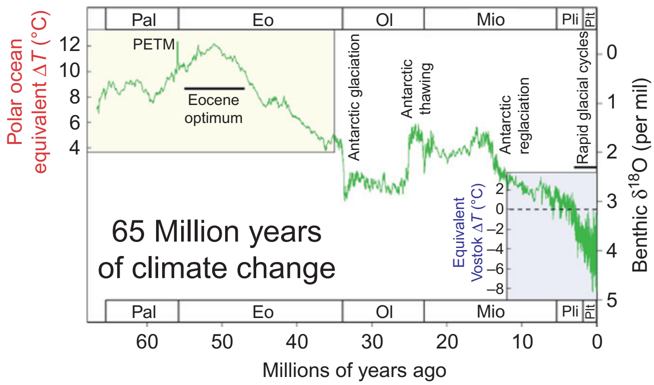

Figure 1.1 Climate change between 65 My ago and the present (0). The climate curve is the mean running line of all the existing deep-sea benthic foraminiferal oxygen-isotope ($\delta^{18}O$) records from DSDP and ODP sites. Benthic foraminiferal $\delta^{18}O$ represents a combination of the temperature changes in this organisms' local living environment and changes in the isotopic composition of seawater derived by the growth and retreat of continental ice sheets. The $\delta^{18}O$ temperature anomaly on the left axis (in red) was computed on the assumption of an ice-free ocean, which is why it applies only to the time preceding the onset of large-scale glaciation on Antarctica (about 35 My ago). The $\delta^{18}O$ temperature anomaly for the most recent data (in blue) was computed considering the tight correlation between the oxygen-isotope measurements of Lisiecki and Raymo (2005), and the temperature changes at the Vostok ice core established by Petit et al. (1999).

Source: After Zachos et al. (2001).

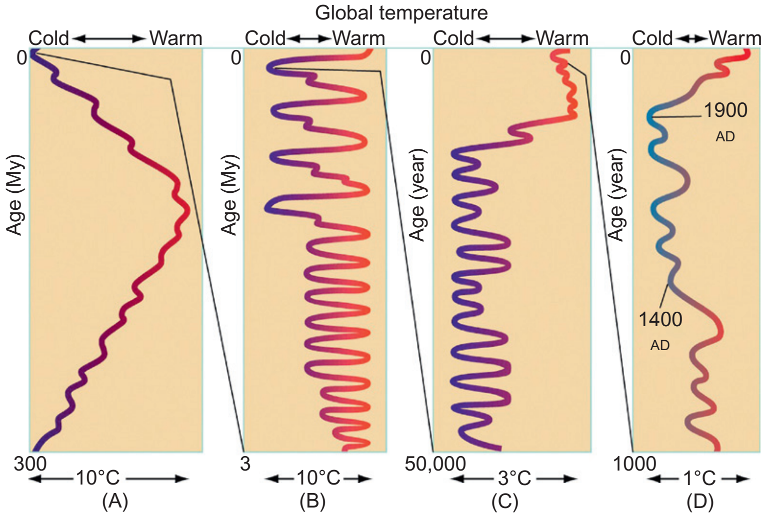

Figure 1.2 The four major timescales of climate variation: (A) tectonic, (B) orbital, (C) deglacial/millennial, and (D) historical.
Source: Adapted from Ruddiman (2001).

4. Historic (centuries to seasons) includes the climatic variations of shorter periods (best observed in historical times) and more recent anthropogenic climate changes on a global scale.

In spite of the intrinsic importance of paleoclimatic studies, recent interest in climate reconstructions has evolved from the perception that understanding the dynamics of past climatic events and their impact is fundamental in modeling and understanding future climate changes.

The main geophysical properties that paleoclimatologists attempt to reconstruct are the same as those that physical, chemical, or biological climatologists grapple with today. However, past climate reconstructions have to be done through the study of "climate archives," such as tree rings, speleothems, ice cores, corals, and sedimentary sequences (lakes and marine). Acting as multichannel recorders, all of these contain multiple pieces of climatic information, but they are different in nature and resolution (Figure 1.3; Ruddiman, 2001).

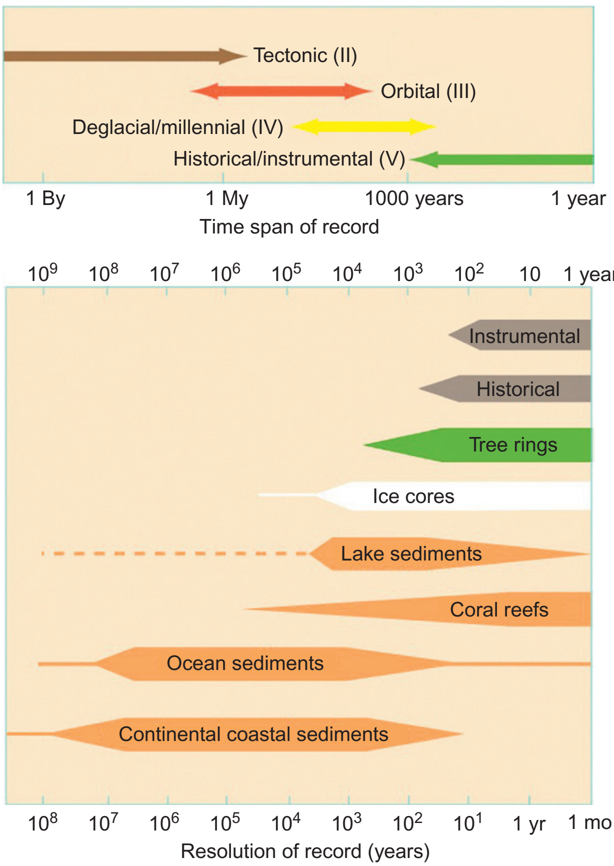

Figure 1.3 Time span covered and resolution of different climate archives in view with the timescales of climate variation.
Source: Adapted from Ruddiman (2001).

Past climatic reconstructions typically take one of two forms: time series or time slices. Time series provide information through time at one or more specific location(s); time-slice reconstructions attempt to ascertain the spatial distribution of a property at a specific time. Independent of the selected approach, their interpretation has to follow the general geology principle of Lyell (1830) that "the present is the key to the past" in order to later allow a turnaround of that principle into "the past is the key to the future." Besides, given the impossibility of directly measuring past oceanic properties using any archive, it is necessary to use indicators, or proxies.

A proxy is an archive property or component that can be related to an environmental parameter or process. A multitude of proxies are in use, from methods based on biological, physical, and chemical sciences, to modern statistical techniques that allow the application of extensive and complex databases. Proxies can be classified on the basis of their type (physical, chemical, biological, isotopic, etc.) or grouped by the type of parameter that they attempt to reconstruct (Fischer and Wefer, 1999).

Paleoclimate proxies can be subtle and complex. This is why most studies use a multiproxy approach. In this chapter, we use a combination of proxies for sea-surface temperature (SST), primary production, bottom / intermediate waters ventilation, and flow strength; for continental climate, we use atmospheric temperature, precipitation, wind strength, and direction. For SST reconstruction, we will incorporate records from foraminiferal $\delta^{18}O$, the C_{37} alkenone unsaturation index ($U^{K'}{}_{37}$), TEX_{86}, the Mg:Ca ratio, and microfossil assemblage transfer functions that relate species distributions to modern hydrographic conditions. Primary production conditions at any time will be estimated from the organic carbon, Ba contents, as well as from microfossil abundance and assemblages. Bottom/intermediate water ventilation will be determined via benthic foraminiferal $\delta^{13}C$ and the geochemical composition of sediments. For bottom water strength, grain size is the proxy mainly used. Continental temperature reconstructions are based primarily on palynological data preserved in sedimentary archives, supplemented by other lake data when available. On land precipitation is also derived from pollen data, continental plants' biomarker data, $\delta^{18}O$ in speleothem carbonate, and Fe, Ti, and clay minerals' abundance and type. The locations of all the records used in this compilation are presented in Figure 1.4, and their position information and original references to all the works used are listed in Table 1.1. Site numbers mentioned in the following text refer to the numbers of the sites shown in Figure 1.4.

Given the nature of climate reconstructions, there are several uncertainties related to any data point. Age uncertainties are the most important since the chronology of the archive constitutes the base for accurate environmental or climatic reconstructions. A good age control is fundamental to estimate rates of change for any one parameter or process in one location as well as to establish relationships between sites. The process or property/proxy relation can also be a source of uncertainty, given that there is no way to verify whether the modern relations hold through geological time. Furthermore, the numeric relationships defined from the proxies to modern conditions may also cause problems by assuming them to be good analogs when in reality modern conditions may result from a combination of natural and anthropogenic forcing. Errors can also derive from the methods and equipment used

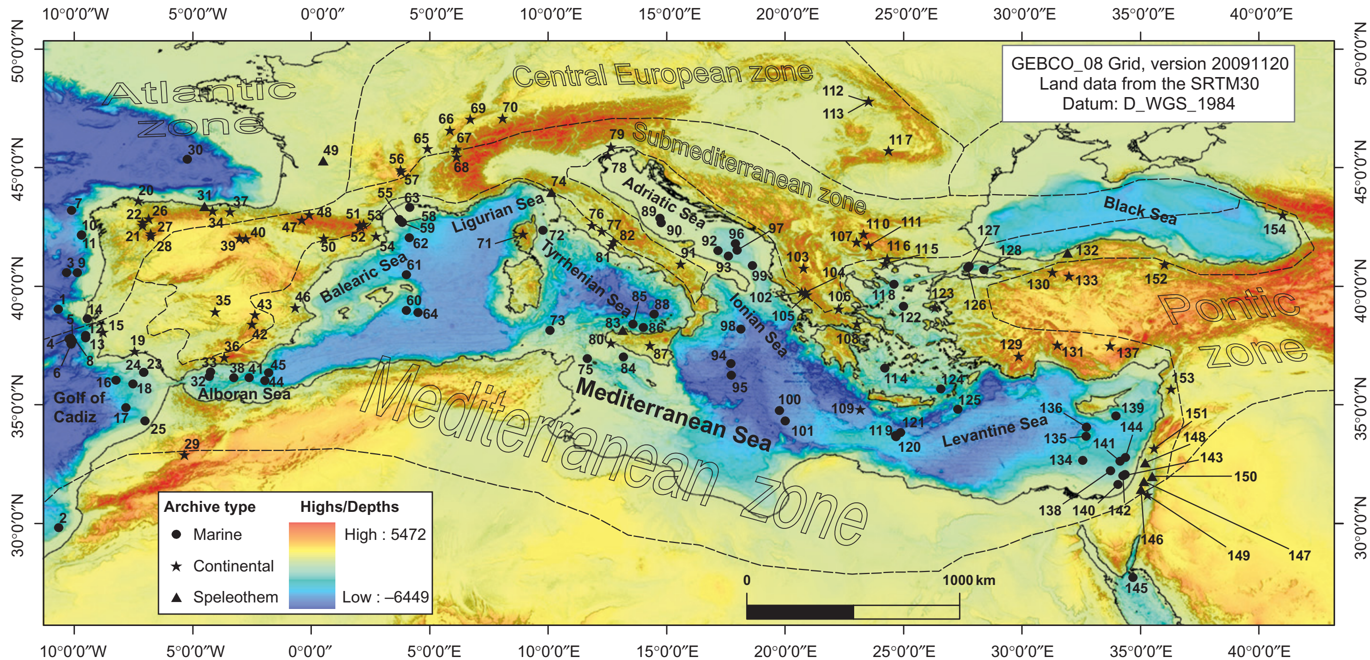

Figure 1.4 Type and location of all the archives used to compile this chapter. For detailed information, see Table 1.1.

Table 1.1 Published Records Used in This Compilation. Sites' ID; Original Site Name; Latitude; Longitude; Elevation/Water Depth; Archive Type; Time-Slice(s); Original Works' Reference

Site ID	Site Name	Latitude	Longitude	Elevation/ Water Depth	Archive Map	Archive Type	Time Slice	References
1	MD03-2699	39.04	−10.67	−1895	Marine	Marine core	LGIT; HO; 8.2 ka	Rodrigues et al. (2010, 2011)
2	M16004-1	29.83	−10.65	−1512	Marine	Marine core	MIS 5e; MIS 3	Hooghiemstra et al. (1992)
3	MD95-2039	40.57	−10.33	−3381	Marine	Marine core	MIS 3; LGIT	Roucoux et al. (2001, 2005)
4	SU81-18	37.77	−10.21	−3135	Marine	Marine core	LGIT; HO; 8.2 ka	Bard et al. (2000), Lézine and Denèfle (1997), Turon et al. (2003)
5	MD95-2042	37.81	−10.15	−3146	Marine	Marine core	MIS 5e; MIS 3; LGIT; HO; 8.2 ka	Pailler and Bard (2002), Salgueiro et al. (2010), Sánchez-Goñi et al. (1999, 2000, 2002, 2005), Shackleton et al. (2000, 2003)
6	MD01-2444	37.57	−10.13	−2656	Marine	Marine core	MIS 5e; MIS 3; LGIT; HO; 8.2ka	Margari et al. (2010), Martrat et al. (2007), Skinner and Elderfield (2007), Vautravers and Shackleton (2006)
7	SU92-03	43.20	−10.11	−3005	Marine	Marine core	MIS 5e; MIS 3	Salgueiro et al. (2010)
8	8057B	37.68	−10.08	−2811	Marine	Marine core	LGIT; 8.2ka	Hooghiemstra et al. (1992)
9	MD95-2040	40.58	−9.86	−2465	Marine	Marine core	MIS 5e; MIS 3	de Abreu et al. (2003), Pailler and Bard (2002), Salgueiro et al. (2010)
10	MD03-2697	42.17	−9.70	−2164	Marine	Marine core	LGIT; HO; 8.2 ka	Naughton et al. (2007b)

11	MD99-2331	42.15	−9.69	−2110	Marine	Marine core	MIS 5e; MIS 3; LGIT	Naughton et al. (2007b, 2009), Sánchez-Goñi et al. (2005, 2008, 2009)
12	MD95-2041	37.83	−9.52	−1123	Marine	Marine core	MIS 3	Voelker and de Abreu (2011), Voelker et al. (2009)
13	SO75-6KL	37.94	−9.51	−1281	Marine	Marine core	LGIT	Boessenkool et al. (2001)
14	D13882	38.63	−9.45	−88	Marine	Marine core	LGIT; HO; 8.2 ka	Abrantes et al. (2005), Rodrigues et al. (2009)
15	Santo Andre lagoon	38.08	−8.78	2.7	Continental	Lagoon core	HO	Santos and Sanchez-Goni (2003)
16	M39029-7	36.04	−8.23	−1917	Marine	Marine core	MIS 3	Colmenero-Hidalgo et al. (2004)
17	M15669-1	34.88	−7.82	−2030	Marine	Marine core	MIS 3	Hooghiemstra et al. (1992)
18	MD99-2339	35.88	−7.53	−1170	Marine	Marine core	MIS 3	Voelker and de Abreu (2011), Voelker et al. (2006, 2009)
19	Guadiana basin	37.27	−7.45	0	Continental	Estuary core	LGIT; HO; 8.2 ka	Fletcher et al. (2007)
20	Area longa	43.60	−7.30	0	Continental	Terrestrial core	MIS 3	Gómez-Orellana et al. (2007)
21	Lagoa de Lucenza	42.58	−7.12	1375	Continental	Terrestrial core (pool)	LGIT	Muñoz-Sobrino et al. (2001)
22	Pozo do Carballal	42.71	−7.11	1330	Continental	Lake core	LGIT	Muñoz-Sobrino et al. (1997)
23	MD99-2341 + GeoB5901	36.38	−7.07	−574	Marine	Marine core	HO; 8.2 ka	Kim et al. (2004), Toucanne et al. (2007)
24	M39008	36.37	−7.07	−576	Marine	Marine core	LGIT; HO; 8.2 ka	Cacho et al. (2001)
25	KS 78007	34.32	−7.02	−700	Marine	Marine core	LGIT; HO	Marret and Turon (1994)
26	Suárbol	42.86	−6.85	1080	Continental	Peatbog core	LGIT	Muñoz-Sobrino et al. (1997)

(*Continued*)

Table 1.1 (Continued)

Site ID	Site Name	Latitude	Longitude	Elevation/ Water Depth	Archive Map	Archive Type	Time Slice	References
27	Laguna de la Roya	42.22	−6.77	1608	Continental	Lake core	LGIT; HO	Allen et al. (1996)
28	Lleguna	42.12	−6.77	1050	Continental	peatbog core	LGIT	Muñoz-Sobrino et al. (2004)
29	Tigalmamine	32.90	−5.35	1626	Continental	Lake core	HO; 8.2 ka	Cheddadi et al. (1998), Lamb et al. (1995, 1989), Lamb and van der Kaars (1995)
30	MD04-2845	45.35	−5.22	−4100	Marine	Marine core	MIS 5e; MIS 3	Sánchez-Goñi et al. (2008)
31	El Pindar	43.38	−4.50		Speleothem	Speleothem	HO; 8.2 ka	Moreno et al. (2010)
32	ODP Site 976	36.20	−4.30	−1108	Marine	Marine core	MIS 3; LGIT; HO; 8.2 ka	Combourieu-Nebout et al. (1998, 2002, 2009)
33	TG-5	36.38	−4.25	−626	Marine	Marine core	HO; 8.2 ka	Bárcena et al. (2001)
34	Enol	43.18	−4.15		Continental	Lake/Peatbog core	HO; 8.2 ka	Moreno et al. (in press)
35	Fuentillejo maar	38.93	−4.05		Continental	Lake core	HO; 8.2 ka	Vegas et al. (2010)
36	Padul	37.00	−3.67	785	Continental	Lake core	LGIT; HO	Florschütz et al. (1971), Pons and Reille (1988)
37	Puerto de los tornos	43.15	−3.43	920	Continental	Peatbog core	8.2 ka	Muñoz-Sobrino et al. (2005), Peñalba (1994)
38	KS8231	36.15	−3.27	−865	Marine	Marine core	HO; 8.2 ka	Bárcena et al. (2001)
39	Quintanar de la sierra	42.03	−3.02	1470	Continental	Marshland core	LGIT	Peñalba et al. (1997)
40	Hoyos de Iregua	42.02	−2.75	1780	Continental	Lake core	LGIT; HO	Gil-García et al. (2002)

41	MD95-2043	36.14	−2.62	−1841	Marine	Marine core	MIS 3; LGIT; HO; 8.2 ka	Cacho et al. (1999, 2000, 2001, 2002, 2006), Fletcher and Sanchez Goñi (2008), Fletcher et al. (2010b), Moreno et al. (2002, 2004, 2005), Sánchez-Goñi et al. (2002, 2008, 2009)
42	Siles lake	38.40	−2.50	1320	Continental	Lake core	LGIT	Carrión (2002)
43	Villaverde	38.80	−2.37	900	Continental	Lake core	HO; 8.2 ka	Carrión (2003), Carrión et al. (2001), Jalut et al. (2005, 2009)
44	ODP Site 977A	36.03	−1.96	−1984	Marine	Marine core	MIS 5e; MIS 3; LGIT; HO; 8.2 ka	Gonzalez-Mora et al. (2008), Martrat et al. (2004)
45	TTR14-300G	36.36	−1.79	−1860	Marine	Marine core	HO; 8.2 ka	Jimenez-Espejo et al. (2008)
46	Navarres peatbog	39.10	−0.68	225	Continental	Peatbog core	LGIT	Carrión and Dupré (1996), Carrión and van Geel (1999)
47	El Portalet	42.80	−0.38	1802	Continental	Peatbog core	LGIT; HO; 8.2 ka	González-Sampériz et al. (2005, 2006, 2008, 2009)
48	Biscaye	43.03	−0.07	410	Continental	Lake core	LGIT	Reille and Andrieu (1995)
49	Villars Cave, France	45.30	0.50		Speleothem	Speleothem	MIS 3	Genty et al. (2003, 2010)
50	Estanya	42.03	0.53		Continental	Lake core	HO; 8.2 ka	Morellón et al. (2009)
51	Balcére	42.59	2.06	1764	Continental	Lake core	LGIT	Reille and Lowe (1993)
52	La Borde	42.53	2.08	1660	Continental	Peatbog core	LGIT	Reille and Lowe (1993)
53	Gourg Negre	42.63	2.22	2080	Continental	Peatbog core	LGIT	Reille and Lowe (1993)

(*Continued*)

Table 1.1 (Continued)

Site ID	Site Name	Latitude	Longitude	Elevation/ Water Depth	Archive Map	Archive Type	Time Slice	References
54	Lago de Banyoles	42.12	2.75	173	Continental	Lake core	MIS 3; LGIT; HO; 8.2 ka	Perez-Obiol and Julia (1994), Valero-Garcés et al. (1998)
55	MD99-2349	42.82	3.73	−126	Marine	Marine core	LGIT	Beaudouin et al. (2007)
56	Lac du Bouchet	44.92	3.78	1200	Continental	Lake core	MIS 5e; MIS 3; LGIT	de Beaulieu and Reille (1984), Reille et al. (1998), Reille and de Beaulieu (1990), Reille and de Beaulieu (1988a,b)
57	Ribains/ Landos/ Velay 1	44.84	3.82	1080	Continental	Lake core	MIS 5e; LGIT	de Beaulieu and Reille (1992, 1984), Reille and Beaulieu (1989)
58	borehole PRGL1	42.69	3.84	−300	Marine	Marine core	MIS 5e; MIS 3	Sierro et al. (2009)
59	MD99-2348	42.70	3.85	−296	Marine	Marine core	LGIT	Beaudouin et al. (2005), Sierro et al. (2009)
60	M40/4-87SL	38.99	4.02	−1900	Marine	Marine core	MIS 5e	Emeis et al. (2003), Weldeab et al. (2003)
61	MD99-2343	40.50	4.03	−2391	Marine	Marine core	MIS 3; HO; 8.2 ka	Frigola et al. (2007, 2008), Sierro et al. (2005)
62	MD99-2346	42.04	4.15	−2100	Marine	Marine core	HO; 8.2 ka	Melki et al. (2009)
63	MD99-2352	43.32	4.17	−70	Marine	Marine core	LGIT	Beaudouin et al. (2007)
64	ODP Site 975B	38.90	4.51	−2416	Marine	Marine core	MIS 5e; HO; 8.2 ka	Doose et al. (1999), Jimenez-Espejo et al. (2007, 2008)

65	les Echets	45.81	4.92	267	Continental	Lake core	MIS 5e; MIS 3	Ampel et al. (2008), de Beaulieu and Reille (1984, 1989)
66	Lake Lautrey	46.59	5.86	788	Continental	Lake core	LGIT	Magny et al. (2006)
67	Lac d'Annecy	45.80	6.13	445	Continental	Lake core	LGIT	David (2001)
68	Ételles	45.47	6.15	700	Continental	Lake core	LGIT	David (2001)
69	Le Locle	47.05	6.72	915	Continental	Lake core	LGIT; 8.2 ka	Magny et al. (2001)
70	Soppensee	47.09	8.08	596	Continental	Lake core	8.2 ka	Tinner and Lotter (2001)
71	Lac de Creno	42.20	8.95	1310	Continental	Lake core	LGIT	Reille et al. (1997)
72	MD01-2434	42.37	9.79	−800	Marine	Marine core	MIS 3	Touyet et al. (2010)
73	LC07	38.15	10.08	−488	Marine	Marine core	MIS 5e	Incarbona et al. (2008)
74	Antro del Corchia	43.98	10.13	840	Speleothem	Speleothem	MIS 5e	Drysdale et al. (2004, 2005, 2009), Essallami et al. (2007), Rouis-Zargouni et al. (2010)
75	MD04-2797	36.95	11.67	−771	Marine	Marine core	LGIT; HO; 8.2 ka	Essallami et al. (2007), Rouis-Zargouni et al. (2010)
76	Lagaccione	42.57	11.85	355	Continental	Lake core	MIS 3; LGIT	Magri and Sadori (1999)
77	Lago di Vico	42.33	12.27	507	Continental	Lake core	MIS 3; LGIT; 8.2 ka	Leroy et al. (1996), Magri (1999), Magri and Parra (2002)
78	Lagoon of Venice	45.52	12.53	−2	Continental	Lagoon	MIS 3; LGIT	Canali et al. (2007)
79	Azzano Decimo core	45.88	12.65	9.9	Continental	Terrestrial	MIS 3	Pini et al. (2009)
80	Lake Gorgo Basso	37.62	12.65	6	Continental	Lake core	HO; 8.2 ka	Tinner et al. (2009)
81	Albano	41.72	12.67		Continental	Lake core	HO; 8.2 ka	Ariztegui et al. (2001)
82	Valle di Castiglione	41.89	12.76	44	Continental	Lake core	MIS 5e; MIS 3; LGIT	Follieri et al. (1989, 1993, 1998), Magri (1994)

(*Continued*)

Table 1.1 (Continued)

Site ID	Site Name	Latitude	Longitude	Elevation/ Water Depth	Archive Map	Archive Type	Time Slice	References
83	Grotta di Carburangeli	38.17	13.16	22	Speleothem	Speleothem	HO; 8.2 ka	Frisia et al. (2006)
84	ODP Site 963A + 963D	37.03	13.18	−470	Marine	Marine core	MIS 5e; HO; 8.2 ka	Incarbona et al. (2008, 2010), Sprovieri et al. (2006a)
85	BS79-38	38.41	13.58	−1489	Marine	Marine core	LGIT; HO; 8.2 ka	Cacho et al. (2001)
86	BS79-33	38.26	14.03	−1282	Marine	Marine core	LGIT; HO; 8.2 ka	Cacho et al. (2001)
87	Lago di Pergusa	37.52	14.30	674	Continental	Lake core	LGIT; HO	Sadori et al. (2010)
88	KET80-03	38.82	14.48	−1900	Marine	Marine core	MIS 3; LGIT	Paterne et al. (1999), Rossignol-Strick (1985), Rossignol-Strick and Planchais (1989)
89	CM92-43	42.88	14.72	−252	Marine	Marine core	8.2 ka	Ariztegui et al. (2000), Asioli et al. (2001)
90	PRAD1-2	42.68	14.77	−185.5	Marine	Marine core	MIS 5e; LGIT; HO; 8.2 ka	Piva et al. (2008)
91	Lago Grande di Monticchio	40.94	15.61	656	Continental	Lake core	MIS 5e; MIS 3	Allen and Huntley (2009), Allen et al. (1999, 2000, 2002), Watts et al. (2000)
92	SA03-1	41.50	17.18	−567	Marine	Marine core	LGIT	Favaretto et al. (2008)
93	MD90-917	41.28	17.62	−1010	Marine	Marine core	LGIT	Combourieu-Nebout et al. (1998), Siani et al. (2010)
94	M25_4-KL11	36.75	17.72	−3376	Marine	Marine core	LGIT; HO; 8.2 ka	Emeis et al. (2000)
95	KC01	36.25	17.74	−3640	Marine	Marine core	MIS 5e; HO; 8.2 ka	Doose (1999)
96	IN68-9	41.80	17.92	−1234	Marine	Marine core	HO; 8.2 ka	de Rijk et al. (1999)

97	KET 8216	41.52	17.98	−1166	Marine	Marine core	LGIT; HO	Rossignol-Strick (1996), Rossignol-Strick et al. (1992)
98	KS205	38.20	18.14	−2384	Marine	Marine core	MIS 5e	Rohling et al. (2002a)
99	AD91-17	40.87	18.64	−844	Marine	Marine core	LGIT; HO; 8.2 ka	Giunta et al. (2001), Melki et al. (2009), Sangiorgi et al. (2002, 2003)
100	M40/1-10	34.76	19.76	−2972	Marine	Marine core	HO; 8.2 ka	Löwemark et al. (2006)
101	BAN 84 09 GC	34.32	20.02	−3405	Marine	Marine core	LGIT; HO	Cheddadi et al. (1991), Rossignol-Strick (1996)
102	Ioannina I	39.75	20.72	470	Continental	Lake core	LGIT	Bottema (1995)
103	K6 lake maliq	40.77	20.78	−818	Continental	Lake core	LGIT; 8.2 ka	Bordon et al. (2009)
104	Ioannina 284	39.75	20.85	319	Continental	Lake core	MIS 5e; MIS 3; LGIT	Frogley et al., (1999), Lawson et al. (2004), Tzedakis et al. (2002)
105	Ioannina 249	39.65	20.92	470	Continental	Lake core	MIS 5e	Tzedakis (1994)
106	Lake Xinias	39.05	22.27	500	Continental	Lake core	MIS 3	Bottema (1979)
107	Lake Sedmo Rilsko	41.88	23.02	2925	Continental	Lake core	LGIT; HO	Bozilova and Tonkov (2000)
108	Kopais	38.43	23.05	95	Continental	Lake core	MIS 3; MIS 5e	Tzedakis (1999)
109	M40/ 4-71SL	34.81	23.19	−2827	Continental	Lake core	MIS 5e	Emeis et al. (2003), Weldeab et al. (2003)
110	Trilistnika lake	42.20	23.32	2216	Continental	Lake core	LGIT	Tonkov et al. (2006)
111	Lake Kremensko-5	41.72	23.53	2124	Continental	Lake core	LGIT	Atanassova and Stefanova (2003)
112	Preluca Tiganului	47.81	23.53	730	Continental	Lake core	LGIT	Björkman et al. (2002), Feurdean et al. (2007), Wohlfarth et al. (2001)
113	Steregoiu	47.81	23.54	790	Continental	Lake core	LGIT	Feurdean (2004), Feurdean et al. (2007)

(*Continued*)

Table 1.1 (Continued)

Site ID	Site Name	Latitude	Longitude	Elevation/ Water Depth	Archive Map	Archive Type	Time Slice	References
114	C69	36.55	24.21	−632	Marine	Marine core	MIS 3; LGIT; HO; 8.2 ka	Geraga et al. (2005)
115	Tenaghi Philippon 2	40.97	24.22	40	Continental	Lake core	8.2ka	Pross et al. (2010)
116	Tenaghi Philippon 1	41.17	24.33	40	Continental	Lake core	MIS 5e; MIS 3; LGIT	Tzedakis et al. (1997), Tzedakis et al. (2003b), Wijmstra (1969), Wijmstra and Smit (1976)
117	AVRIG	45.72	24.38	400	Continental	Lake core	LGIT	Feurdean et al. (2007), Tantau et al. (2006)
118	GeoTü SL152	40.09	24.61	−978	Marine	Marine core	LGIT; 8.2 ka	Kotthoff et al. (2008a,b)
119	ODP Site 971A	33.72	24.68	−2026	Marine	Marine core	MIS 5e	Marino et al. (2007), Osborne et al. (2010), Rohling et al. (2002a, 2006)
120	M40/1-22	33.66	24.69	−2004	Marine	Marine core	HO; 8.2 ka	Löwemark et al. (2006)
121	ODP Site 969E	33.84	24.88	−2212	Marine	Marine core	MIS 5e	Emeis et al. (2003), Weldeab et al. (2003)
122	MNB3	39.15	25.00	−800	Marine	Marine core	LGIT; 8.2 ka	Geraga et al. (2010), Gogou et al. (2007)
123	Megali Limni basin	39.10	26.33	323	Continental	Lake core	MIS 3	Margari et al. (2009)

124	LC21	35.67	26.58	−1522	Marine	Marine core	HO; 8.2 ka, MIS 5e	de Rijk et al. (1999), Marino et al. (2007), Osborne et al. (2010), van der Meer et al. (2007)
125	M40/4-67SL	34.81	27.30	−2158	Marine	Marine core	MIS 5e	Emeis et al. (2003), Schmiedl et al. (2003), Weldeab et al. (2003)
126	MD01-2430	40.80	27.73	−580	Marine	Marine core	LGIT; HO	Vidal et al. (2010)
127	M44-1-KL71	40.84	27.76	−566	Marine	Marine core	HO; 8.2 ka	Sperling et al. (2003)
128	MAR97-11	40.70	28.40	−111	Marine	Marine core	LGIT	Mudie et al. (2002)
129	Söğüt	37.05	29.88	1383	Continental	Lake core	LGIT	Bottema (1995)
130	Abant	40.60	31.30	1375	Continental	Lake core	LGIT	Bottema (1995)
131	Beyşehir	37.53	31.50	1120	Continental	Lake core	LGIT	Bottema (1995)
132	Sofular Cave	41.42	31.93	700	Speleothem	Speleothem	MIS 3; HO	Fleitmann et al. (2009)
133	Yeniçağa	40.43	32.00	980	Continental	Lake core	LGIT	Bottema (1995)
134	MD84642	32.67	32.57	−1260	Marine	Marine core	MIS 5e	Cheddadi and Rossignol-Strick (1995a,b)
135	KC20B	33.68	32.71	−882	Marine	Marine core	MIS 5e	Doose et al. (1999)
136	ODP Site 967C	34.07	32.73	−2550	Marine	Marine core	MIS 5e; LGIT; HO; 8.2 ka	Emeis et al. (1998, 2000, 2003), Fleitmann et al. (2009), Rohling et al. (2002a, 2006), Scrivner et al. (2004)
137	Akğöl Konya	37.50	33.73	1000	Continental	Lake core	LGIT	Bottema (1995)
138	MD84627	32.22	33.75	−1185	Marine	Marine core	8.2 ka	Cheddadi and Rossignol-Strick (1995a,b)
139	9501	34.53	33.98	−980	Marine	Marine core	MIS 3	Almogi-Labin et al. (2009)
140	GeoB7702-3	31.65	34.07	−562	Marine	Marine core	LGIT; HO; 8.2 ka	Castañeda et al. (2010)

(*Continued*)

Table 1.1 (Continued)

Site ID	Site Name	Latitude	Longitude	Elevation/ Water Depth	Archive Map	Archive Type	Time Slice	References
141	GeoTü KL83	32.62	34.15	−1433	Marine	Marine core	MIS 5e	Schmiedl et al. (2003), Weldeab et al. (2003)
142	9509	32.02	34.27	−884	Marine	Marine core	MIS 3	Almogi-Labin et al. (2009)
143	MD84629	32.07	34.35	−745	Marine	Marine core	8.2 ka	Cheddadi and Rossignol-Strick (1995a,b)
144	MD84632	32.78	34.37	−1425	Marine	Marine core	LGIT; HO; 8.2 ka	Essallami et al. (2007)
145	GeoB5844-2	27.71	34.68	−963	Marine	Marine core	LGIT; HO; 8.2 ka	Arz et al. (2003)
146	Soreq Cave	31.45	35.03	400	Speleothem	Speleothem	MIS 5e; MIS 3; HO; 8.2 ka	Affek et al. (2008), Bar-Matthews et al. (1999, 2003), Vaks et al. (2006)
147	Jerusalem West Cave	31.78	35.15	700	Speleothem	Speleothem	MIS 5e	Frumkin et al. (1999, 2000)
148	Peqiin Cave	32.58	35.19	650	Speleothem	Speleothem	MIS 5e; MIS 3	Bar-Matthews et al. (2003)
149	Lake Lisan	31.21	35.31	410	Continental	Lake core	MIS 3; HO	Bartov et al. (2003), Schramm et al. (2000), Stein et al. (2010), Waldmann et al. (2009, 2010)
150	Ma' ale Efrayim cave, Israel	32.00	35.50	250	Speleothem	Speleothem	MIS 3	Vaks et al. (2003)
151	Hula	33.17	35.58	300	Continental	Lake core	LGIT	Bottema (1995)
152	Lâdik	40.92	36.02	800	Continental	Lake core	LGIT	Bottema (1995)
153	Ghab	35.68	36.30	300	Continental	Lake core	LGIT; MIS 3	Bottema (1995), Niklewski and van Zeist (1970)
154	Dziguta River	43.02	41.02	120	Continental	River core	MIS 3; LGIT	Arslanov et al. (2007)

to do the proxy measurements. Typically, however, a final error can be the sum of its different components (dating, sampling, counting, etc.).

Values obtained by reconstructions should not be seen as exact. However, when calibration is done and replicate estimations are accurate, they constitute the best source of information on the reaction of the different components of the earth's climatic system to past external forcing or internal reorganization, on the range of natural variability as well as on the rate of change of any process through time.

Regional reconstructions of environmental and climatic variability have been recognized by the Intergovernmental Panel on Climate Change (IPCC; Solomon et al., 2007) as essential for better understanding specific local reactions to global climatic trends. The Mediterranean basin is particularly suitable for providing information on the climatic connection between high and low latitudes in the Northern Hemisphere because of its midlatitude location. Furthermore, as a semi-enclosed sea, it has the potential to amplify global paleo-environmental and -oceanographic changes (Kennett, 1982).

In this chapter, we attempt to compile the currently available quantitative data for the Mediterranean region for selected time intervals and to investigate regional scale change during specific climatic conditions through spatial patterns of natural variability. Furthermore, results from some climate modeling studies of the Holocene are discussed in the context of our well-constrained data sets. Although climate models have their own limitations (e.g., spatial resolution, temporal coverage, missing physical processes, and model uncertainty), these comparisons offer the potential for identifying flaws in the models, weaknesses in the data, critical geographic regions at key time slices as well as independent means of validating the climate model's response to applied "forcings" (Webb, 1997). However, it should be noted that climate models only simulate "responses" (outputs) that are consistent with prescribed forcings (inputs): if the forcing is not well understood, then the response may not be informative. The nature of the forcing is somewhat dependent on the components included in the model (e.g., some models include ocean dynamics or dynamic vegetation while others do not; Braconnot et al., 2007a), but they will generally include at least some of the following: changes in orbital parameters, greenhouse-gas concentrations, sea-surface height, ice-sheet extent, land-surface properties, and ocean circulation. Clearly then, some of these forcings are better constrained than others. The responses produced by climate models are therefore subject to interpretation, based on a physical understanding of the forcings applied and an understanding of the physical processes of the climate system (and their representation in the model). It is, therefore, in this more nuanced context that we undertake a model-data comparison in this chapter rather than contrasting the two data sets on a site-by-site basis.

1.1.1 Reconstruction Approach

After summarizing the birth and early evolution of the modern Mediterranean Sea, we discuss a selection of specific time intervals that experienced different climate forcings. For the latter, we consider marine records with radiocarbon chronologies for defining the time-slice patterns for marine isotope stage (MIS) 3 and younger. For continental records, we include both lake and speleothems. In lakes, ages are derived both from varve chronology, ^{14}C ages or $\delta^{18}O$ stratigraphy, while U–Th dates are the base for speleothems' age models. However, given our intent to focus on the main features, any property or process reconstruction aims to include mainly records that have estimations from different proxies, but values based on a single proxy will be considered, given that a multiple approach has been applied on only a very small number of sites. Age models and records were adopted as published by the authors, making no attempt to harmonize the data toward any particular calibration or method. Absolute chronology is usually based on radiocarbon measurements of carbonaceous (mainly marine) and organic matter (continental) samples, but given the radiocarbon-based age constraints, the (usually small) analytical error of the ^{14}C dates as well as errors and uncertainties in the paleoreservoir ages (Sabatier et al., 2010; Siani et al., 2001), a tolerance on the order of several centuries to one millennium, as we move back in time, is used for the timing of events. Furthermore, the data presented represent a "mean state" calculated as the average value for the considered time slice at each site.

Note that ages are referred to as My (million years) and ky (thousand years), but ka is used if referring to a specific age level.

1.2 The Geological History of the Mediterranean Through the Meso-Cenozoic: From a Global Latitudinal Ocean to an Enclosed Sea

1.2.1 Origin of the Mediterranean

The Mediterranean history is the result of the complex interaction between plate tectonics, the formation of orogenic belts, global eustatic changes, and climate, which have continuously changed its geographic extension, its water exchange with the global ocean, and its local hydrological budget. It originated from the Tethys Ocean, which was a vast ocean located along the eastern coast of Laurasia and Gondwana during the Mesozoic and early Cenozoic. Since the Eocene (ca. 38 My) to the Miocene (23 My), the African plate rotated counterclockwise and moved northward into the Eurasian Plate (Rögl, 1999), leading to the progressive restriction of the Tethys connection with the Indian Ocean and the formation of the Paratethys and the Mediterranean (Rögl and Hansen, 2009). At that time, the connection between the Mediterranean Sea and the Indo-Pacific Ocean was through a wide and deep gateway located between the Arabian and Anatolian plates along Southern Turkey and Iraq (Hüsing et al., 2009; Rögl, 1999), but this gateway shoaled to subtidal marine environments, leading to a severe restriction of the Indian–Mediterranean connection by the end of the Oligocene (23 My) (Hüsing et al., 2009; Rögl, 1999). However, another shallow-water gateway may have developed during the middle Miocene in response to the subduction between the Arabian plate and the Asian plate south of the Bitlis Massif (Hüsing et al., 2009). This connection, which was located north of the Arabian Peninsula, deepened to at least 300–600 m between 13.8 and 11. 8 My. It remained open until 11 My ago, during the early Tortonian, when the gateway emerged and the Mediterranean finally became disconnected from the Indian Ocean (Hüsing et al., 2009).

1.2.2 The Mediterranean and the Paratethys

The history of Mediterranean and Eurasian climate cannot be understood without knowing its relationship with the Paratethys Sea, the large marginal sea that existed along the Southern margin of Eurasia approximately 33 My ago, around the Eocene–Oligocene boundary (Allen and Armstrong, 2008; Rögl, 1999; Schulz et al., 2005). The tectonic uplift of the Alps and Carpathian orogenic belts led to the formation of a large basin that stretched from the Alps to the Aral Sea, with a connection with the Mediterranean toward the south. The isolation of the Paratethys from the Mediterranean since the Oligocene was recorded by a significant change from open marine planktonic floras and faunas to less diverse or monospecific microfossil assemblages usually characteristic of brackish or freshwater environments as well as the development of stagnant conditions at the bottom (Popov and Stolyarov, 1996; Schulz et al., 2005). Conditions were similar to those of the modern Black Sea, which is in fact the reminiscent basin of the ancient Paratethys. This marginal sea was characterized by brackish waters because of a positive freshwater budget and a strong stratification of the water column that favored accumulation of organic carbon in bottom sediments, which constitute the source for hydrocarbons (Sachsenhofer et al., 2009). European rivers are the main source of freshwater for the Mediterranean today and probably also were during the Miocene; therefore, the isolation of the Paratethys from the Mediterranean is likely to have generated a strong hydrological deficit in the Mediterranean, as most of the freshwater was collected in the Paratethys.

Over the Oligocene and Miocene, the geographic boundary between the Paratethys and the Mediterranean, and therefore water exchange between the two basins, changed in response to the intense tectonic activity of the orogenic belts of southern Eurasia and global eustatic changes (Clauzon et al., 2005; Harzhauser and Piller, 2007; Rögl, 1998). The first isolation occurred near the Eocene–Oligocene boundary (33.9 My) and may have been triggered by the global sea-level fall associated with the onset of the Antarctic ice sheets. During the late Miocene and especially during the Pliocene and Quaternary, the original size of the Paratethys Sea was substantially reduced, and various separated basins, such as the actual Black, Caspian, and Aral Seas, appeared as a consequence of the uplift in the Carpathian mountains and the Caucasus (Popov et al., 2006; Rögl, 1999).

The presence of the Paratethys, a large epicontinental sea, had a strong effect on Eurasian climate since it was a significant source of water vapor for the atmosphere. Besides, the heat capacity of this large volume of water contributed to reducing the seasonal thermal gradient (Fluteau et al., 1999; Ramstein et al., 1997). The shrinkage of the Paratethys during the late Miocene and Pliocene changed the Eurasian climate from oceanic to more continental conditions with much colder winter temperatures and a larger seasonal thermal contrast (Ramstein et al., 1997).

The progressive closure of the Tethys–Indian connection from the Oligocene to the Miocene also resulted in drier climates in Anatolia and the Arabian Peninsula as well as in northeast Africa (Ramstein et al., 1997). Furthermore, the northward drift of the African continent from the Eocene to the present contributed to an expansion of the subtropical desert along North Africa, with a strong impact on the Mediterranean hydrological budget (Fluteau et al., 1999).

1.2.3 Mediterranean Salinity Crisis

After the final closure of the Indian gateway (11 My), the Mediterranean was connected with the Atlantic Ocean through two gateways, the northern Betic Strait located in Southern Spain and the south Riffian gateway in Northern Morocco. However, the convergence between the African and Iberian plates progressively restricted those gateways contributing to the Mediterranean "salinity crisis" between 7.25 and 5.96 My.

The term *Mediterranean salinity crisis* was first used by Mediterranean geologists to explain the widespread presence of evaporites (gypsum, salts) all over the Mediterranean marginal basins such as those in Spain (Figure 1.5), Italy, Crete, Turkey, and North Africa (Gentil, 1918). However, the deep implications of this crisis were not fully recognized until the discovery of giant evaporite deposits in the deepest basins of the Mediterranean during the Deep Sea Drilling Project (DSDP) Leg 13 in 1970 (Cita et al., 1978; Hsü et al., 1973, 1977). The discovery of huge

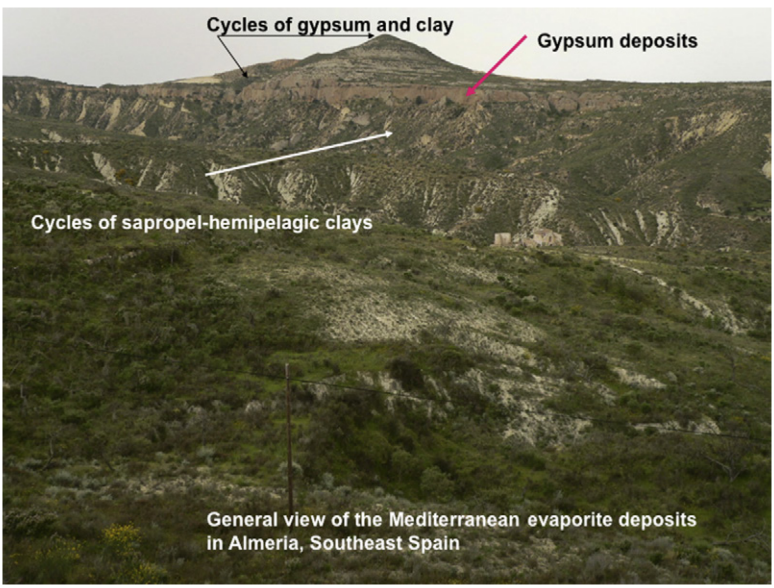

Figure 1.5 General view of the Mediterranean evaporite deposits in Almeria, Southeast Spain, showing massive gypsum deposits of around 40 m thick overlaid by gypsum–pelite cycles. The gypsum deposits are overlying astronomically driven hemipelagic cyclical sediments. *Source*: Photo by F.J. Sierro.

saline bodies buried by thousands of meters of Plio-Pleistocene pelagic sediments led scientists to recognize that the Mediterranean had to have been completely or partially desiccated during the late Miocene. This was one of the most exciting scientific discoveries in earth sciences. The late Miocene Mediterranean desiccation has been the focus of intensive research both on land and in the deep marine basins of the Mediterranean, generating passionate debates in scientific meetings that ended with new ideas about the origin of this dramatic episode of Mediterranean history.

Up to today, only the top of the evaporites has been drilled and cored in the deep sea, but nothing is yet known about the evaporites underneath, which can only be interpreted through the study of seismic profiles. The few meters recovered from the uppermost evaporites indicate that they were deposited in a shallow-water desiccated Mediterranean (Cita et al., 1978; Hsü et al., 1973, 1977), in sharp contrast to the pelagic oozes deposited afterward, during the early Pliocene. Since indications on the sediments underlying the evaporites point to material deposited in a deep marine environment, it was concluded that the Mediterranean Sea desiccation was an exceptional event during the Messinian (5.9–5.3 My; Hsü et al., 1973).

Seismic profiles in the western Mediterranean deep basins allowed the recognition of three evaporite units, the so-called Messinian trilogy (Lofi et al., 2005, 2008; Montadert et al., 1970), with a total thickness of around 1600 m. These three distinct seismic units were defined as the Lower Unit, Mobile Unit, and Upper Unit (LU, MU, and UU, respectively; Lofi et al., 2005, 2008) with thicknesses of 500–800 m for the UU, 600–1000 m for the MU, and 500–700 m for the LU.

Because we have no record from the deeper Mediterranean Sea evaporites, most of the geological interpretations and the desiccation scenarios proposed so far are based on observations made in marine sediments preserved on the marginal basins, such as in Spain (Figure 1.5), Italy, Greece, and Morocco. In particular, today outcropping deposits in the Caltanissetta basin in Sicily (Decima and Wezel, 1973) and the Northern Apennines (Manzi et al., 2005, 2007, 2009; Roveri et al., 2001, 2008; Roveri and Manzi, 2006) were probably deposited in deep marine settings and consequently may be equivalent to the western Mediterranean trilogy. The LU has usually been related to the lower evaporites cropping up in Sicily, Spain, and all over the Mediterranean marginal basins; the MU with the halite unit in Sicily; and the UU with the upper evaporites in Sicily and the Apennines.

High-resolution astrochronological studies on several sections of the pre-evaporitic deposits in Spain (Figure 1.5), Italy, and Greece concluded that the onset of the Messinian salinity crisis, at least in the marginal basins, was isochronous all over the Mediterranean, with an astronomical age of 5.96 My (Hilgen and Krijgsman, 1999; Krijgsman et al., 1999). Since the basal age of the Pliocene is 5.33 My (Hilgen, 1991b), the time period of the Messinian salinity crisis is well constrained, with a total duration of 630 ky. However, while the age of the onset of evaporites on land is precisely known, there is still a lot of controversy about the synchronous or diachronous onset of the deep Mediterranean evaporites (see Rouchy and Caruso, 2006, for a review). Over the last several decades, numerous desiccation scenarios have been proposed (Braga et al., 2006; Butler et al., 1995; CIESM, 2008; Clauzon et al., 1996; Riding et al., 1998; Rouchy and Caruso, 2006). Below we will summarize the main phases of the Messinian salinity crisis.

The History of Mediterranean Desiccation

Based on land and deep Mediterranean observations, the scenario proposed for the Messinian desiccation (CIESM, 2008) is the following. The time, 7.2 My, when compression between North Africa and the Iberian Peninsula restricted the Betic–Riffian corridors that severely reduced the Atlantic–Mediterranean water exchange is likely to represent the beginning of the Mediterranean salinity crisis because of the severe restriction of the Atlantic–Mediterranean water exchange. A sudden drop in benthic foraminiferal $\delta^{13}C$, well below the Atlantic benthic carbon isotope signal, and the onset of sapropel (i.e., a sediment layer rich in organic matter) deposition at times of precession minima are the evidence for this restriction (Kouwenhoven et al., 1999, 2003; Seidenkrantz et al., 2000; Sierro et al., 2003). A second and more severe restriction of the connection with the Atlantic occurred at 6.7 My, as evidenced by widespread deposition of laminated sediments all over the Mediterranean and a significant drop in benthic foraminiferal diversity as well as an increase in the abundance of species typically living in dysoxic waters (Kouwenhoven et al., 1999, 2003; Sierro et al., 1999, 2001, 2003; van Assen et al., 2006). An increase in benthic foraminiferal $\delta^{18}O$ in combination with warmer temperatures also indicates higher Mediterranean salinities (Sierro et al., 2003).

Preceding the deposition of evaporites on the marginal basins, the first signs of high surface salinities were recorded in Spain and Italy by the cyclical disappearance of planktonic foraminifera during the so-called aplanktonic zones that usually occur between 6.3 and 6.2 My and coincide with times of minimum summer insolation (Manzi et al., 2007; Sierro et al., 2001). Progressive restriction of the Atlantic–Mediterranean water exchange, in combination with the cyclical oscillations between periods of higher and lower Mediterranean water deficits led to surface salinities exceeding 49 psu, the maximum tolerable limit for most planktonic foraminiferal species (Fenton et al., 2000).

The Onset of Gypsum Deposition on the Marginal Basins

In the beginning of the Messinian salinity crisis, huge amounts of gypsum were deposited in peripheral basins all over the Mediterranean (Figure 1.5). These deposits, usually called the "lower evaporites," contain geochemical evidence for deposits under marine conditions. In consequence, the connection to the Atlantic, though limited, was still open, and the sea level in the Mediterranean was possibly the same as that in the Atlantic. The lower evaporites consist of approximately 16/17 sedimentary cycles formed by the alternation of gypsum and marl beds, which, based on the tuning of the gypsum beds to cycles of maximum Earth precession (Krijgsman et al., 1999, 2001), were deposited between 5.96 and 5.59 My. Alternatively, gypsum deposition may have been triggered by eustatic sea-level changes on a millennial scale (Rohling et al., 2008). The onset of gypsum deposition was an isochronous event in all peripheral basins, with an astronomical age of 5.96 My (Gautier et al., 1994; Krijgsman et al., 1999; Sierro et al., 1999).

Some studies suggest that gypsum deposition was restricted to the marginal, shallow basins, whereas black euxinic shales, barren of microfossils, were laid down in the deep sea, suggesting the existence of a completely anoxic deep Mediterranean

Sea at the time of gypsum deposition in the margins (CIESM, 2008; De Lange and Krijgsman, 2010; Lugli et al., 2010).

Box models using the present Mediterranean annual freshwater deficit suggest that with a continuous Atlantic inflow but a restricted outflow, the salinity of Mediterranean water progressively increased to reach gypsum saturation at values up to 145 g/L in 6 ky (Krijgsman and Meijer, 2008).

The Sea-Level Drawdown and Salt Precipitation

The deposition of the lower evaporites in the margins ended with a major sea-level drawdown of at least 1500 m in the Mediterranean. This took place approximately 5.59 My ago and led to the subaerial exposure of the continental margins and to the excavation of deep canyons by the major rivers. Canyons up to 1000 and 2500 m deep were excavated by the Rhone and the Nile, respectively, in response to this drastic base-level lowering that generated the Messinian erosion surface (MES) visible in seismic lines all over the Mediterranean (Clauzon, 1973; Lofi et al., 2005). Because of this massive erosion of the Mediterranean continental shelves and slopes, huge amounts of sediments, including the gypsum of the lower evaporites that were previously deposited in the margins, were transported downslope and redeposited in the deep Mediterranean basins. By comparison with the Northern Apennines outcrops, it has been hypothesized that these redeposited sediments formed the LU recognized in the Mediterranean seismic profiles (CIESM, 2008; Lofi et al., 2005). The bottom of the LU in the deep basins and the MES on the continental margins consequently mark the first complete disconnection of the Mediterranean from the Atlantic, occurring approximately 5.59 My ago. As a result, and immediately overlaying the LU, deposition of 600–1000 m of halite in the deep basins started. It has been estimated that salt precipitation took place in the deep basins between 5.59 and 5.52 My, during a time interval of only 70 ky that has been correlated with glacial isotope stages TG14-12 (Hilgen et al., 2007; van der Laan et al., 2005). In deposits in Sicily, considered to be the equivalent of the deep Mediterranean setting, the halite unit is deposited between the lower and upper evaporites (Decima and Wezel, 1973).

Oceanographic models suggest that halite saturation in the Mediterranean, which takes place at salinities of 350 g/L, could be reached only with a continuous Atlantic inflow and a blocked outflow (Krijgsman and Meijer, 2008; Meijer, 2006). These models also indicate that with the present freshwater deficit, after a complete disconnection with the Atlantic, the Mediterranean water level would drop rapidly to reach an equilibrium level at –2500 m in 10 ky (Meijer and Krijgsman, 2005).

The Lago Mare Phase

The last phase of the Messinian salinity crisis, which lasted from 5.55 to 5.33 My, is marked by the deposition of the upper evaporites and is usually known as the Lago Mare event (Hsü et al., 1973). This period is characterized by 7/10 precessional cycles defined by the alternation of gypsum or conglomerates and marl beds, suggesting cyclical fluctuations in salinity (Hilgen et al., 2007; Roveri et al., 1998, 2001, 2008).

Strontium isotope values and the presence of fresh and brackish water ostracods and mollusks of Paratethyan origin have been interpreted as a proof of Mediterranean flooding with freshwater from the Paratethys (Çagatay et al., 2006; Cita et al., 1978; Flecker and Ellam, 2006; Hsü et al., 1973, 1977; Lugli et al., 2008). Although a major change in the Mediterranean hydrological budget can also explain this shift from hyperhaline to hypohaline waters at the onset of the Lago Mare event, no significant change in the Mediterranean climate has been detected at this time (Suc, 1984).

Contradictory information has been found with respect to the Mediterranean water level during the Lago Mare phase. Shallow-water deposits were recorded in deep Mediterranean basins immediately below the Pliocene pelagic sediments, documenting a deep, almost desiccated Mediterranean during this period (Cita et al., 1978; Hsü et al., 1973; Iaccarino and Bossio, 1999). However, a deepwater habitat for brackish water microfossils cannot be completely ruled out. By contrast, Lago Mare deposits with mollusks and ostracods of Paratethys origin have been reported in many marginal basins, such as in Spain, Italy, Cyprus, northeast Morocco, Algeria, and Turkey (Aguirre and Sánchez-Almazo, 2004; Bassetti et al., 2006; Fortuin and Krijgsman, 2003; Guerra-Merchán et al., 2010; Rouchy et al., 2001, 2003, 2007). This documents that the Mediterranean water level was not below the paleodepth of these marginal basins, which was probably very shallow as suggested by the abundant presence of shallow-water ostracods and foraminifera. The cyclical occurrence of Lago Mare and fluvial deposits with evidence of paleosoils in some of the marginal basins (Fortuin and Krijgsman, 2003; Rouchy et al., 2001) suggests that significant oscillations in the water base level may have occurred during this period and that the lake level in the Mediterranean Sea was, at least temporarily, well below that of the Ocean. Alternatively, the existence of various marginal disconnected lacustrine basins with different water levels cannot be completely ruled out.

1.2.4 The Pliocene Mediterranean Flooding

The Mediterranean salinity crisis abruptly ended at the Miocene–Pliocene boundary, 5.33 My ago, with the opening of the Strait of Gibraltar and the reestablishment of open marine conditions when the Atlantic water discharge flooded into the Mediterranean. The Mediterranean inundation has been related to either a global eustatic sea-level rise at the end of the Miocene or to tectonic or erosive processes in the Strait of Gibraltar.

The analysis of benthic foraminiferal $\delta^{18}O$ records from the North Atlantic and its detailed correlation with the Mediterranean show that the Mediterranean flooding was not triggered by any major eustatic rise at the beginning of the Pliocene (Hilgen et al., 2007; Hodell et al., 2001; van der Laan et al., 2006). On the other hand, several studies have revealed that tectonic processes in the Gibraltar Arc, such as the activity of strike-slip faults or subsidence, are probably responsible for the opening of the Strait of Gibraltar (Duggen et al., 2003; Sierro et al., 2008).

Some models suggest that enhanced fluvial regressive erosion may have developed in the Mediterranean side of Gibraltar in response to the sea-level drop of more than 1500 m, which eventually captured the Atlantic waters (Blanc, 2002; Loget and van den Driessche, 2006). One study suggested that, although the initial opening of the strait may have been caused by river incision, once Atlantic water discharge began, it was the huge hydraulic energy of this water generated by the large difference in altitude of sea levels at the two sides of the Strait that excavated the long and deep channel that exists today across the Strait of Gibraltar (Garcia-Castellanos et al., 2009). Water discharge, which may have been low at the beginning, exponentially increased as the rate of incision rapidly opened the floodgate to the Mediterranean to finally generate a catastrophic flood that filled the Mediterranean in less than 2 years with a water discharge of more than 108 m^3/s (Garcia-Castellanos et al., 2009). This study also suggests that at the time of maximum water discharge, the Mediterranean may have been filled at a rate of 10 m/day.

1.2.5 Mediterranean Climate During the Pliocene

Pollen records indicate that during the early Pliocene, the Mediterranean climate was warmer and wetter than it is today (Fauquette et al., 1998, 1999; Jimenez-Moreno et al., 2010; Suc, 1984). Based on the quantitative changes of warm-water planktonic foraminiferal species, a relative SST record was elaborated for the whole Pliocene in sections from Southern Italy (Lourens et al., 1996). Although SST oscillated at a precession scale, warm-water species were dominant during the early Pliocene, with a special warm interval between 4.1 and 3.7 My. The first evidence of cooling is found at 3.7 My and a second one between 3.5 and 3.2 My (MIS MG5-M2; Lourens et al., 1996; Sprovieri et al., 2006b). Pollen records from the Black Sea and northwest Mediterranean also reflect a sharp change in the Mediterranean vegetation during this later interval. This event is recorded by a decrease of subtropical trees that were partially replaced by herbs, indicating lower temperatures but still relatively humid conditions (Fauquette et al., 1998; Popescu et al., 2010). This transitional period of cooling was interrupted by the Mid-Pliocene warmth event between 3.2 and 3 My (Dowsett et al., 2009). Pliocene Mediterranean temperatures have been estimated to be 1–2°C warmer than at present (Dowsett et al., 2009), and atmospheric carbon dioxide concentrations were about 30% higher than pre-anthropogenic values (Tripati et al., 2009; van der Burgh et al., 1993); consequently the climate during this period has been considered a good analog for future climate conditions. On the basis of model simulations, the climate of Western Europe and Mediterranean was warmer and wetter because of the enhanced atmospheric and oceanic transport of heat and moisture to the North Atlantic and Mediterranean from the Equatorial Atlantic, especially during winter (Haywood et al., 2000).

Pollen data found in sediments from the early and mid-Pliocene fit well with these predictions of a warmer and more humid climate in the northern Mediterranean (1–4°C warmer) and 400–700 mm higher annual rainfall than today (Fauquette et al., 1999; Jost et al., 2009). In the southern Mediterranean, however, climate was warmer by 1–5°C, but present-day arid conditions appear to have been in place since the beginning of the Pliocene (Fauquette et al., 1999).

SST changes during the late Pliocene reflect the progressive intensification of the Northern Hemisphere glaciation, but the first pronounced glacial cycle is not recorded until the late Pliocene, cotemporaneous with an intensification of the Northern Hemisphere glaciation at around 2.7 My. In particular, very cool planktonic foraminiferal assemblages have been found in MIS G6 and MIS 100-98-88 (Lourens et al., 1996), coincident with prominent glacial stages in the Equatorial and North Atlantic Ocean (Haug and Tiedemann, 1998; Lisiecki and Raymo, 2005). From 2.7 My ago up to the present, pollen records from the northwest Mediterranean indicate alternations between steppe and forest that have been associated with the glacial–interglacial climate oscillations (Combourieu-Nebout et al., 2000; Fauquette et al., 1998; Popescu et al., 2010).

Contourite deposits (e.g., the Faro Drift) suggest that the Mediterranean outflow water (MOW) was already flowing along the southern Iberian margin in the early Pliocene, though its onset has not yet been precisely dated (Hernandez-Molina et al., 2006). Continuous deposition in the Faro contourite drift seems to indicate that the Atlantic–Mediterranean water exchange was anti-estuarine from the early Pliocene to the present. In consequence, we may conclude that the Mediterranean hydrological budget has remained negative since then. A MOW intensification between 3.5 and 3.3 My ago, probably in response to enhanced aridification of the Mediterranean climate, was recorded in the Ireland continental margin (Khelifi et al., 2009).

Throughout the Pliocene and Pleistocene, the Mediterranean experienced numerous anoxic events recorded by the cyclical deposition of organic-rich layers (ORLs), or sapropels, whose formation is linked to the monsoon influence on the Mediterranean area and subsequent Nile river runoff and/or enhanced annual rainfall in peri-Mediterranean regions (Cramp and O'Sullivan, 1999; Rohling, 1994; Rossignol-Strick et al., 1982; Thunell et al., 1984; Wehausen and Brumsack, 1998). Sapropel formation is linked to summer insolation maxima in the Northern Hemisphere (see also Section 1.3.1), and the patterns of sapropel deposition have been used to elaborate the astronomical timescale (Hilgen, 1991a; Lourens et al., 1996). Eighteen sapropels (S63 to S80) were deposited in the eastern Mediterranean Sea between 2.6 and 3.2 My (Kroon et al., 1998). Around some of those sapropels, alkenone-based SST values reached 23–26°C during the warmer periods and 20–21.5°C during the colder ones (Emeis et al., 1998), in agreement with the warmer-than-Pleistocene SST estimated by Dowsett et al. (2009). Prior to sapropel deposition, export productivity was high. Overall, productivity was higher in the eastern than in the western basin and higher in the Pliocene than in the Pleistocene (Diester-Haass et al., 1998).

1.3 Sensitivity and Variability at Different Climate States

1.3.1 Warm Climate Intervals of the Pleistocene: The Case of the Last Interglacial

The glacial–interglacial cycles that characterize the last 2.6 My of Earth's climate have been shown to be related to changes in the Earth's orbital elements that affect radiation received at the top of the atmosphere (insolation) and are a function of hemisphere, latitude, and season (Hays et al., 1976; Milankovitch, 1920). On orbital timescales, full glacial and stadial (i.e., less cold) periods were in general associated with colder global temperatures and lower atmospheric greenhouse-gas concentrations and interglacial and interstadial (i.e., less warm) intervals with warmer global temperatures and higher greenhouse-gas concentrations (Jouzel et al., 2007; Loulergue et al., 2008; Petit et al., 1999). In the marine realm, interglacials are marked by sea-level highstands indicated by lower benthic $\delta^{18}O$ values (Lisiecki and Raymo, 2005; Shackleton and Opdyke, 1973). On land, interglacial climate conditions are often associated with forest expansion (Sánchez-Goñi et al., 2005; Tzedakis et al., 1997, 2004). However, no interglacial period in the last 800 ky was exactly like another (EPICA members, 2004; Tzedakis et al., 2009). The climate of the Holocene, the current interglacial, will be discussed separately (Section 1.3.4).

In this section, we concentrate mainly on the last interglacial period called MIS 5e in the marine isotope stratigraphy and referred to as the Eemian period in continental records based on the palynological evidence. As the multiproxy study of site 5 (core MD95-2042) off southwestern Portugal revealed, the boundaries of the two periods are not the same (Kukla et al., 2002; Shackleton et al., 2003). The base of MIS 5e, defined as the midpoint of the glacial–interglacial transition, appears to be 6 ky older than the onset of the Eemian forest phase, while the onset of the sea-level highstand-related benthic $\delta^{18}O$ plateau preceded the Eemian by about 2 ky (Shackleton et al., 2003; Figure 1.6B and C). Here, we follow Kukla et al. (2002) and consider the interval from 128 to 116 ka to calculate the mean SST for MIS 5e (Table 1.1sm (supplementary material available at http://www.elsevierdirect.com/companion.jsp?ISBN=9780124160422) Figure 1.7), while the Eemian lasted from 126 to 110 ka and thus extended into the MIS 5d stadial when continental ice sheets were already growing. MIS 5e global sea level was about 5 ± 2 m higher than today (Rohling et al., 2008; Thompson and Goldstein, 2005). Around the Mediterranean Sea, evidence for past eustatic highstands is still sparse and linked to sedimentary gaps on the continental shelf in the Gulf of Lions (Sierro et al., 2009), deltaic deposits of the Tiber river (Marra et al., 2008), and submerged cave deposits (Bard et al., 2002; Dorale et al., 2010).

One interglacial phenomenon particular to the Mediterranean Sea is the deposition of the above-mentioned organic-rich and thus dark-colored sapropel layers (Figure 1.6H), especially in the eastern basin (Emeis et al., 1998; Kroon et al., 1998; Rossignol-Strick, 1985; Rossignol-Strick et al., 1982). Sapropel deposition not only followed (by 1–3 ky) the insolation maxima associated with the glacial–interglacial transitions (Figure 1.6G) but also occurred along with glacial insolation maxima (Schmiedl et al., 2003; Weldeab et al., 2003). During MIS 5e, a sapropel called S5 formed between 124 and 119 ky (Figure 1.6H), but its duration and intensity varied regionally (Weldeab et al., 2003; Figure 1.6H), reaching a thickness of 120 cm in the southern Aegean Sea (site 124, core LC21; Marino et al., 2007; Table 1.1; Figures 1.4 and 1.6). Although some sapropel layers are laminated, indicating variable hydrographic conditions, most of them, including S5, were associated with anoxic conditions—as indicated by the absence of benthic foraminifera (Jorissen, 1999; Schmiedl et al., 2003)—in the intermediate and deep waters in the eastern basin. The shallowest sapropels were detected at 120 m in sediment cores from the Aegean Sea (Casford et al., 2002), while, in general, they were present below 300 m in the open eastern

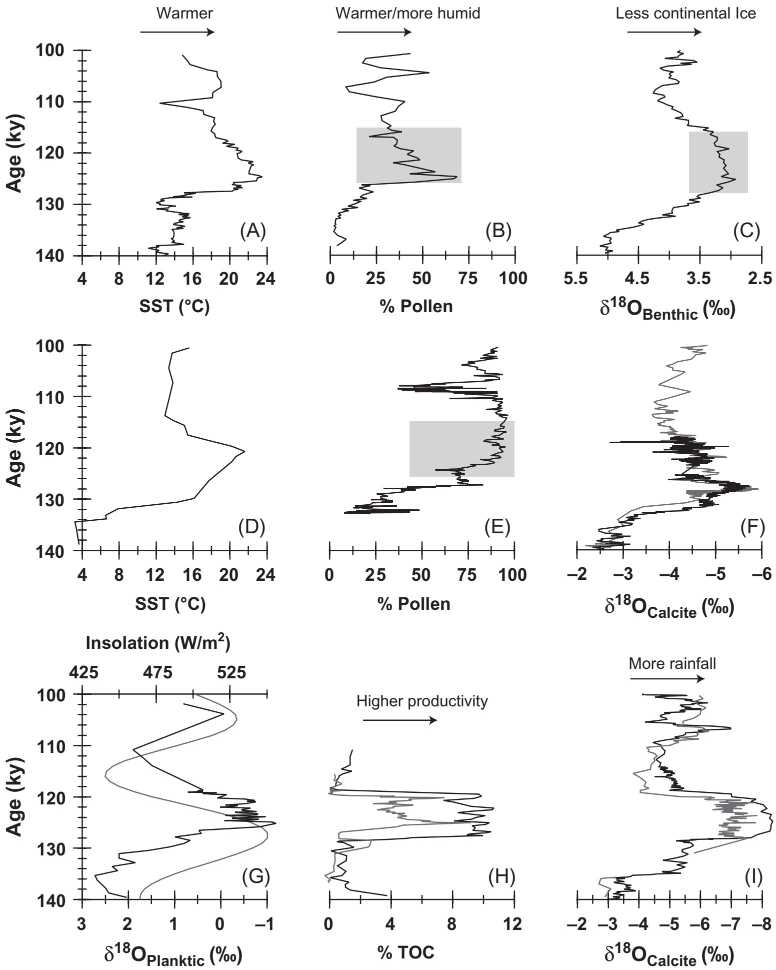

Figure 1.6 Climate records from the last interglacial period for the western Iberian margin and Mediterranean Sea (A–C) and for the central (D–F) and eastern (G–I) Mediterranean region. (A) Sea-surface temperature (SST) record of ODP Site 977 (Alboran Sea; Martrat et al., 2004). (B) Pollen percentages of Mediterranean taxa included in core MD95-2042 (Sánchez-Goñi et al., 1999). The gray square marks the Eemian interval (115–127 ka; Kukla et al., 2002). (C) Benthic foraminiferal $\delta^{18}O$ record of core MD95-2042 from the Portuguese margin (Shackleton et al., 2000) with the gray square highlighting the period of the MIS 5e sea-level highstand (116–128 ka). (D) SST record of borehole PRAD1-2 in the central Adriatic Sea (Piva et al., 2008). (E) Abundance of arboreal pollen in the Lake Monticchio sequence (central Italy; Allen and Huntley, 2009) (gray square as in B). (F) Corchia cave speleothem records (central Italy; Drysdale et al., 2005, 2009). (G) Planktonic foraminiferal *Globigerinoides ruber* (white) $\delta^{18}O$ record of core SL 67 near Crete (black; Weldeab et al., 2003) and June 21 insolation at 65°N (gray; Laskar et al., 2004). (H) Total organic carbon (TOC) records (maxima represent Sapropel 5) of sediment cores SL 67 (gray) and ODP Site 969E from the Mediterranean ridge south of Crete (black; Weldeab et al., 2003). (I) Speleothem records from Soreq Cave (black; central Israel) and Peqiin Cave (gray; northern Israel) (Bar-Matthews et al., 2003).

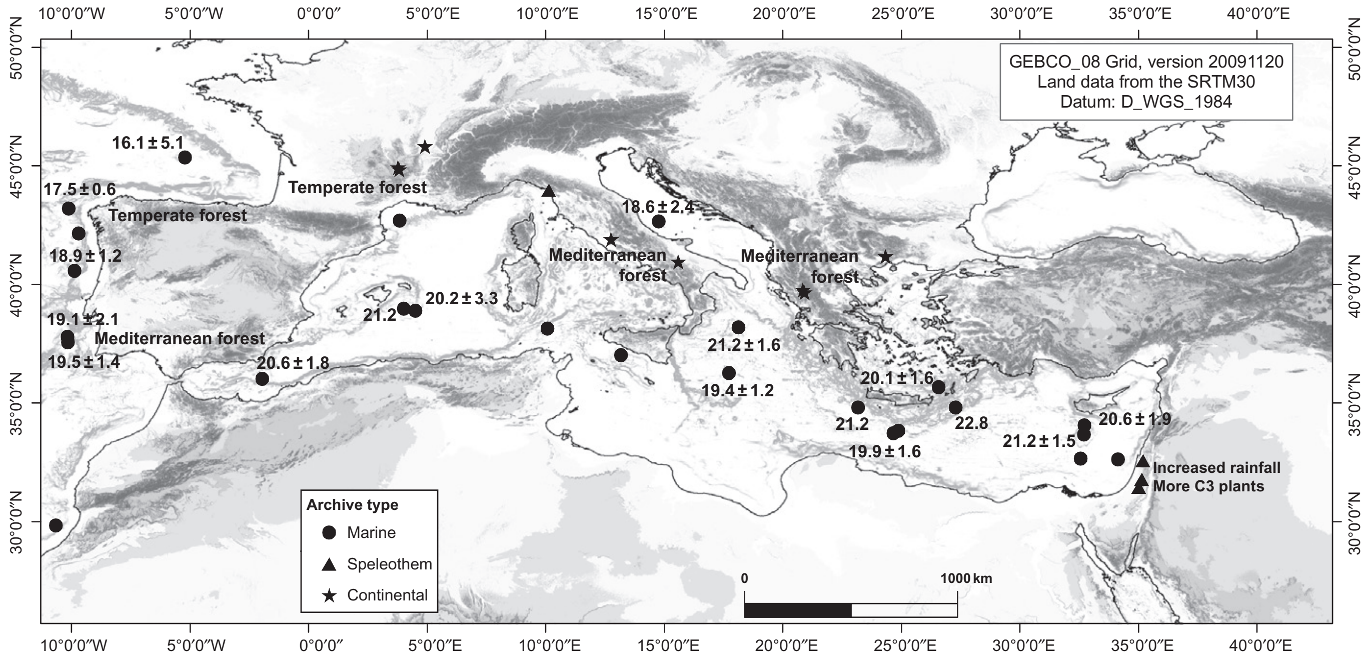

Figure 1.7 Map showing sites with MIS 5e/Eemian records and mean SST values for MIS 5e (Table 1.1sm).

Mediterranean (Rohling et al., 1993) and below 400 m in the Adriatic Sea (Jorissen et al., 1993). Although benthic foraminifera were absent, planktonic foraminifera can be found in the sapropel sediments and used to establish isotope stratigraphies (Figure 1.6G) and to reconstruct hydrographic conditions. Pollen and geochemical evidence have revealed that the formation of sapropels is linked to episodes of enhanced freshwater discharge, especially from the Nile River (Cheddadi and Rossignol-Strick, 1995a; Osborne et al., 2010; Scrivner et al., 2004) because of an intensification of the African monsoon (by precessional forcing) and the northward migration of the Intertropical Convergence Zone (Rohling et al., 2002a; Waldmann et al., 2010). A mark of the increased rainfall is well preserved in speleothem, travertine, and lake records from Israel (Figure 1.6I; Bar-Matthews et al., 1999, 2003; Frumkin et al., 1999, 2000; Waldmann et al., 2010). Because of the freshwater flux into the eastern Mediterranean basin, δw was depleted at the beginning of S5 (Emeis et al., 2003) and evidence from site 124 indicates a salinity drop of >4 psu in the eastern Aegean Sea (van der Meer et al., 2007). The combination with the slightly cooler SST at the onset of S5 (Emeis et al., 2003; Marino et al., 2007; Rohling et al., 2002a) led to temperature and salinity stratification, which inhibited convection and sustained the poor ventilation of the deeper water column and thus preserved organic matter (C_{org}). Marino et al. (2007) showed that the subsurface ventilation collapsed within 40 ($\pm$20) years in the Aegean Sea and 300 ($\pm$120) years later throughout the eastern Mediterranean Sea. The euxinic conditions, extending up to a water depth of about 200 m, persisted for 650–900 years (Marino et al., 2007; Rohling et al., 2006), followed by a >4 ky-long period of variable conditions in the winter mixed-layer and water-column stratification (Rohling et al., 2006). At site 141 (core GeoTüKL83) off Israel, Schmiedl et al. (2003) showed that oxygenation had already recovered during the later S5 phase, at a water depth of 1433 m, indicating at least local convection. Besides, reduced ventilation increased productivity (Rohling et al., 2006; Weldeab et al., 2003) and hence enhanced carbon flux to the seafloor also played a role in sapropel formation. Different theories are being debated for the nutrient supply that sustains the high productivity: riverine supply (Martinez-Ruiz et al., 2000), development of a deep chlorophyll maximum and productivity therein (Rohling and Gieskes, 1989; Rohling et al., 2004), and trapping of nutrients in the eastern basin (Struck et al., 2001). At site 73 (core LC07), at the Sardinian–Sicilian sill, plankton productivity was already high prior to the deposition of S5 (Incarbona et al., 2008).

Mean SST values for MIS 5e, most of them based on alkenone concentrations ($U^{K'}_{37}$ index) and limited to the S5 interval, are shown in Figure 1.7 and listed with their minimum and maximum values in Table 1.1sm. Colder mean SSTs were recorded off western Iberia, reflecting the effect of the upwelling system, and a 2°C gradient from north to south (Figure 1.7), similar to modern conditions (Salgueiro et al., 2010). Within the Mediterranean Sea, both mean and maximum SSTs were similar throughout the Mediterranean, from the western to the eastern basins, with values around 21°C, which is 1–2°C warmer than the late Holocene SST (see Introduction). At site 90 (borehole PRAD1-2) in the central Adriatic Sea, a relatively colder mean value is observed, and the SST cooled rapidly and faster than in other records after the SST peak at 120.7 ky (Figure 1.6D versus 1.6A). The mean value of 19.4°C at site 95 (core KC01) in the central Ionian Sea, on the other hand, includes only data from the late MIS 5e when the SST was already declining (Marino et al., 2007; Martrat et al., 2004; Rohling et al., 2002a). The record from site 98 (core KS205), in the same region (Rohling et al., 2002a), reveals that the SST was overall more variable in the Ionian Sea and shows a slight cooling during S5 that is even more strongly depicted by the planktonic foraminiferal records. Rohling et al. (2002a) interpret this fluctuation with a timing of 122.5–121.4 ky as a disruption in the African monsoon—supported by slightly higher $\delta^{18}O$ values in the Corchia and Peqiin speleothem records (Figure 1.6F and I)—and link it to the Eemian cold fluctuation identified in pollen records from Greece (Tzedakis et al., 2003a,b), Italy (Allen and Huntley, 2009), and a French lake (Thouveny et al., 1994). The timing also fits with a reduction in coccolith diversity at site 73 (core LC07; Incarbona et al., 2008). A second and more pronounced cooling event is recorded in the planktonic and benthic foraminiferal $\delta^{18}O$ climate records of site 84 (Ocean Drilling Program (ODP) site 963) during late MIS 5e (Sprovieri et al., 2006a). This cooling event is coeval with the C25 cooling event recorded in North Atlantic sediments (Oppo et al., 2006) and with the Greenland Stadial (GS) 26 of the North Greenland Ice Core Project (NGRIP) ice core (NGRIP members, 2004). However, Incarbona et al. (2008) point out that the surface-water cooling at site 84 might be linked to local changes since the same event is not as well defined in the records of nearby site 73.

On land, the Eemian pollen records around the Mediterranean region clearly show that the major forested period occurred between 126 and 120 ka. However, they also reveal four main climatic phases of low amplitude, in particular, in the southwestern Iberian Peninsula (Sánchez-Goñi et al., 1999, 2005) and in Greece (Tzedakis et al., 2003a). Between 126 and 120 ka, southwestern Iberia experienced a warm and relatively humid climate, as indicated by the expansion of the Mediterranean forest (Figure 1.6B), while a deciduous oak forest is found in northwestern Iberia (Sánchez-Goñi et al., 2005). Here, the beginning of the Eemian interglacial period was actually marked by the expansion of pioneer species 1 ky prior to the establishment of Mediterranean forest conditions, suggesting pre-cool and wet conditions (Sánchez-Goñi et al., 2005). Annual precipitation in this same region was around 800 mm and the warmest month mean temperature must have varied between 20°C and 24°C, while the coldest month is likely to have had temperatures around 5°C (Sánchez-Goñi et al., 2005). In northwestern Iberia, precipitation levels were similar but temperatures were lower, close to 18°C in the warmest month and 3°C in the coldest month. Studies of the isotopic composition of water in fluid inclusions ($\delta D_{(H2O)}$) of two stalagmites and oxygen isotopes of mammal's teeth phosphate ($\delta^{18}O_{(PO4)}$) in the Soyons Cave, Rhone Valley, France, also indicate comparable contrasting seasonal temperatures during the same time interval, with mean summer and winter values of 16°C and 2°C, respectively (Gardien et al., 2010). The Mediterranean climate of southern Iberia was gradually replaced by oceanic (cool and wet) conditions that were well established between 120 and 116 ka and turned into warm and dry conditions between 116 and 110 ka (Sánchez-Goñi et al., 1999, 2005). At latitudes north of 36°N but further to the east, the climatic phases described for the northwestern Iberian margin are also detected in the Ioannina record (Greece; Tzedakis et al., 2003b). In central Italy, the temperatures during the coldest month were similar to the ones registered in the southwestern Iberian margin—i.e., 4–5°C (Allen and Huntley, 2009).

In the Levant, the Israeli speleothem $\delta^{13}C$ records indicate a greater abundance of C3 plants (e.g., trees), indicating humid and cool conditions, especially during the time of S5 (Bar-Matthews et al., 2003; Frumkin et al., 2000).

During the last 450 ky, MIS 5e stands out as the warmest interglacial period within the Mediterranean Sea. The warm periods preceding MIS 5e were MIS 7 and MIS 9e (338–324 ka). MIS 7 includes the three warm substages MIS 7e (246–229 ka), 7c (216.8–206.8 ka), and 7a (200–190 ka), of which MIS 7e is the warmest in the Antarctic ice-core records (EPICA members, 2004); sapropels 9, 8, and 7, respectively, are associated with these substages. Relative sea-level data for the Mediterranean Sea exist only for MIS 7a, when the sea level was between 9 and 18 m lower than it is in the present (Bard et al., 2002). SSTs in the Mediterranean region were fairly similar during all three substages, but on average, they were 1°C colder than during MIS 5e (Emeis et al., 2003; Martrat et al., 2004, 2007; Piva et al., 2008). Similar to MIS 5e, SSTs were warmer (by about 1°C) in the eastern basin than in the western basin (Emeis et al., 2003). Also comparable to MIS 5e, SSTs at site 90 (borehole PRAD1-2; Piva et al., 2008) in the central Adriatic Sea started to decline earlier than in the Alboran Sea (site 44/ODP Site 977; Gonzalez-Mora et al., 2008; Martrat et al., 2004) and off southwestern Portugal (MD01-2443; Martrat et al., 2007) during MIS 7e and 9e. In surface water records from the Alboran Sea and off southwestern Portugal MIS 7e, 7c and 7a were recorded as long warm periods. In the subsurface waters (*Neogloboquadrina pachyderma* (r) record of Gonzalez-Mora et al., 2008), on the other hand, only MIS 7e and 7a were continuously warm. During MIS 7c, subsurface waters in the Alboran Sea warmed only during the later phase, similar to the $U^{K'}_{37}$ SST at site 90, indicating that the two records might be linked via the Levantine Intermediate Water (LIW) formed in the Adriatic Sea. For MIS 9e, few SST data exist within the Mediterranean Sea. The $U^{K'}_{37}$ SST record at site 90 (Piva et al., 2008) indicates values (around 17.2°C) similar to those for MIS 7a and thus colder than during MIS 5e while at site 136 in the Levantine basin temperatures of 21.5°C were reached during the formation of sapropel 10 (Emeis et al., 2003). Along the western Portuguese margin, average SSTs decreased from 19.5°C at 37.8°N (core MD01-2443; Martrat et al., 2007) to 19.2°C at site 1 (Rodrigues et al., 2011) and to values around 18.5°C at site 10 (Desprat et al., 2009) and were therefore within the MIS 5e range (Figure 1.7).

In the pollen records, the MIS 7 substages and MIS 9e also show differences from MIS 5e. Although all three MIS 7 substages and MIS 9e were associated with a forest expansion (Follieri et al., 1998; Reille et al., 1998; Wijmstra and Smit, 1976), the forested periods were shorter than the MIS substages (Tzedakis et al., 2004) and the forest during MIS 7c was more diverse than the one during MIS 7e (Follieri et al., 1998; Tzedakis et al., 2003b). For MIS 9e, on other hand, the southern Iberian pollen record of core MD01-2443 (Roucoux et al., 2006; Tzedakis et al., 2004)—opposite northern Iberia (Desprat et al., 2009)—reveals a short tree pollen maximum that is replaced by a higher abundance of *Ericaceae* pollen in the later phase of the interglacial period. However, a much stronger climate contrast to MIS 5e is observed in the records from the Levant. The higher lake level in the Lake Lisan–Dead Sea system, the formation of travertine, and the prevalence of C3 plants (trees) as shown by the lighter $\delta^{13}C$ data from the Soreq Cave clearly indicate that MIS 7 was a much wetter period than was MIS 5e (Bar-Matthews et al., 2003; Waldmann et al., 2010).

1.3.2 High-Frequency Variations: The Case of MIS 3

The millennial-scale climate variability consisting of cycles of warmer (interstadial) and colder (stadial) periods was first described in detail in ice-core records from Greenland (Grootes and Stuiver, 1997; Johnsen et al., 1992) but can be found in climate records all over the world (Voelker, 2002). The abrupt warming at the transition from a stadial to an interstadial is referred to as Dansgaard–Oeschger event and the cycles are called Dansgaard–Oeschger cycles (Broecker and Denton, 1989) and consist of a Greenland interstadial (GI) and a GS (NGRIP members, 2004). During some of the GS the well-known Heinrich ice-rafting events occurred in the North Atlantic Ocean (Bond et al., 1993), events that because of their supply of freshwater into the North Atlantic's convection areas led to a shutdown of the Atlantic Meridional Overturning Circulation (AMOC) (Ganopolski and Rahmstorf, 2001). During a "regular" GS, AMOC was not only slowed down but also shallower than it is today. As a result of the reduced convection in the North Atlantic, the interface between the North Atlantic Deep Water (NADW) and the Antarctic Bottom Water (AABW) shoaled and the AABW filled the water column up to a depth of 2000 m (Oppo and Lehman, 1995; Vidal et al., 1997). The duration of a Heinrich ice-rafting event varied with a longer (apparent) duration in more northern latitudes and closer to the calving ice sheets and a shorter toward the southern edge of the North Atlantic's ice-rafted debris belt (Sanchez-Goñi and Harrison, 2010). Since icebergs themselves did not enter the Mediterranean Sea—just their meltwater—it is impossible to clearly distinguish a Heinrich event in that region. Thus, we follow Sanchez-Goñi and Harrison (2010) and use the term Heinrich stadial (HS) for those GSs associated with a Heinrich event. The temporal duration of a HS is equal to the associated GS as recorded in the Greenland ice-core records and thus sometimes longer than the ice-rafting event itself. For the time slices discussed here, we selected HS 4 and the subsequent GI 8. Heinrich event 4 was one of the major ice-rafting events during MIS 3 and thus had a strong impact on the climate. GI 8, on the other hand, was one of the longer-lasting GIs (NGRIP members, 2004). HS 4 lasted between 39.92 and 38.46 calendar (cal) ka before the present (BP = AD 1950) in the Greenland Ice Sheet Project 2 (GISP2) chronology (Grootes and Stuiver, 1997) and between 39.81 and 38.31 cal ka in the GICC05 chronology of the NGRIP ice core (NGRIP members, 2004; note that GICC05 ages are before AD 2000). The respective age ranges for GI 8 are 38.44–36.22 cal ka BP (GISP2) and 38.29–36.55 cal ka (NGRIP). The waxing and waning of the continental ice sheets left their imprints in the MIS 3 sea-level record (see Siddall et al., 2008, for a recent review) and can also be detected in the Mediterranean Sea where flooding of the Gulf of Lions continental shelf occurred in general by the onset of the GI following an HS (site 58—PRGL1; Sierro et al., 2009).

High-resolution SST records for the Mediterranean Sea are sparse and concentrated in the western basin. Both $U^{K'}_{37}$ SST records from the Alboran Sea reveal the GI/GS cycles, with warmer SSTs during the GI (Figure 1.8G; sites 41 and 44; Cacho et al., 1999; Martrat et al., 2004). The coldest SST during MIS 3 occurred during the HS, especially HS 4, both in the Alboran Sea (Figure 1.8G) and north of Menorca (site 61; Sierro et al., 2005). For the central basin, the data of site 88 in the Tyrrhenian Sea (core KET80-03; Paterne et al., 1999) is present, and in the eastern basin, the SST record of site 114 (core C69) in the southern Aegean Sea prevails (Figure 1.9; Geraga et al., 2005). Both sites experienced a cooling during HS 4. The temperature evolution in the Levantine basin is partly revealed by the planktonic foraminiferal $\delta^{18}O$ records of sites 139 and 142 (cores 9501 and 9505; Almogi-Labin et al., 2009) but those two seem to follow more Northern Hemisphere insolation (Figure 1.8E) rather than the millennial-scale pattern. However, the $\delta^{18}O$ records of both cores show some oscillations during HS 4, indicating less stable surface-water conditions.

On the western Iberian margin, SST records show millennial-scale oscillations (Figure 1.8B–D; Salgueiro et al., 2010). SSTs were colder in the north, where the impact of the southward advance of the polar front and thus the appearance of iceberg-bearing subpolar waters was felt more strongly (Eynaud et al., 2009; Naughton et al., 2009; Salgueiro et al., 2010). The southward shift of the polar front had a stronger impact north of 39°N because SST values in the Mediterranean Sea north of this latitude were not much colder than those off the shore of Portugal during HS 4 (Figure 1.9A). Likewise, SSTs south of this latitude was similar on the Portuguese margin and in the Mediterranean Sea. The Gulf of Cadiz record of site 18 (core MD99-2339) stands out with the warmest mean SST, but this location experienced only short-term cooling episodes during HS 4 (Figure 1.8D; Voelker and de Abreu, 2011; Voelker et al., 2006) because it was located close to the boundary separating the colder northern surface waters from the waters to the south, which were derived from the Azores Current. For the younger HS 2 and HS 1, Penaud et al. (2010) showed that the waters off Morocco clearly had a different origin from that of the Alboran Sea, and Rogerson et al. (2004) revealed that the Azores Front penetrated into the Gulf of Cadiz. In comparison to the Gulf of Cadiz data, the Alboran Sea mean values—for sites 41 and 44—appear relatively cold, but one needs to keep in mind that the Alboran Sea $U^{K'}_{37}$ data reflect annual mean temperatures and those in the Gulf of Cadiz summer SSTs. Mg:Ca-based temperatures derived from the shells of *Globigerina bulloides,* a surface-dwelling foraminiferal species, from site 41 (core MD95-2043) give a mean value of 14.5 ± 0.8°C for HS 4 (Cacho, unpublished data) and thus in the range of the site 18 (core MD99-2339) value.

For the GI 8 time slice, the major boundary was again located near 39°N, especially on the Portuguese margin (Figure 1.9B; Table 1.2sm available at http://www.elsevierdirect.com/companion.jsp?ISBN=9780124160422). One peculiarity associated with GI 8—and only with this GI—is that the planktonic foraminiferal faunas recorded colder SSTs at the beginning of the GI than at its end and not an immediate warming at the onset of the GI (Figure 1.8B and D; Salgueiro et al., 2010). The

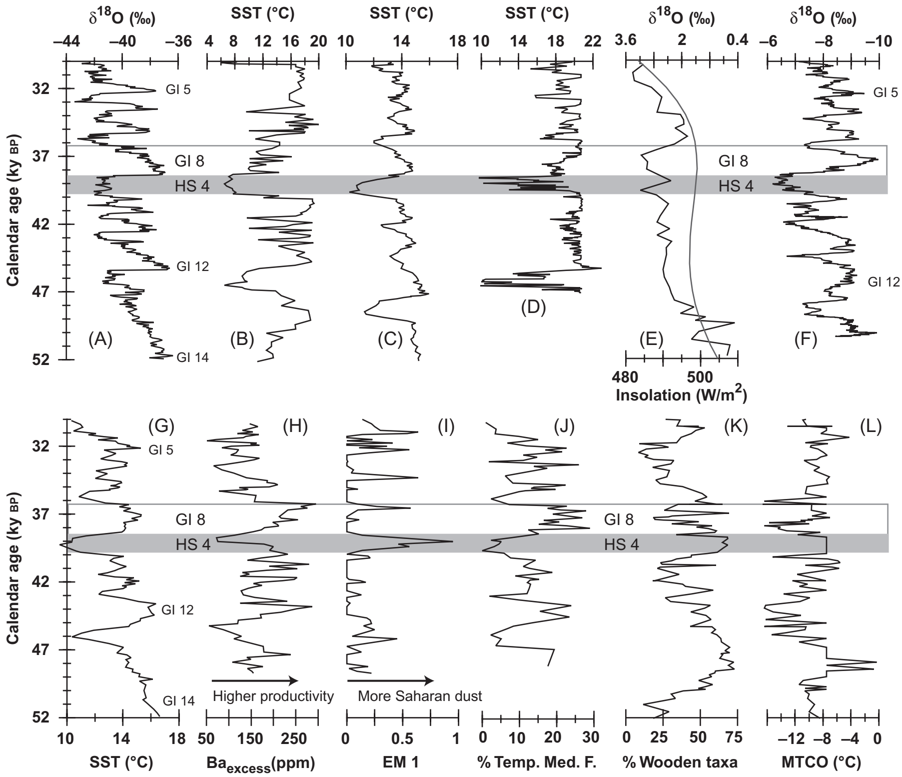

Figure 1.8 Climate records for the interval from 30 to 52 cal ka BP (i.e., most of MIS 3) reveal millennial-scale variability. (A) $\delta^{18}O$ record of the GISP2 ice core (Grootes and Stuiver, 1997) from central Greenland, to whose chronology many of the records presented were linked for their respective age models. (B) Foraminiferal-fauna-based SST record of core MD95-2040 off northern Portugal (Salgueiro et al., 2010). (C) Alkenone-based SST record of core MD01-2444 off southwestern Portugal (Martrat et al., 2007). (D) Foraminiferal-fauna-based SST record of core MD99-2339 in the Gulf of Cadiz (Voelker and de Abreu, 2011). (E) $\delta^{18}O$ record of planktonic foraminifera *G. ruber* (white) from core 9501 south of Cyprus (Almogi-Labin et al., 2009) and June 21st insolation at 65°N (gray curve; Laskar et al., 2004). (F) Speleothem $\delta^{18}O$ record from Sofular Cave in northern Turkey (Fleitmann et al., 2009). Note that the speleothem's U/Th chronology diverges from the GISP2 chronology show in (A) for some of the Greenland interstadials (GIs) and conforms more with the GICC05 chronology of the NGRIP ice core (NGRIP members, 2004). (G–J) Records from core MD95-2043 in the Alboran Sea: (G) Alkenone-based SST (Cacho et al., 1999); (H) Ba_{excess} data indicating biogenic Ba and thus productivity (Moreno et al., 2004); (I) modeled end member (EM) 1 reflects the intensity of Saharan winds (Moreno et al., 2005); (J) Sum of pollen representing the temperate Mediterranean forest (Fletcher et al., 2010a), higher percentages of which indicate warmer and more humid conditions in southern Spain. (K) Percentage of wooden taxa as recorded in Lago Grande di Monticchio in central Italy (Allen et al., 2000). (L) Mean temperature of the coldest month (MTCO) estimated from the pollen data of Lago Grande di Monticchio (Allen et al., 2000). The gray bar marks the interval of HS 4, and the gray rectangle that of GI 8. Additional GIs are listed in (A) and (F).

(A)

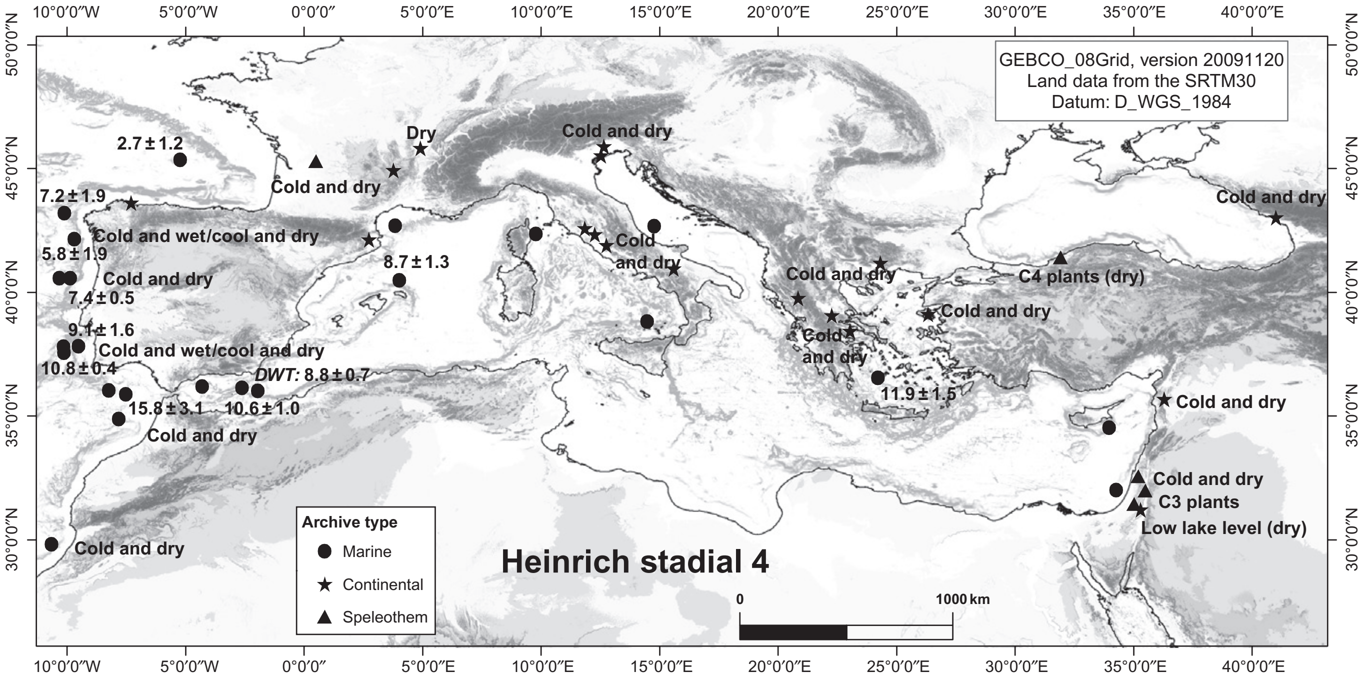

Figure 1.9 Map showing sites covering MIS 3 and mean SST values (Table 1.2sm) for HS 4 (A) and for GI 8 (B).

(B)

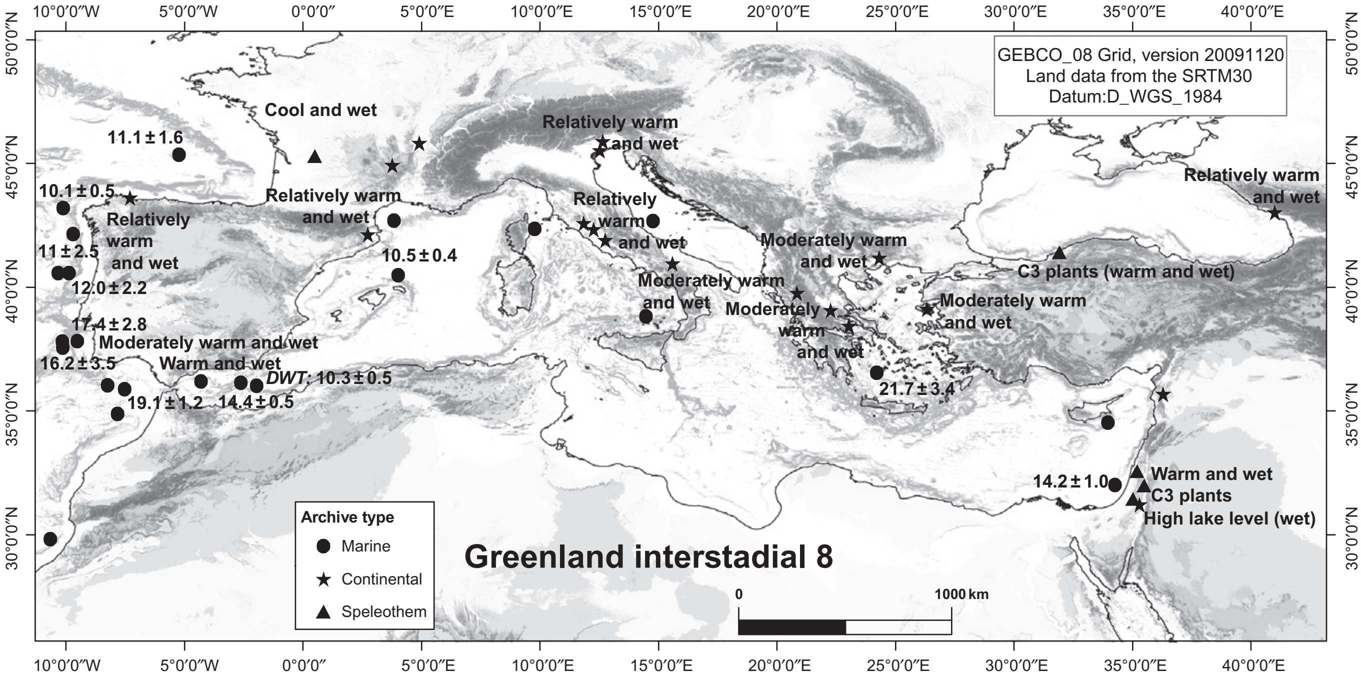
10°0'0"W
5°0'0"W
0°0'0"
5°0'0"E
10°0'0"E
15°0'0"E
20°0'0"E
25°0'0"E
30°0'0"E
35°0'0"E
40°0'0"E
50°0'0"N
45°0'0"N
40°0'0"N
35°0'0"N
30°0'0"N
GEBCO_08 Grid, version 20091120
Land data from the SRTM30
Datum:D_WGS_1984
Cool and wet
11.1 ± 1.6
Relatively warm and wet
10.1 ± 0.5
Relatively warm and wet
Relatively warm and wet
11 ± 2.5
10.5 ± 0.4
12.0 ± 2.2
Relatively warm and wet
Relatively warm and wet
Moderately warm and wet
C3 plants (warm and wet)
Moderately warm and wet
Moderately warm and wet
Moderately warm and wet
17.4 ± 2.8
Moderately warm and wet
16.2 ± 3.5
Warm and wet
DWT: 10.3 ± 0.5
19.1 ± 1.2
14.4 ± 0.5
21.7 ± 3.4
14.2 ± 1.0
Warm and wet
C3 plants
High lake level (wet)
Archive type
Marine
Continental
Speleothem
Greenland interstadial 8
0
1000 km

$U^{K'}_{37}$ SST values for the two Alboran Sea sites (41 and 44) and site 142 (core 9505) off Israel with 14.2–14.4°C are again mean annual SSTs, which might explain why they are so much colder than the SST recorded off the southern Portuguese margin or in the southern Aegean Sea. Also, for this time slice the *G. bulloides* Mg:Ca temperatures for site 41 (core MD95-2043) are significantly warmer, at 18.4 ± 1.0°C (Cacho, unpublished data), and more in the range of those off southern Portugal.

For the Mediterranean Sea itself, little evidence exists for the impact of millennial-scale climate change on ocean productivity. The various paleoproductivity proxy records generated for site 41 (core MD95-2043; Figure 1.8H; Moreno et al., 2004) indicate that in the Alboran Sea productivity was reduced during stadials and high during interstadials. Productivity during HS 4 was comparable to that during other HS or GS and during GI 8 to other GI. However, maxima in interstadial productivity occurred not at the beginning of a GI but later on. The site 84 (ODP Site 963) abundance record of *Florisphaera profunda*, a deep-dwelling coccolithophore, which abundance is anticorrelated with the chlorophyll a concentration, also shows millennial-scale variations that seem to support reduced/increased productivity during stadials/interstadials (Incarbona et al., 2008). Site 114 (core C69) in the southern Aegean Sea recorded a total organic carbon (TOC) peak at the onset of GI 8, indicating the formation of an ORL (Geraga et al., 2005). If hydrographic conditions during the formation of this layer were similar to those during sapropel formation, then the increase in organic matter could result from enhanced productivity.

More evidence for productivity variations is available for the western Iberian margin. A latitudinal transect compiled by Salgueiro et al. (2010) revealed that the same boundary affecting the SST variations also existed with regard to productivity. North of 39°N, the southward migrating subpolar surface waters inhibited upwelling and thus led to reduced productivity during HS and GS. South of this boundary, productivity during HS and GS varied—sometimes it was reduced, sometimes not. During HS 4, export productivity was increased at site MD95-2042—even higher than during GI 8. North of 39°N, productivity increased during the GI to levels similar to those of the interglacial periods (Salgueiro et al., 2010). GI 8 stands out a bit because off of Cape Finisterre (site 7, core SU92-03) productivity—such SSTs—increased only toward the end of the GI. Coccolith evidence from the Gulf of Cadiz supports high phytoplankton productivity during interstadials (Colmenero-Hidalgo et al., 2004), consistent with the total alkenone concentration data from sites 5 and 9 (cores MD95-2042 and MD95-2040) on the western Iberian margin (Pailler and Bard, 2002). Voelker et al. (2009), on the other hand, showed for site 18 (core MD99-2339) in the central Gulf of Cadiz that export productivity—estimated from the planktonic foraminiferal fauna—was high during HS 1, HS 2, and HS 3, potentially linked to frontal upwelling. Export productivity at this site was also high during HS 4 but increased even further and remained high during GI 8 (Voelker, unpublished data).

Ventilation of the Western Mediterranean Deep Water (WMDW) strongly followed the millennial-scale variations (Figure 1.10C and D; sites 41 and 61; Cacho et al., 2000; Sierro et al., 2005), with better ventilation during the GS and most parts of the HS and poor ventilation during the GI. This relationship is opposite to the one observed in the deep North Atlantic ocean, for example, at site 5 (core MD95-2042;

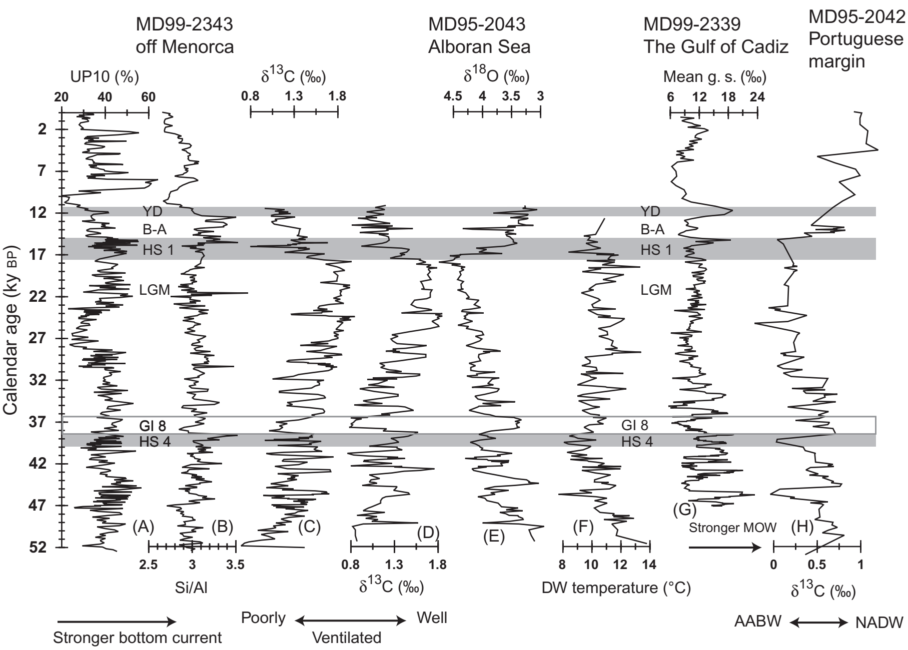

Figure 1.10 Evidence for Mediterranean deepwater variability during the last 52 cal ky BP in comparison to a MOW record and depth changes in the boundary between NADW and AABW on the Portuguese margin. (A–C) Records of core MD99-2343 from a depth of 2391 m with (A) the UP10 grain-size data, (B) Si/Al, both of which reflect bottom-current strength (Frigola et al., 2007, 2008), and (C) the benthic foraminiferal $\delta^{13}C$ record, with higher $\delta^{13}C$ values reflecting a better ventilation and thus formation of WMDW in the Gulf of Lions (Sierro et al., 2005). (D–F) Conditions in the deep Alboran Sea, core MD95-2043 from a depth of 1841 m, with the benthic foraminiferal $\delta^{13}C$ (D) and $\delta^{18}O$ (E) data and DWTs estimated from benthic foraminifera Mg:Ca data in (F) (Cacho et al., 2000, 2006). On the Atlantic side, the mean grain size in the fraction $<63\,\mu m$ measured in core MD99-2339 (G) shows changes in the bottom-current strength, that is, the lower MOW core (Voelker et al., 2006). In the deeper western Iberian margin, the benthic foraminiferal $\delta^{13}C$ record of core MD95-2042 (H) (Shackleton et al., 2000) reflects changes in the strength of the AMOC, with AABW ($\delta^{13}C < 0.5‰$) bathing the site's depth of 3146 m during colder climate intervals when AMOC was reduced, and NADW being present during warmer intervals when AMOC was strong.

Figure 1.10H), where the AMOC proxies indicate a slowdown during GSs and a shutdown during most HSs that led to a shoaling of the interface between NADW and AABW. Consequently, a seesaw pattern existed between the ventilation state of the deep Mediterranean Sea and the Atlantic Ocean (Sierro et al., 2005). The high-resolution record of site 61 (core MD99-2343), however, revealed that deep convection in the Gulf of Lions—driving WMDW ventilation—was interrupted during parts of the HSs, such as HS 4 (Figure 1.10C), because of the capping by less saline surface waters entering through the Strait of Gibraltar (Sierro et al., 2005). In general, the WMDW current off Menorca had a higher flow speed during most of the HSs and all GSs (Figure 1.10A and B; site 61; Frigola et al., 2008), supporting formation of WMDW by deep convection in the Gulf of Lions. Off Corsica, the grain-size record of site 72 (core MD01-2434; Toucanne et al., 2012) from a depth of 800 m also showed an increase in bottom-current strength during all the GSs and HSs, hinting at enhanced production of intermediate-depth water masses, such as LIW, in the eastern Mediterranean. Currently, benthic stable isotope data for MIS 3 exist for only one intermediate-depth core site in the Mediterranean Sea—M69/1-348, recovered in the Alboran Sea from a depth of 802 m and covering the last 34 cal ky BP. The benthic $\delta^{13}C$ record of this core reveals a pattern similar to those of sites 61 and 41 (cores MD99-2343 and MD95-2043) with better ventilation during GSs 5 and 4 (Schönfeld, unpublished data). Thus, it appears that convection, most likely stronger than it is today, took place in both Mediterranean basins during the cold-climate periods of MIS 3. Since surface waters were colder during GSs and HSs than they are today or were during GIs (Figures 1.8 and 1.9), the deeper and intermediate waters of the Mediterranean Sea should also have been colder, and the deepwater temperature (DWT) record of site 41 (core MD95-2043) from the Alboran Sea (Figure 1.10F; Cacho et al., 2006) confirms that they were. However, the DWT and benthic $\delta^{18}O$ records do not mimic each other (Figure 1.10E and F), indicating that the $\delta^{18}O$ signal—a pattern similar to that of core MD95-2043 is also seen in the Sicily Strait at site 84 (ODP Site 963; Incarbona et al., 2008)—is partly driven by salinity changes.

Since production of both intermediate- and deepwater masses took place in the Mediterranean Sea, both of them likely contributed to the MOW in the Gulf of Cadiz. Grain-size records from core sites in the Gulf of Cadiz indicate the formation of contourite layers (grain-size maxima; Figure 1.10G) during GSs and HSs, revealing that bottom-current strength was enhanced not only in the Mediterranean Sea but also in the upper and lower MOW levels (sites 23 and 18; Toucanne et al., 2007; Voelker et al., 2006). Because signal responses in mean grain size and benthic $\delta^{13}C$ at site 18 (core MD99-2339) were similar to those of sites 41 and 61 (cores MD95-2043 and MD99-2343) in the deep western Mediterranean Sea, Voelker et al. (2006) postulated that WMDW contributed more to the deeper MOW during GSs and HSs than it does at present.

The millennial-scale variations also affected the vegetation in the wider Mediterranean region. Several short-term events of forest expansion and reduction have been detected in Europe and in particular in some Mediterranean continental sites (Burjachs and Julià, 1994; Follieri et al., 1998; Magri, 1999) and tentatively correlated with the GS/GI cycles and the North Atlantic Heinrich events (Allen et al., 1999, 2000; Arslanov et al., 2007; Burjachs and Julià, 1994; Guiter et al., 2003; Leroy et al., 1996; Margari et al., 2009). However, this correlation is not direct and based on independent chronologies that preclude the perfect match (Fletcher et al., 2010a). Marine sequences, in turn, usually present continuous, long records and can be used for direct sea–land correlations. In recent years, large efforts have been made to understand the vegetation response to millennial-scale climate changes using sediment cores from the eastern North Atlantic midlatitudes and the Mediterranean Sea (Fletcher et al., 2007, 2010a; Fletcher and Sanchez Goñi, 2008; Margari et al., 2010; Naughton et al., 2007b, 2009; Roucoux et al., 2001, 2005; Sánchez-Goñi et al., 2000, 2002, 2008). Based on these studies, the strong/weak reduction of

Mediterranean forests is likely the result of cold/cool conditions, while the expansion of these floristic associations reflects warm conditions. Also, the growth/decline of semidesert plants might be associated with dry/wet conditions (Figure 1.8J and L).

HS 4 was characterized by cold or extremely cold and dry conditions in the Mediterranean region that not only affected the vegetation—a shift to a steppic flora (Allen et al., 1999; Sánchez-Goñi et al., 2002)—but also lake levels, such as site 149 (Lake Lisan; Bartov et al., 2003; Waldmann et al., 2010) or site 65 (Les Echets; Ampel et al., 2008), and precipitation as reflected in speleothem $\delta^{18}O$ records (Figure 1.8F; Bar-Matthews et al., 1999, 2003; Fleitmann et al., 2009; Genty et al., 2003). The arid conditions were associated with increased intensity of Saharan winds (site 41; Figure 1.8I; Moreno et al., 2002, 2005), and Saharan dust has also been found in Italy (Narcisi, 2001). The shift to a dominance of steppic and thus C4 plants (e.g., grasses, herbs) is also seen in the Sofular speleothem $\delta^{13}C$ data and Fleitmann et al. (2009) showed that an approximate 100-year phase lag existed between the climate change and the ecosystem response. Pollen data from extremely high-resolution Iberian margin records, however, indicate a more complex pattern for HS 4, composed of alternating cold and wet/cool and dry phases (Fletcher and Sanchez Goñi, 2008; Naughton et al., 2009; Sánchez-Goñi et al., 2000, 2002, 2008).

GI 8, on the other hand, was associated with wetter conditions (Figure 1.9, bottom), resulting in higher lake levels and increased precipitation (Figure 1.8F). A gradual temperature increase from 47 to 35°N is depicted from pollen records. North of 45°N, GI 8 was detected in only a few sequences, such as site 30 in the Bay of Biscay (core MD04-2845; Sánchez-Goñi et al., 2008) and at site 79 in northern Italy (Azzano Decimo; Pini et al., 2009). Both records are marked by the slight expansion of temperate and Mediterranean forests (Figure 1.8J and K), reflecting cool/relatively warm and wet conditions. A review of European vegetation records revealed that during the last glacial period, the temperate forest's northern limit was displaced further south, to latitudes around 45°N in comparison with the 60°N today (Fletcher et al., 2010a). South of 45°N, GI 8 is more evident in high-resolution marine and terrestrial pollen records (Figure 1.8J and K). Relatively warm and wet conditions were detected between 44°N and 40°N, moderately warm and wet conditions between 40°N and 37°N, and warm and wet conditions above 37°N (Figure 1.9, bottom; Table 1.2sm).

1.3.3 Deglaciation(s): The Case of the Last Glacial–Interglacial Transition (LGIT)

The deglaciation is the transition period between the end of a glacial period and the beginning of the subsequent interglacial period. Here we will concentrate on the last deglacial period, the transition from the Last Glacial Maximum (LGM) at 21 cal ka BP to the Holocene. The increase in high-latitude summer insolation that followed the LGM, favored the retreat of the Northern Hemisphere ice sheets and triggered a 120–130 m increase in global sea level (starting around 19 cal ka BP; Fairbanks, 1990; Fairbanks et al., 2005; Peltier and Fairbanks, 2006; Stanford et al., 2006), which led to a gradual deepening of the (shallower) straits and to flooding of the northern Adriatic Sea (Asioli et al., 2001). The last deglaciation is marked by a succession of accelerated melting events superimposed on a smooth continuous sea-level rise, the so-called meltwater peak (mwp) 1A occurring at around 14 cal ka BP and mwp 1B at around 11.3 cal ka BP (Bard et al., 1996, 2010). Millennial-scale climate variability, which includes two extreme cold episodes: (HS 1; Figure 1.10) and the Younger Dryas (YD; Figure 1.11) further interrupted the deglacial-warming trend. HS 1 is the result of abrupt and massive iceberg discharges into the North Atlantic region (Bond et al., 1993), while the YD is related to catastrophic drainage episodes of the proglacial Lake Agassiz (Teller et al., 2002). Between HS 1 and the YD, a short warm phase occurred, the Bølling–Allerød episode (B–A; Bond et al., 1993; Dansgaard et al., 1993; Hughen et al., 1996; Iversen, 1954; Johnsen et al., 2001; Keigwin and Lehman, 1994; Mangerud et al., 1974; McManus et al., 2004; Naughton et al., 2007b; Teller et al., 2002).

Figure 1.11 shows a west-to-east transect of $U^{K'}{}_{37}$ SST records from the Iberian margin to the eastern Mediterranean basins for the above-described period (21–9 cal ka BP). An SST increase from the LGM to the Holocene emerges as the general deglaciation pattern, with a more evident SST rise between the end of the YD and the beginning of the Holocene. The Holocene temperatures are close to 20°C almost all along the transect, but warmer values are observed in the Gulf of Cadiz (around 22°C) at sites 41 and 44 (Table 1.1) and in the easternmost Levantine basin, with values around 24°C (site 145; Table 1.1).

The LGM was associated with generally cool sea-surface conditions, with SSTs close to 12°C in the Alboran Sea and central basin, 14°C in the southwestern Iberian margin, and around 16°C in the Levantine basin (Figure 1.11). These data show a southwestern Iberian margin and Alboran Sea 4–6°C colder in the LGM than today, while the central and Levantine basin SSTs were around 8°C colder. The $U^{K'}{}_{37}$ SST estimates for the LGM indicate lower values (by 1–2°C) than those determined by Hayes et al. (2005) based on planktonic foraminiferal faunas, especially in the eastern Mediterranean Sea, where new data (site 144) point to a 6°C cooling (Essallami et al., 2007), confirming the alkenone values from nearby site 136 (Table 1.1; Emeis et al., 2000, 2003).

The HS 1 and YD events were well imprinted on the Iberian margin and Alboran Sea records. However, the cold HS 1 signal is less evident in the central and Levantine basin as compared with the other sites (Figure 1.11). The YD cold event was well recorded in the Tagus mud patch (site 14; Figure 1.11; Table 1.1), with cold temperatures close to 8°C but less severe (~12°C), although well recorded, in other Iberian margin sites and in the western and central Mediterranean basins. In the Levantine basin (sites 140 and 144) and northern Red Sea (site 145; Figures 1.4 and 1.11), a cooling episode also interrupted the LGIT but occurred about 2 ky earlier than the YD; as a consequence the rapid SST rise preceded the one at the other sites.

The B–A interstadial interval was recorded at most sites with SSTs around 2–4°C colder than during the Holocene.

Two areas stand out in the compilation—the Adriatic Sea (site 90; Piva et al., 2008) and the Red Sea (site 145; Arz et al., 2003). The Adriatic Sea (despite the low resolution) recorded extremely cold conditions during HS 1, with SSTs close

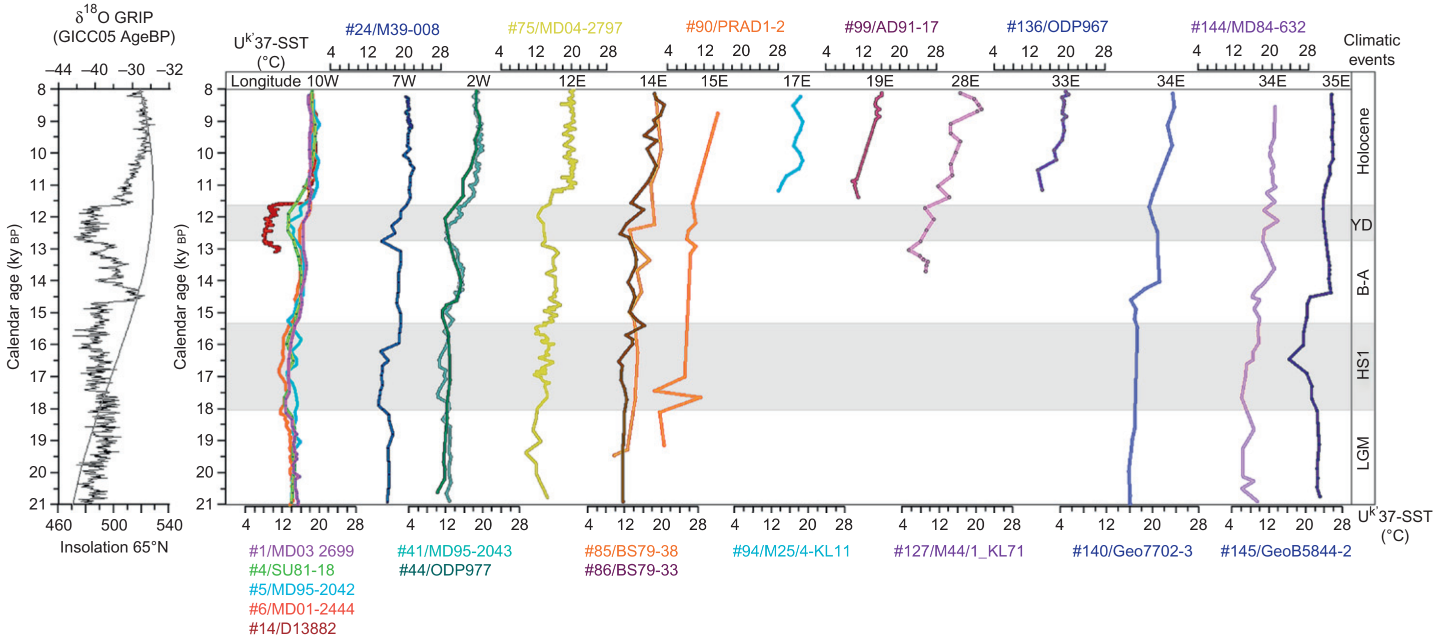

Figure 1.11 West-to-east transect of $U^{K'}_{37}$ SST records from the Iberian margin to the eastern Mediterranean basins for the LGIT period (21–8 cal ka BP). On the left, in gray are plotted the $\delta^{18}O$ record of the Greenland ice-core GRIP (Johnsen et al., 1992, 2001; on GICC05 age scale) and the insolation curve at 65°N (Berger, 1978). The SST records are organized from left (west) to right (east) and are numbered according to the site numbers in Table 1.1 and Figure 1.4; original work is referenced in Table 1.1.

to 3°C. Afterward the SSTs rose to around 10°C during the B–A and decreased to 8°C during the YD. The transition to the interglacial period is recorded as a gradual SST increase until the early Holocene. A similar pattern occurred in the Marmara Sea (site 127; Sperling et al., 2003), with SSTs increasing from 6°C during the YD to 20°C at 9 cal ka BP. In contrast to these cold conditions, the site located in the Red Sea experienced warmer SSTs during the whole period with the warmest values during the Holocene (26°C) and only 2°C lower SSTs during the LGM. The interval between 18 BP and 14.5 cal ka BP shows the lowest values, around 20°C, and the rapid increase to interglacial conditions occurred at the end of this interval (site 145 in Figures 1.4 and 1.11).

In summary, the "Mediterranean" $U^{K'}_{37}$ SST record for the last deglaciation shows lower values in the Adriatic Sea during HS 1 and in the Tagus mud patch area off Lisbon during the YD. Warmer conditions were recorded during the present interglacial period with values close to 20°C and with around 4–6°C lower values during the B–A interstadials. The LGIT is marked by a rapid SST increase, in its last warming phase, in the southwestern Iberian Margin, the Alboran Sea, and the central Mediterranean basin.

Reconstruction of a δw west-to-east transect, combining $\delta^{18}O$ of planktonic foraminifera (*Globigerina bulloides* and *Globigerinoides ruber*) and $U^{K'}_{37}$ SSTs, reveals a progressive isotopic enrichment of the surface water from the North Atlantic to the Levantine basin, except for a slight depletion in the central Mediterranean Sea (Essallami et al., 2007). This result indicates that the salinity gradient was steeper during the LGM than it is today. Although δw values in the central Mediterranean basin are slightly lower than today, δw increased sharply from the Sicily Strait to the East, suggesting a higher salinity gradient in the eastern basin. Therefore, even though colder temperatures may account for less evaporation at the LGM, the eastern Mediterranean Sea underwent higher excess evaporation over precipitation than today. Lake-level curves support this with a lowering in the Lake Lisan/Dead Sea system (site 149; Bartov et al., 2003; Stein et al., 2010) and in Lake Tiberias (Jordan Valley; Hazan et al., 2004; Robinson et al., 2006) during HS 1 and HS 2. Halite deposition in the paleo-Dead Sea during the YD has been interpreted as reflecting extremely arid conditions (Stein et al., 2010), although according to the Levantine basin δw curve, HS 1 was more arid than the YD. Speleothem $\delta^{18}O$ records from Israel (Bar-Matthews et al., 2003) agree with the lake-level fluctuations, with the most positive values (i.e., lowest rainfall) during the YD.

LGIT-related variations in productivity for the area have been investigated by many authors (Abrantes, 1988, 1990; Bárcena et al., 2001; Caralp, 1988; Targarona, 1997; Vergnaud-Grazzini and Pierre, 1991; Weaver and Pujol, 1988). Although controversial results arise when different proxies are compared, strong changes in primary productivity and an ORL have been described from the Alboran deglaciation sediments, at a time of no sapropel deposition in the eastern Mediterranean (Jimenez-Espejo et al., 2007; Sierro et al., 1999). In the central Mediterranean Sea, surface-water productivity increased during the colder climate phases of the LGIT—the LGM, the YD, and the century-scale cold oscillations within the B–A interstadial complex (Asioli et al., 2001; Sangiorgi et al., 2002; Sprovieri et al., 2003)—with the colder conditions often aiding deep winter mixing and thus nutrient replenishment.

Increased productivity in the Adriatic Sea during the B–A cold oscillations might, on the other hand, be linked to nutrients supplied by the Po River (Asioli et al., 2001; Sangiorgi et al., 2002). In the upwelling centers along the western Iberian margin, summer export productivity was high during the LGM, crashed during HS 1, especially in the northern region, and then increased again during the YD (Salgueiro et al., 2010). YD levels were, however, lower than during the LGM and more comparable to the early Holocene.

Conditions in the deeper water masses were also affected by the deglacial climate oscillations. During the LGM, the WMDW was well ventilated (Figure 1.10D and E; sites 41 and 61; Cacho et al., 2000; Sierro et al., 2005), indicating that deepwater convection took place in the Gulf of Lions. The glacial WMDW was also relatively cold (Figure 1.10F; Cacho et al., 2006). Furthermore, the UP10 record of site 61 (core MD99-2343; Figures 1.4 and 1.9A; Frigola et al., 2008) reveals that the current strength of the WMDW branch near Menorca was highly variable. Benthic isotope records from intermediate-depth core sites in the Aegean and Levantine Seas reveal that the LIW was well ventilated from the LGM to the YD (Schmiedl et al., 2010) and indicate continuous LIW formation in those regions. Records from the Adriatic Sea, on the other hand, indicate that deep convection was interrupted in the Adriatic Sea, especially during the YD (Asioli et al., 2001). Studies in the Gulf of Cadiz and along the southern Portuguese margin showed that the lower MOW settled deeper in the water column (lower boundary near 2000 m) during the LGM (Rogerson et al., 2005; Schönfeld and Zahn, 2000), but current strength was also partly enhanced in the upper MOW core (site 23; core MD99-2341; Toucanne et al., 2007).

During HS 1 and the YD, the WMDW was less well ventilated (in contrast to the LIW), but relatively cold. The WMDW's current strength off Menorca declined from the LGM until the transition from the YD to the Holocene. Nevertheless, the records of site 61 related to current strength (Figure 1.10A and B; Frigola et al., 2008) indicate that periods with a stronger current existed during parts of HS 1 and the YD. Similar to the MIS 3 GS and HS, the enhanced WMDW flow during the later phase of HS 1 might have contributed to the increased current strength of the lower MOW core in the Gulf of Cadiz (Figure 1.10G; Voelker et al., 2006). However, the grain-size record at site 72 (core MD01-2434), collected from a depth of 800 m east of Corsica, also reveals maxima during HS 1 and the YD (Toucanne et al., 2012) indicating that current strength was also enhanced close to the LIW level—concordant with the evidence of LIW formation in the eastern basins (Schmiedl et al., 2010)—so that strengthening of the MOW might more be related to the LIW, which contributes much more to the export through the Strait of Gibraltar. The YD contourite layer formed in the Gulf of Cadiz is well known and recorded in water depths bathed by the lower as well as the upper MOW core (Toucanne et al., 2007; Vergnaud-Grazzini et al., 1989; Voelker et al., 2006). Because epibenthic foraminiferal species become sparse to absent in the Holocene, no stable isotope data exist for the deeper Mediterranean Sea (WMDW level) younger than 11.2 cal ka BP (Figure 1.10). Thus, WMDW conditions at the beginning of the Holocene can only be deducted from site 61 (core MD99-2343) through grain size and Si/Al records, both of which show an extended minimum at the transition into the Holocene, indicating a sluggish WMDW current. LIW production in the eastern basin remained relatively strong until about 11 cal ka BP and then declined toward the period of sapropel S 1 formation (Kuhnt et al., 2008; Schmiedl et al., 2010).

On land, and in particular in the western Iberian Peninsula and western Mediterranean region, the climate was cool and relatively wet (Boessenkool et al., 2001; Combourieu-Nebout et al., 2002; Fletcher and Sanchez Goñi, 2008; Naughton et al., 2007b; Roucoux et al., 2001, 2005; Turon et al., 2003). These cool and wet conditions were probably the response to a more vigorous AMOC than during the previous HS 2, as proved by $^{231}Pa/^{230}Th$ measurements that estimate an AMOC slowdown of 30–40% or less during this period (Gherardi et al., 2005; McManus et al., 2004), as also predicted by numerical climate models (Ganopolski and Rahmstorf, 2001). In contrast, further east the climate seems to have been relatively drier during the LGM, as shown by pollen sequences from Italy (Allen et al., 1999, 2000; Magri and Sadori, 1999), Greece (Lawson et al., 2004), and the Black (Arslanov et al., 2007), Tyrrhenian (Rossignol-Strick, 1996), and southern Aegean Seas (Geraga et al., 2005).

As during HS 4, the continental climate became extremely cold and dry during the HS 1 episode, as revealed by several pollen sequences (Allen et al., 1999; Arslanov et al., 2007; Boessenkool et al., 2001; Combourieu Nebout et al., 1999, 2002, 2009; de Beaulieu and Reille, 1984; Geraga et al., 2005; Lawson et al., 2004; Magri and Sadori, 1999; Rossignol-Strick, 1996; Roucoux et al., 2001, 2005; Turon et al., 2003; Tzedakis et al., 1997, 2003b). However, a complex pattern composed of two or even three phases (cold/wet and cool/dry; cold/wet, cool/dry, and cold/wet) is detected in a few high-resolution pollen records from the western Iberian margin and the Alboran Sea (Fletcher and Sanchez Goñi, 2008; Naughton et al., 2007b, 2009). A similar complex pattern has also been observed in a high-resolution lacustrine record in central Italy (Lake Albano; Chondrogianni et al., 2004; Reille and Beaulieu, 1989).

During the B–A warm period, numerous marine and terrestrial pollen sequences (Allen et al., 1996; Arslanov et al., 2007; Atanassova and Stefanova, 2003; Boessenkool et al., 2001; Bordon et al., 2009; Cheddadi et al., 1991; Combourieu Nebout et al., 2009; Fletcher et al., 2007; Fletcher and Sanchez Goñi, 2008; Follieri et al., 1989; Lamb et al., 1989; Lawson et al., 2004; Magri and Sadori, 1999; Muñoz-Sobrino et al., 2004; Naughton et al., 2007b; Peñalba et al., 1997; Reille and Beaulieu, 1989; Reille and Lowe, 1993; Rossignol-Strick and Planchais, 1989; Turon et al., 2003) reveal warm and wet conditions along the entire Mediterranean region, supported by lake-level increases such as in Lake Albano (Chondrogianni et al., 2004). Furthermore, high-resolution pollen sequences show that this period was punctuated by centennial-scale climatic variations such as the Older Dryas and the intra-Allerød events (Combourieu-Nebout et al., 2002; de Beaulieu and Reille, 1984; González-Sampériz et al., 2005; Magny et al., 2006). This complexity of vegetation changes during the B–A event parallels the rapid episodes detected in the Greenland ice cores during the GI 1 known as GI-1e, d, c, b, and following the INTIMATE (INTegrating Ice core, MArine, and TErrestrial records) event stratigraphy (Lowe et al., 2008).

The YD is marked by a strong to moderate reduction of the temperate Mediterranean forests and the high to moderate expansion of semidesert plants in the Mediterranean region that indicate cold/cool and dry/relatively dry conditions, respectively (see B–A references above). The vegetation changes linked to this short event appear to be more drastic at latitudes above 42°N and in high-altitude sites rather than in lower-latitude records (Naughton et al., 2007a). Also, the conditions became less cold and dry further east (Bottema, 1995).

1.3.4 Holocene Climate

General North Hemispheric Climate

The last period discussed in this Mediterranean compilation corresponds to the interglacial period in which we presently live, the Holocene. This relatively warm period started at about 11.7 cal ka BP (Walker et al., 2009) and has generally been considered to be an epoch of climate stability, as compared with the rapid and intense variability that characterized the last glacial period (Dansgaard et al., 1993; see Section 1.3.2). However, more high-resolution studies, completed within the last decade, have revealed the existence of significant short-term decadal to centennial climate variability (Mayewski et al., 2004).

In general terms, most of the extratropical Holocene records suggest maximum temperatures right at the beginning of the Holocene, during the so-called Holocene Climatic Optimum (HO; centered at 9 cal ka BP), followed by a continuous and pronounced trend toward cooler conditions (DeMenocal et al., 2000a,b; Kim et al., 2004; Marchal et al., 2002). In the tropics, the same period shows roughly the reverse trend (Jansen et al., 2007). These changes are associated with changes in the terrestrial orbit (Berger, 1978), which led to markedly stronger seasonality in the Northern Hemisphere during the HO, with annual mean insolation increased at high latitudes and reduced at low latitudes. Nevertheless, an increasing number of high-resolution regional studies reveal the existence of differences in magnitude and intensity of this trend, which is also indicative of the parallel action of regional processes of different intensity (Renssen et al., 2009).

Climatic oscillations of short duration are, to some extent, superimposed on this general Holocene evolution, and, in the literature, these have been associated with a combination of internal climate system variability and external forcings (Debret et al., 2009). Variability at this timescale was first identified in the North Atlantic and linked to an external forcing in the form of changes in the intensity of the solar activity (Bond et al., 2001), although the physical mechanisms to establish the link within the climate system remain somewhat unclear. These authors found that periods of less intense solar activity were associated with relatively cold conditions and larger numbers of icebergs, the last of which is believed to have been the Little Ice Age (LIA) that followed a time of warmer climatic conditions known as the Medieval Warm Period (MWP). These two periods are well differentiated in the Northern Hemisphere, and a wide range of historical documentation is available; they are therefore discussed separately and in detail in Chapter 2.

Within the Holocene centennial oscillations identified in the North Atlantic (Bond et al., 2001), the one that left the strongest imprint was the so-called 8.2 event, a cold period whose occurrence was centered at 8.2 cal ka BP (Alley and Agustsdottir, 2005; Alley et al., 1997). It is well marked in the Greenland ice cores and with a climatic expression in most of the Northern Hemisphere records. The 8.2 event shows many of the typical characteristics as the most prominent glacial cold events (i.e., Heinrich events). This event is believed to have been forced by the rapid discharge of freshwater from proglacial Lakes Agassiz and Ojibway through Hudson Bay and the Hudson Strait into the Labrador Sea (Barber et al., 1999) or into the Arctic Ocean (Born and Levermann, 2010) marking the final demise of the Laurentide ice sheet.

The Holocene in the Mediterranean Region

In the Mediterranean region, the most abundant Holocene temperature data are $U^{K'}_{37}$ SST records; their evaluation reveals an HO development following the previously described Northern Hemisphere extratropical cooling trend (Kim et al., 2004; Marchal et al., 2002), best marked off of western Iberia and in the western Mediterranean (Cacho et al., 2001). After maximum SST values, a 1°C cooling trend toward present day is observed in the western Iberian margin and the Alboran Sea (Cacho et al., 2001; Martrat et al., 2004); a pattern also visible in other more central regions of the Mediterranean, although more intense at the Tyrrhenian Sea, north of Sicily, with a 1.5°C cooling (Cacho et al., 2001). Another SST record north of Menorca confirms the maximum at the beginning of the Holocene and a cooling trend of 1°C during the Holocene (Herrera and Cacho, unpublished data), but SST records from the south of Sicily and the eastern Levantine basin do not show a clear cooling pattern and support comparable temperatures during the early and late Holocene (Castañeda et al., 2010; Essallami et al., 2007).

This Holocene SST evolution seems to be better established in the marine records than in the terrestrial ones, given the complexity of separating the thermal from the hydrologic imprint on land. One of the few continuous atmospheric records is from Lake Redó in the central Pyrenees (Pla and Catalan, 2005). This record shows marked millennial-scale oscillations, but the warmer temperatures are still observed at the beginning of the Holocene (Pla and Catalan, 2005).

Pollen records are direct indicators of the vegetation type and state, and as such, they correspond to an integral of the atmospheric temperature and humidity conditions. Several efforts have been made to reconstruct the atmospheric temperature from pollen sequences both from northern and southern Europe, and the results found in southern France and the northern Iberian Peninsula point to minimum temperatures at the beginning of the Holocene followed by a continuous warming trend of 2°C toward the present (Davis et al., 2003). However, these reconstructions do not agree with other reconstructions (also pollen-based) that also show 1–2°C higher temperatures at the beginning of the Holocene relative to present-day values (Huntley and Prentice, 1988). Although this might still be a problem connected to the small number of records available, it also reveals the difficulty of reconstructing atmospheric temperatures from pollen. Indeed, important variations in the hydrological conditions are clearly detected for the Mediterranean from pollen information, suggesting that precipitation might be more important than temperature in defining the terrestrial vegetation. Such variations have allowed the separation of three intervals in the Holocene for the circum-Mediterranean region: (1) a primarily humid period (11.5–7 cal ka BP),

(2) a transition phase (7–5.5 cal ka BP), and (3) a more recent arid period (5.5–0 cal ka BP; Jalut et al., 2000). Southern European lake levels also indicate a primarily humid beginning for the Holocene and drier conditions after 5 cal ka BP (Harrison and Digerfeldt, 1993). This evolution is quite well recorded in the Iberian Peninsula, but the variations do not appear to be synchronous (Carrión et al., 2007). In the Pyrenees, the period of maximum humidity is concentrated at 9–8 cal ka BP, where the arid phase starts around 8–7.5 cal ka BP (Gonzalez-Samperiz et al., 2006; Morellón et al., 2008). The Lake Banyoles pollen record confirms an initial humid phase in Catalonia for the Holocene (Perez-Obiol and Julia, 1994), while the saline levels in the Ebro valley point to more arid conditions after 5 ka BP (González-Sampériz et al., 2008).

In terms of oceanic primary productivity, diatom data for both western Iberia and the Alboran basin point to the early- to mid-Holocene as the time of the lowest productivity level of the last 23 cal ky BP (Abrantes, 1988, 1990; Bárcena et al., 2001) and indicate a reestablishment of more productive conditions toward the Recent (ca. last 3 cal ka BP). Very low productivity conditions are also indicated for the Algero–Balearic basin by Ba_{excess} data (Jimenez-Espejo et al., 2007), the Gulf of Lions by benthic foraminiferal data (Melki et al., 2009), and the Tyrrhenian Sea by planktonic foraminiferal assemblages (Ciampo, 2004). In contrast, in the eastern Mediterranean, higher abundances of crenarchaeol and alkenones support increased productivity in a high-nutrient stratified environment (Castañeda et al., 2010), as also shown by major and minor trace-element distributions and solid-phase phosphorus contents in a core from the Cretan Ridge (Gennari et al., 2009). However, the early Holocene sediments of the Alboran Sea show the formation of an ORL (Cacho et al., 2002; Comas et al., 1996; Emeis et al., 1996). A layer that, although not found in other parts of the western Mediterranean, corresponds in time to manganese-rich layers in the Balearic basin (Canals-Artiguas, 1980) and layers containing organic traces in the Tyrrhenian Sea (Kallel et al., 1997b).

ORL/sapropel formation is associated with either a high flux of organic matter to the seafloor from high-productivity conditions at the surface or increased preservation of organic matter in the ocean bottom due to deep waters devoid of oxygen. Given the indication of low primary production shown by the traditional productivity proxies, such as diatoms, for the Alboran Sea, this ORL was associated with a deep oxygen-depleted environment (Cacho et al., 2002). Besides, this layer is coeval with the deposition of the well-known sapropel S1 in the eastern Mediterranean, which occurred during the early Holocene in two phases S1a (10.8–8.8 cal ka BP) and S1b (7.8–6.1 cal ka BP) interrupted at about 8.2 ka BP (Ariztegui et al., 2000; de Lange et al., 2008; Mercone et al., 2001; Rohling et al., 1997).

S1 is just the last of a large number of sapropel layers, occurring over a long interval, in the eastern Mediterranean. Its formation is related to global changes in climate and circulation that derived from strong freshwater runoff of nutrients and resulted in enhanced stratification of the water column, increased productivity, and reduction of dense water formation (see Section 1.2.1). In the western Mediterranean, one needs to also consider the Mediterranean in its relation to the Atlantic Ocean. As discussed in the Introduction and Chapter 3, the fact that the Gibraltar Strait is the Mediterranean Sea's sole connection to the Atlantic Ocean results in a west-to-east sea-surface salinity and SST increase and a corresponding productivity decrease (Antoine et al., 1995; Malanotte-Rizzoli et al., 1999; Pinardi and Masetti, 2000). The inflowing Atlantic surface waters have their main influence in the western basin, while the strong evaporation toward the central and eastern basins leads to a 1.7-psu increase in salinity. The resulting rise in water density, associated with the cold dry Arctic air that penetrates into the eastern Mediterranean region during the winter, leads to the formation of deep waters in the Levantine (LIW) and Ionian basins (see the Introduction and Chapter 3). This dense Mediterranean water is pumped over the sill of Gibraltar, and exported as MOW into the Atlantic, where its presence is easily depicted by both higher temperature and salinity at depths between 600 and 1200 m. The salinity of the Atlantic Ocean surface waters depend on the freshwater budget, but the salinity of the intermediate layer depends on processes occurring in the North Atlantic (Labrador and Norwegian Seas), where those waters are formed.

The primary sources of precipitation in the Mediterranean region over the Holocene period have typically been associated with two main processes: (1) fronts that originate in the northeast Atlantic Ocean, passing over Europe and the Mediterranean Sea, generally associated with cyclonic "storm" systems (Rindsberger et al., 1983), and (2) the monsoonal system that originates in the tropical Atlantic or the southern Indian Ocean and passes over northeast Africa and is associated with the low-latitude rainfall system (Rossignol-Strick, 1985).

The monsoonal system fluctuates, in time reaching maximum strength during periods of maximum insolation in the Northern Hemisphere summer (Rossignol-Strick, 1985; Rossignol-Strick et al., 1982). As mentioned above, the major forcing for the HO was the strong Northern Hemisphere extratropical insolation along with a marked increase in seasonality (Berger, 1978), which is known also to have had a strong impact in the tropical, subtropical, and Mediterranean precipitation regime at the beginning of the Holocene (Braconnot et al., 2007a,b; Marchal et al., 2002), such that currently deserted regions in the African continent were then marked by humid conditions determined by a strong African monsoon (Calvert et al., 1992; Rossignol-Strick et al., 1982). The northward extension of the summer African monsoon is widely simulated by climate modeling experiments using General Circulation Models (GCMs) and is enhanced by both vegetative feedbacks over North Africa (Claussen et al., 2006) and oceanic processes (Zhao et al., 2005). Despite this, most GCMs appear to underestimate the extent of the northward shift in precipitation relative to paleo-observations under mid-Holocene-like conditions (Braconnot et al., 2007a,b).

These changes mean that sapropel S1 was deposited simultaneously in the western and eastern Mediterranean basins, under warmer and wetter climatic conditions, which are likely to have reduced or even nullified the present-day Atlantic–Mediterranean salinity gradient, and consequently reduced deep water formation and bottom ventilation (Schmiedl et al., 2010). The reconstructed surface-salinity record for the Gulf of Lions shows strong negative excursions, confirming the low salinity of the Atlantic surface water entering the Mediterranean at the time (Melki et al., 2009), coinciding with elevated discharge of the Nile River (Calvert et al., 1992; Fontugne et al., 1994; Rossignol-Strick et al., 1982; Scrivner et al., 2004). Furthermore, although it is perhaps unlikely that direct monsoonal precipitation (of tropical origin) reached the southern coastline of the eastern Mediterranean—consistent with the so-called monsoon-desert proposed by Rodwell and Hoskins (1996), discussed in the Holocene context by Brayshaw et al. (2011) and in agreement with paleodata from the Red Sea (Arz et al., 2003)—rivers from the Tibesti Mountains, formed as a result of a northward shift of the monsoonal belt over Africa, are additional sources of freshwater into the eastern Mediterranean during this period (Almogi-Labin et al., 2009; Osborne et al., 2008; Rohling et al., 2002a,b). In addition to the monsoonal precipitation, there is evidence for stronger rainfall on the entire Mediterranean Sea from Atlantic sources (Bar-Matthews et al., 2000; Kallel et al., 1997a; Roberts et al., 2008), perhaps consistent with enhanced winter storm activity in the Mediterranean during the earlier part of the Holocene (Brayshaw et al., 2010) and stronger westerly mean flow over southern Europe and the Mediterranean—consistent with the pollen-based study of Bonfils et al. (2004), although it should be noted that GCM simulations of the associated atmospheric circulation anomalies over the Atlantic and Europe remain highly uncertain (Gladstone et al., 2005). At around the same period, the influx of fresher Black Sea water (Aksu et al., 1995; Bahra et al., 2005) was also contributing to a fresher Mediterranean Sea.

HO in the Mediterranean Region

The hydrological information gathered from pollen data as well as oxygen isotopic composition measured in lakes and speleothems for HO, a period contained in the first phase of the S1 deposition time (Figure 1.12), is consistent with widespread wet and warm conditions in the landmass surrounding the Mediterranean as a whole. As for the SST, the $U^{K'}{}_{37}$ data contained in Figure 1.12, with the exception of the 25°C found at site 145 in the Red Sea, and considering the standard deviation (Table 1.3sm available at http://www.elsevierdirect.com/companion.jsp?ISBN=9780124160422), reveals values that are very similar across the entire basin, with a mean Mediterranean SST of 18.8 ± 1.8°C and 18.6 ± 2.05°C in the western basin, 18.3 ± 1.93°C in the central basin, and 19.8 ± 1.21°C in the eastern basin. Planktonic foraminiferal assemblages dominated by the species *Globigerinoides ruber* together with other warm-water species confirm the presence of warm surface waters in most of the basin (Asioli et al., 2001; Jorissen et al., 1993; Rohling et al., 2002b; Sbaffi et al., 2004; Siani et al., 2010; Sprovieri et al., 2003). Foraminiferal estimated SSTs (Table 1.3sm) as well as TEX_{86}-based SST, although showing higher values relative to the $U^{K'}{}_{37}$ SST, which probably indicates increased seasonality in the early Holocene (Castañeda et al., 2010), confirm widespread warm conditions throughout the Mediterranean. This observation supports a major reduction of the modern thermal gradient, as suggested by Rohling and de Rijk (1999). Furthermore, the presence of infaunal and low-oxygen-tolerant benthic foraminiferal species throughout the central and eastern basins, points to a decrease of the oxygen content into the sediment levels (Asioli, 1996; Jorissen, 1999; Melki et al., 2009). Anoxic conditions confirmed by de Lange et al. (2008) for the whole eastern Mediterranean basin below 1.8 km during the entire period of sapropel S1 formation

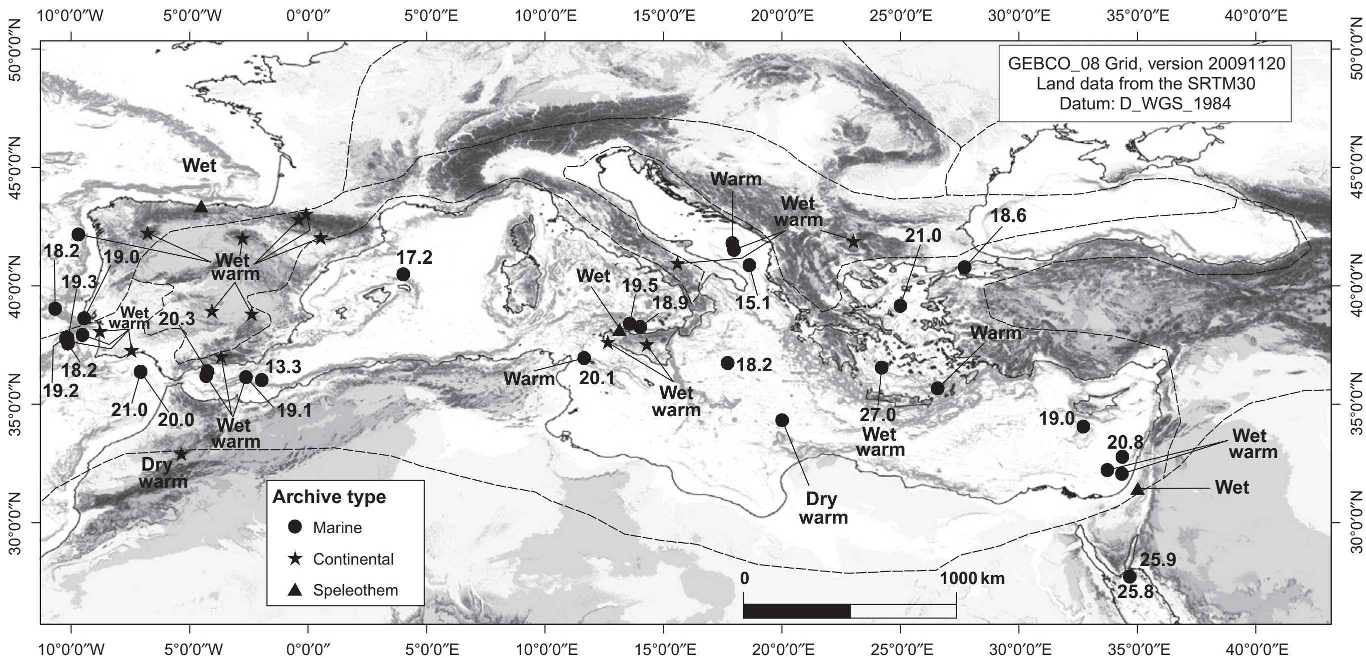

Figure 1.12 Climate conditions in the HO period (9 ± 0.250 cal ka BP; Table 3sm) for the Mediterranean region. SST estimated through $U^{K'}_{37}$ in marine cores. Qualitative information is derived from pollen data in marine cores as well as other proxies from lakes, peat bogs, lagoons, and speleothem records. Map legend is as in Figure 1.4. Original work referenced in Table 1.1.

Table 1.2 Means (±SD) of the Existing $U^{K'}_{37}$ SST Values for the Mediterranean Sea as a Whole and its Three Main Basins (Western, Central, and Eastern), at the Time of the HO and the 8.2 Event, as Reported in Figures 1.11 and 1.12.*

	SST HO	SST 8.2	ΔSST (HO—8.2)
Western (9 sites W)	19.2 ± 1.1	18.8 ± 0.8	0.4
Central (7 sites C)	18.3 ± 1.9	17.8 ± 1.5	0.6
East (5 sites E)	19.8 ± 1.2	18.6 ± 1.4	1.3
Total (21 sites W–E)	19.1 ± 1.4	18.4 ± 1.2	0.7

*For original data, see references in Table 1.1.

(10.8–6.1 ka cal BP) sustain the hypothesis that during the first phase of S1 deposition (S1a), the entire Mediterranean Sea suffered a major change in circulation toward poor ventilation conditions (de Rijk et al., 1999; Myers and Rohling, 2000; Table 1.2).

Climate simulations of the HO with sufficient resolution to discern the detailed topography of the Mediterranean are scarce. However, Brayshaw et al. (2010, 2011), using a nested regional climate model within a global GCM, provide a picture that broadly concurs with the description above in that the Mediterranean was generally wetter during the HO (particularly in the north and east), with a considerably stronger seasonal cycle of surface temperatures (summer temperatures are much warmer, particularly over land in the south and east of the basin, consistent with the large-scale response of most climate models; Braconnot et al., 2007a). However, somewhat in contrast to the surface temperature changes inferred from proxy evidence, the annual mean surface temperature in Brayshaw et al. (2011) shows little change or even a slight reduction over much of the basin (in their model, this is consistent with a response to reduced atmospheric greenhouse-gas concentrations in their HO period experiments).

The 8.2 Event in the Mediterranean Region

Several paleoclimatic records from Greenland, Europe, and America show evidence of a rapid reorganization of the atmospheric system occurring exactly at this time (the 8.2 event; Alley and Agustsdottir, 2005; Mayewski et al., 2004; Rohling and Pälike, 2005). The agreement observed between the periodicity of the Holocene abrupt events marked in the westernmost Mediterranean region, and the cooling events of the North Atlantic region support a strong Atlantic–Mediterranean climatic link at high-frequency time intervals. Furthermore, proxies for deepwater conditions reveal the occurrence of episodes of deepwater overturning reinforcement in the western Mediterranean basin, which supports not only the good ventilation conditions needed to stop the formation of the ORL in the Alboran Sea (Cacho et al., 2002) but also the interrupted sapropel S1 in the eastern Mediterranean basin (Mercone et al., 2001; Rohling et al., 1997). Furthermore, it also indicates a rapid response of the Mediterranean thermohaline circulation to climate change in the North Atlantic and stresses the importance of atmospheric processes in linking climate variability between high latitudes and midlatitudes. A mechanism similar to one defended by Cacho et al. (2002) and Sierro et al. (2005) for the glacial Dansgaard–Oeschger variability has also been proposed by Frigola et al. (2007) to explain the Holocene cooling events. That is, a strengthened westerly system enhancing the marine overturning cell in the Gulf of Lions would lead to a more efficient formation of Mediterranean Deep Waters in both the eastern and western Mediterranean (Cacho et al., 2002; Frigola et al., 2007; Marino et al., 2009) and to the enhancement of deep circulation.

Spatial distribution of climate conditions at 8.2 cal ka BP within the Mediterranean region is shown in Figure 1.13 and compiled in Table 1.4sm. The temperatures documented in the $U^{K'}{}_{37}$ SST records relative to the HO values are 0.7°C lower (for the entire basin). The western basin shows a lower difference between 8.2 ka and HO (0.4°C), while a larger difference (1.3°C) is found in the eastern basin (Table 1.3sm). Lower temperature and/or humidity are also indicated by planktonic foraminiferal $\delta^{18}O$ values from the central Aegean Sea (Geraga et al., 2010) and low Ca contents in the Black Sea (Bahra et al., 2005). This sea-surface cooling is coupled with sharply smaller contents of the marine and terrestrial biomarkers in the water column and point to reductions of organic fluxes or more active oxidation on the seafloor and stronger water-column ventilation (Gogou et al., 2007). An inference also supported by the benthic foraminiferal records (Aksu et al., 1995; Kuhnt et al., 2007; Rohling et al., 1997).

Most high-resolution pollen sequences from the Mediterranean region show a slight decrease of temperature during the 8.2 event (Combourieu Nebout et al., 2009; Fletcher et al., 2007; Geraga et al., 2005; Jalut et al., 2000). Pollen records from the Adriatic Sea indicate an increase in high-altitude trees (*Abies* and *Picea*; Giunta et al., 2003) possibly related to a slight temperature decrease in the continental climate, perhaps induced by an increase in intensity of the northeastern and eastern winds. Nevertheless, the presence of the Mediterranean taxa that require mild winters indicates that winter temperatures did not drastically decrease (Sangiorgi et al., 2003).

South of 42°N, in the central and eastern Mediterranean regions (Carrión et al., 2001; Fletcher et al., 2007; Jalut et al., 2000, 2005; Magri, 1999; Magri and Parra, 2002; Muñoz-Sobrino et al., 2005; Peñalba, 1994; Tinner et al., 2009) and northern Aegean Sea (Ariztegui et al., 2000; Cheddadi et al., 1998; Combourieu Nebout et al., 2009; Geraga et al., 2005; Kotthoff et al., 2008a,b; Lamb et al., 1995; Lamb and van der Kaars, 1995), dry conditions persisted during the 8.2 event. The prevalence of arid conditions in northeastern Africa and the Middle East has also been documented by multiproxy data (Kiage and Liu, 2006, and references therein). In contrast, pollen sequences located north of 42°N, such as those from the northwestern Iberian margin as well as the ones from the Swiss and French Jura mountains, detect an increase in precipitation (Magny et al., 2001; Naughton et al., 2007b; Tinner and Lotter, 2001).

The terrestrial records, however, do not show any major change, except in the Pyrenees, where the signal is toward relatively cold and arid conditions (Gonzalez-Samperiz et al., 2006). On the other hand, archeological evidence from the Ebro Depression points to a quite strong impact on the Neolithic settlings in the region. This period appears to coincide with the period known in the region as the "archeological silence," during which most of the higher-altitude sites were abandoned (Gonzalez-Samperiz et al., 2009).

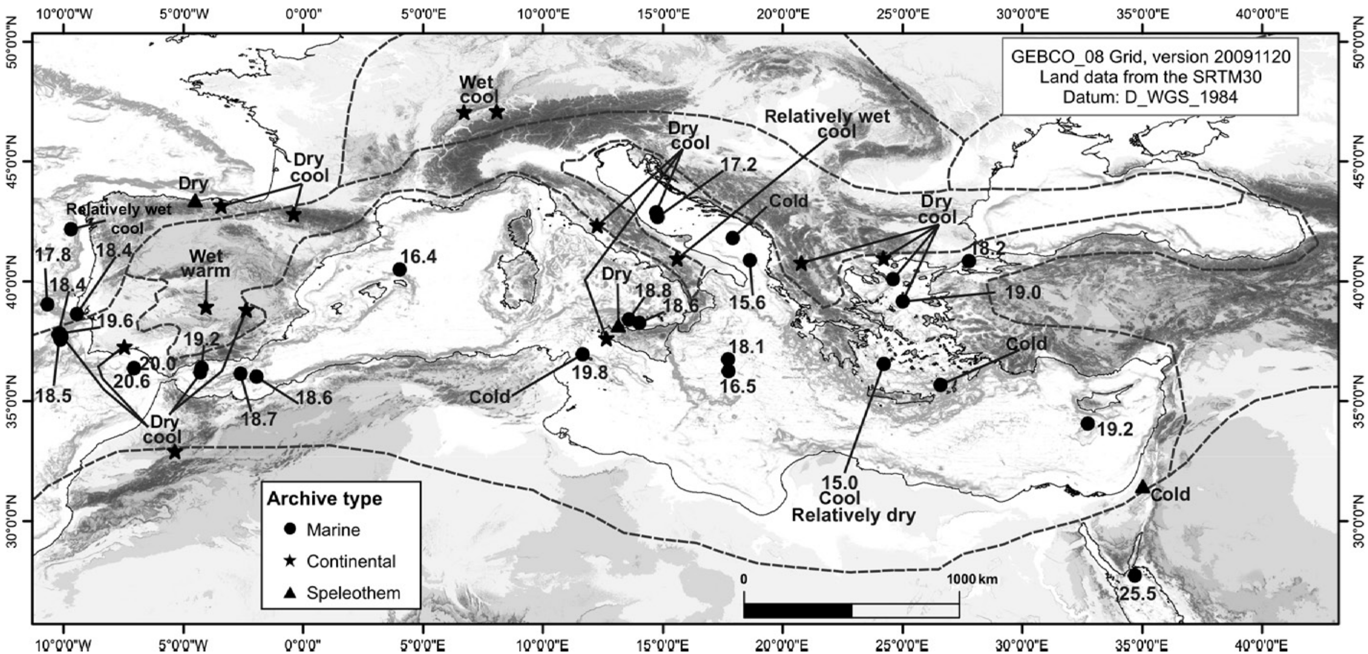

Figure 1.13 Climate conditions at 8.2 ± 0.250 cal ka BP (Table 4sm) for the Mediterranean region. The SSTs are estimated through $U^{K'}_{37}$ in marine cores. Qualitative information derived from pollen data in marine cores as well as other proxies from lakes, peat bogs, lagoons, and speleothem records. Map legend is as in Figure 1.4. Original work referenced in Table 1.1.

Model reconstructions focusing on the short-lived 8.2 event anomaly convincingly link this event to a reduction of the AMOC due to a meltwater pulse (Alley and Agustsdottir, 2005; LeGrande et al., 2006; Wiersma and Renssen, 2006). Sortable silt size (a proxy of deep-current flow speed) records for the Gardar and the Erik Drift (cores MD99-2251 and MD03-2665, respectively; Ellison et al., 2006; Kleiven et al., 2008), sites under the influence of the Iceland-Scotland, and the total integrated Nordic Seas overflows (Ellison et al., 2006; Hansen and Østerhus, 2000; Hansen et al., 2001; Hunter et al., 2007; Kleiven et al., 2008) show cooling and deepwater circulation disturbance at virtually the same time. Specifically, a reduction in NADW production slightly precedes and spans the sea-surface cooling event, in striking agreement with the sequence of events found by the above-mentioned climate models.

However, this data compilation shows a stronger impact of this event on the eastern basin, confirming severe far-field impacts of North Atlantic events in Mediterranean basins such as the Aegean Sea (Marino et al., 2009), which are isolated from the North Atlantic oceanic circulation, and pointing to a signal transmitted through atmospheric processes as proposed by Ariztegui et al. (2000), Mayewski et al. (2004), and Rohling et al. (2002b). Rohling et al. (2002b) showed that the event at 8.2 ka coincided in time with intensifications of the Siberian High, as reflected in the GISP2 nss [K^+] record. This ice peak in K^+ also coincides with periods of dry Indian monsoon (Qunf Cave $\delta^{18}O$ speleothem record; Fleitmann et al., 2003), hinting at large (hemispheric) scale teleconnections during the early Holocene on centennial timescales (Marino et al., 2009; Rohling and Pälike, 2005).

Some insight into these large-scale teleconnections can, perhaps, be gained through the so-called AMOC shutdown experiments using GCMs (Alley and Agustsdottir, 2005). Many of these experiments can, in some senses, be considered to be a "forced" version of the 8.2 event (whereby the sinking water in the high-latitude North Atlantic is completely shutdown by applying a large freshwater pulse or hosing). Such simulations typically indicate markedly cooler temperatures over the whole Northern Hemisphere extratropics (Vellinga and Wood, 2002) and weaker precipitation (lower temperatures are associated with reduced atmospheric humidity despite increased storm activity; Jacob et al., 2005). Although precipitation is reduced over Europe and almost all of the Mediterranean, this change is not uniform (e.g., results presented by Brayshaw et al., 2009, suggest that the precipitation signal is particularly weak in the southeast corner of the Mediterranean basin). However, it is important to note that many of these experiments are performed against a "recent" background climate rather than conditions specifically pertaining to the 8.2 event.

In modern times, outbreaks of cold northerly air masses strongly affect the Aegean winter SST regime, impacting on the rates of Aegean deepwater formation and consequently on the ventilation of the entire eastern Mediterranean Sea (see Introduction and Roether et al., 1996; Theocharis and Georgopoulos, 1993; Zervakis et al., 2003). It may well be that the frequency and/or intensity of such events varies in association with the North Atlantic Oscillation (Tsimplis and Josey, 2001), generating a stronger signal on the eastern than on the western Mediterranean, where the signal appears to be transmitted mainly via thermohaline circulation.

This relation between relative aridity and cold temperatures, however, is not likely to have been maintained during the whole Holocene, given that during the cold LIA conditions the glaciers of the Pyrenees have greatly expanded (Copons and Bordonau, 1994) and evidence for strong precipitation and even increased flooding have been found in the littoral Catalan (Vallve and Martin-Vide, 1998) and off the west coast of the Iberian Peninsula (Abrantes et al., 2005, 2011).

1.4 Outlook

The time-slice reconstructions that constitute the basis for this chapter are of great importance for climate modeling, both as a source of information for the mapped variables and as a form of evaluation of the model results and revealed the lack of data for key sites of this region, which will certainly give rise to the recovery of new sedimentary sequences from such locations. This compilation has also shown a lack of information for geological time intervals during which major oceanographic/climatic changes are known to have occurred, such as between 3 Ma and MIS 11. A gap that is mainly a result of the existing coring facilities and results from the extensive use of long piston coring that allowed the production of large volumes of high-resolution information back to MIS 11 in the last 10 years or so, versus the much smaller number of long DSDP/ODP/Integrated Ocean Drilling Program (IODP) coring needed to reach the older sediments. However, the upcoming IODP Expedition 339, the main objective of which is to better understand the broader significance of the MOW on the North Atlantic circulation and global climate, will certainly provide new data for this specific region and the above-mentioned time intervals. Moreover, a specific site on the southwest Portuguese margin, which has shown the unique strength of correlating millennial-scale variability from the marine environment with ice cores from Greenland and Antarctica and with European terrestrial sequences for the last two climatic cycles, will also be drilled with the expectation of providing a marine reference section of Pleistocene climate variability.

Another conclusion from this work is that given the interdisciplinary aspects of climate research, more conceptually robust climatic reconstructions with a higher potential for achieving more dependable projections of future climate will be accomplished with an increased interaction between the paleoclimatologists' community and the (paleo)climate modelers and modern climatologists.

Acknowledgments

This work is a result of the Mediterranean Climate Variability and Predictability (MedCLIVAR), a European Science Foundation (ESF) program that has provided the funds for meeting(s) that helped shape this contribution. I would like to thank those who provided preprints or unpublished material used in this chapter. Thanks are also due to Alessandra Asioli and Alan Haywood, whose review of this chapter is greatly appreciated.

References

Abrantes, F., 1988. Diatom productivity peak and increased circulation during latest Quaternary deglaciation: western Mediterranean. Mar. Micropaleontol. 13, 76–96.

Abrantes, F., 1990. Increased upwelling off Portugal during the last glaciation: diatom evidence. Mar. Micropaleontol. 17, 285–310.

Abrantes, F., Lebreiro, S., Rodrigues, T., Gil, I., Bartels-Jonsdottir, H., Oliveira, P., et al., 2005. Shallow-marine sediment cores record climate variability and earthquake activity off Lisbon (Portugal) for the last 2000 years. Quat. Sci. Rev. 24 (23–24), 2477–2494.

Abrantes, F., Rodrigues, T., Montanari, B., Santos, C., Witt, L., Lopes, C., et al., 2011. Climate of the last millennium at the southern pole of the North Atlantic Oscillation: an inner-shelf sediment record of flooding and upwelling. Clim. Res. 48 (2–3), 261–280.

de Abreu, L., Shackleton, N.J., Schoenfeld, J., Hall, M.A., Chapman, M.R., 2003. Millennial-scale oceanic climate variability off the Western Iberian margin during the last two glacial periods. Mar. Geol. 196 (1–2), 1–20.

Affek, H.P., Bar-Matthews, M., Ayalon, A., Matthews, A., Eiler, J.M., 2008. Glacial/interglacial temperature variations in Soreq Cave speleothems as recorded by “clumped isotope” thermometry. Geochim. Cosmochim. Acta 72 (22), 5351–5360.

Aguirre, J., Sánchez-Almazo, I.M., 2004. The Messinian post-evaporitic deposits of the Gafares area (Almería-Níjar basin, SE Spain). A new view of the “Lago-Mare” facies. Sediment. Geol. 168, 71–95.

Aksu, A.E., Yasar, D., Mudie, P.J., 1995. Paleoclimatic and paleoceanographic conditions leading to development of sapropel layer S1 in the Aegean Sea. Palaeogeogr. Palaeoclimatol. Palaeoecol. 116, 71–101.

Allen, J.R.M., Huntley, B., 2009. Last interglacial palaeovegetation, palaeoenvironments and chronology: a new record from Lago Grande di Monticchio, southern Italy. Quat. Sci. Rev. 28 (15–16), 1521–1538.

Allen, J.R.M., Huntley, B., Watts, W.A., 1996. The vegetation and climate of northwest Iberia over the last 14 000 yr. J. Quat. Sci. 11 (2), 125–147.

Allen, J.R.M., Brandt, U., Brauer, A., Hubberten, H.-W., Huntley, B., Keller, J., et al., 1999. Rapid environmental changes in southern Europe during the last glacial period. Nature 400, 740–743.

Allen, J.R.M., Watts, W.A., Huntley, B., 2000. Weichselian palynostratigraphy, palaeovegetation and palaeoenvironment; the record from Lago Grande di Monticchio, southern Italy. Quat. Int. 73/74, 91–110.

Allen, J.R.M., Watts, W.A., McGee, E., Huntley, B., 2002. Holocene environmental variability—the record from Lago Grande di Monticchio, Italy. Quat. Int. 88 (1), 69–80.

Allen, M.B., Armstrong, H.A., 2008. Arabia–Eurasia collision and the forcing of mid-Cenozoic global cooling. Palaeogeogr. Palaeoclimatol. Palaeoecol. 265, 52–58.

Alley, R.B., Agustsdottir, A.M., 2005. The 8k event: cause and consequences of a major Holocene abrupt change. Quat. Sci. Rev. 24, 1123–1149.

Alley, R.B., Mayewski, P.A., Sowers, T., Stuiver, M., Taylor, K.C., Clark, P.U., 1997. Holocene climatic instability: a prominent, widespread event 8200 yr ago. Geology 25, 483–486.

Almogi-Labin, A., Bar-Matthews, M., Shriki, D., Kolosovsky, E., Paterne, M., Schilman, B., et al., 2009. Climatic variability during the last ~90 ka of the southern and northern Levantine Basin as evident from marine records and speleothems. Quat. Sci. Rev. 28 (25–26), 2882–2896.

Ampel, L., Wohlfarth, B., Risberg, J., Veres, D., 2008. Paleolimnological response to millennial and centennial scale climate variability during MIS 3 and 2 as suggested by the diatom record in Les Echets, France. Quat. Sci. Rev. 27 (15–16), 1493–1504.

Antoine, D., Morel, A., Andre, J.-M., 1995. Algal pigment distribution and primary production in the eastern Mediterranean as derived from coastal zone colour scanner observations. J. Geophys. Res. 100 (C8), 16, 193–16,209.

Ariztegui, D., Asioli, A., Lowe, J.J., Trincardi, F., Vigliotti, L., Tamburini, F., et al., 2000. Palaeoclimatic reconstructions and formation of sapropel S1: inferences from Late Quaternary lacustrine and marine sequences in the Central Mediterranean region. Palaeogeogr. Palaeoclimatol. Palaeoecol. 158, 215–240.

Ariztegui, D., Chondrogianni, C., Lami, A., Guilizzoni, P., Lafargue, E., 2001. Lacustrine organic matter and the Holocene paleoenvironmental record of Lake Albano (central Italy). J. Paleolimnol. 26 (3), 283–292.

Arslanov, K.A., Dolukhanov, P.M., Gei, N.A., 2007. Climate, Black Sea levels and human settlements in Caucasus Littoral 50,000–9000 BP. Quat. Int., 121–127.

Arz, H.W., Lamy, F., Pätzold, J., Müller, P.J., Prins, M.A., 2003. Mediterranean moisture source for an early-Holocene humid period in the northern Red Sea. Science 300 (5616), 118–121.

Asioli, A., 1996. High resolution foraminifera biostratigraphy in the central Adriatic basin during the last deglaciation: a contribution to the PALICLAS project. Memorie dell'Istituto Italiano di Idrobiologia 55, 197–217.

Asioli, A., Trincardi, F., Lowe, J.J., Ariztegui, D., Langone, L., Oldfield, F., 2001. Submillennial scale climatic oscillations in the central Adriatic during the Lateglacial: palaeoceanographic implications. Quat. Sci. Rev. 20 (11), 1201–1221.

van Assen, E., Kuiper, K.F., Barhoun, N., Krijgsman, W., Sierro, F.J., 2006. Messinian astrochronology of the Melilla Basin: stepwise restriction of the Mediterranean–Atlantic connection through Morocco. Palaeogeogr. Palaeoclimatol. Palaeoecol. 238 (1–4), 15–31.

Atanassova, J., Stefanova, I., 2003. Late-glacial vegetational history of Lake Kremensko-5 in the northern Pirin Mountains, southwestern Bulgaria. Veg. Hist. Archaeobot. 12 (1), 1–6.

Bahra, A., Lamy, F., Arz, H., Kuhlmann, H., Wefer, G., 2005. Late glacial to Holocene climate and sedimentation history in the NW Black Sea. Mar. Geol. 214, 309–322.

Bar-Matthews, M., Ayalon, A., Kaufman, A., Wasserburg, G.J., 1999. The eastern Mediterranean paleoclimate as a reflection of regional events: Soreq Cave, Israel. Earth Planet. Sci. Lett. 166, 85–95.

Bar-Matthews, M., Ayalon, A., Kaufman, A., 2000. Timing and hydrological conditions of Sapropel events in the eastern Mediterranean, as evident from speleothems, Soreq Cave, Israel. Chem. Geol. 169, 145–156.

Bar-Matthews, M., Ayalon, A., Gilmour, M., Matthews, A., Hawkesworth, C.J., 2003. Sea-land oxygen isotopic relationships from planktonic foraminifera and speleothems in the eastern Mediterranean region and their implication for paleorainfall during interglacial intervals. Geochim. Cosmochim. Acta 67 (17), 3181–3199.

Barber, D.C., Dyke, A., Hillaire-Marcel, C., Jennings, A.E., Andrews, J.T., Kerwin, M.W., et al., 1999. Forcing of the cold event of 8,200 years ago by catastrophic drainage of Laurentide Lakes. Nature 400, 344–348.

Bárcena, M.A., Cacho, I., Abrantes, F., Sierro, F.J., Grimalt, J.O., Flores, J.A., 2001. Paleoproductivity variations related to climatic conditions in the Alboran Sea (western Mediterranean) during the last glacial–interglacial transition: the diatom record. Palaeogeogr. Palaeoclimatol. Palaeoecol. 167, 337–357.

Bard, E., Jouannic, C., Hamelin, B., Pirazzoli, P., Arnold, M., Fraure, G., et al., 1996. Pleistocene sea levels and tectonic uplift based on dating of corals from Sumba Island, Indonesia. Geophys. Res. Lett. 23 (12), 1473–1476.

Bard, E., Rostek, F., Turon, J.-L., Gendreau, S., 2000. Hydrological impact of Heinrich events in the subtropical northeast Atlantic. Science 289, 1321–1324.

Bard, E., Antonioli, F., Silenzi, S., 2002. Sea-level during the penultimate interglacial period based on a submerged stalagmite from Argentarola Cave (Italy). Earth Planet. Sci. Lett. 196 (3–4), 135–146.

Bard, E., Hamelin, B., Delanghe-Sabatier, D., 2010. Deglacial meltwater pulse 1B and Younger Dryas sea levels revisited with Boreholes at Tahiti. Science 327 (5970), 1235–1237.

Bartov, Y., Goldstein, S.L., Stein, M., Enzel, Y., 2003. Catastrophic arid episodes in the eastern Mediterranean linked with the North Atlantic Heinrich events. Geology 31 (5), 439–442.

Bassetti, M.A., Miculan, P., Sierro, F.J., 2006. Evolution of depositional environments after the end of Messinian Salinity Crisis in Nijar basin (SE Betic Cordillera). Sediment. Geol. 188–189, 279–295.

Beaudouin, C., Suc, J.-P., Acherki, N., Courtois, L., Rabineau, M., Aloisi, J.-C., et al., 2005. Palynology of the northwestern Mediterranean shelf (Gulf of Lions): first vegetational record for the last climatic cycle. Mar. Pet. Geol. 22 (6–7), 845–863.

Beaudouin, C., Jouet, G., Suc, J.-P., Berné, S., Escarguel, G., 2007. Vegetation dynamics in southern France during the last 30 ky BP in the light of marine palynology. Quat. Sci. Rev. 26, 1037–1054.

de Beaulieu, J.L., Reille, M., 1984. A long Upper Pleistocene pollen record from Les Echets, near Lyon, France. Boreas 13, 111–132.

de Beaulieu, J.L., Reille, M., 1989. The transition from temperate phases to stadials in the long upper Pleistocene sequence from Les Echets (France). Palaeogeogr. Palaeoclimatol. Palaeoecol. 72, 147–159.

de Beaulieu, J.L., Reille, M., 1992. Long Pleistocene pollen sequences from the Velay Plateau (Massif Central, France). Veg. Hist. Archaeobot. 1, 233–242.

Berger, A., Loutre, M.F., 1992. Astronomical solutions for paleoclimate studies over the last 3 million years. Earth Planet. Sci. Lett. 111 (2–4), 369–382.

Berger, A.L., 1978. Long-term variations of daily insolation and quaternary climatic change. J. Atmos. Sci. 35, 2362–2367.

Björkman, L., Feurdean, A., Cinthio, K., Wohlfarth, B., Possnert, G., 2002. Lateglacial and early Holocene vegetation development in the Gutaiului Mountains, NW Romania. Quat. Sci. Rev. 21, 1039–1059.

Blanc, P.L., 2002. The opening of the Plio–Quaternary Gibraltar Strait: assessing the size of a cataclysm. Geodinamica Acta 15, 303–317.

Boessenkool, K.P., Brinkhuis, H., Schönfeld, J., Targarona, J., 2001. North Atlantic sea-surface temperature changes and the climate of western Iberia during the last deglaciation; a marine palynological approach. Global Planet. Change 30 (1–2), 33–39.

Bond, G., Broecker, W., Johnsen, S., McManus, J., Labeyrie, L., Jouzel, J., et al., 1993. Correlations between climate records from North Atlantic sediments and Greenland Ice. Nature 365, 143–147.

Bond, G., Kromer, B., Beer, J., Muscheler, R., Evans, M.N., Showers, W., et al., 2001. Persistent solar influence on North Atlantic climate during the Holocene. Science 294, 2130–2136.

Bonfils, C., de Noblet-Ducoudre, N., Guiot, J., Bartlein, P., 2004. Some mechanisms of mid-Holocene climate change in Europe, inferred from comparing PMIP models to data. Clim. Dyn. 23, 79–98.

Bordon, A., Peyron, O., Lézine, A.-M., Brewer, S., Fouache, E., 2009. Pollen-inferred Late-Glacial and Holocene climate in southern Balkans (Lake Maliq). Quat. Int. 200, 19–30.

Born, A., Levermann, A., 2010. The 8.2 ka event: abrupt transition of the subpolar gyre toward a modern North Atlantic circulation. Geochem. Geophys. Geosyst. 11, Q06011. doi: 10.1029/2009GC003024.

Bottema, S., 1979. Pollen analytical investigations in Thessaly (Greece). Palaeohistoria 21, 20–40.

Bottema, S., 1995. The Younger Dryas in the eastern Mediterranean. Quat. Sci. Rev. 14 (9), 883–891.

Bozilova, E.D., Tonkov, S.B., 2000. Pollen from Lake Sedmo Rilsko reveals southeast European postglacial vegetation in the highest mountain area of the Balkans. New Phytol. 148 (2), 315–325.

Braconnot, P., Otto-Bliesner, B., Harrison, S., Joussaume, S., Peterchmitt, J.Y., Abe-Ouchi, A., et al., 2007a. Results of PMIP2 coupled simulations of the Mid-Holocene and Last Glacial Maximum—Part 1: experiments and large-scale features. Clim. Past 3, 261–277.

Braconnot, P., Otto-Bliesner, B., Harrison, S., Joussaume, S., Peterchmitt, J.Y., Abe-Ouchi, A., et al., 2007b. Results of PMIP2 coupled simulations of the Mid-Holocene and Last Glacial Maximum—Part 2: feedbacks with emphasis on the location of the ITCZ and mid- and high latitudes heat budget. Clim. Past 3, 279–296.

Braga, J.C., Martín, J.M., Riding, R., Aguirre, J., Sanchez-Almazo, I.M., Dinares-Turell, J., 2006. Testing models for the Messinian salinity crisis: the Messinian record in Almería, SE Spain. Sediment. Geol. 188–189, 131–154.

Brayshaw, D.J., Woollings, T., Vellinga, M., 2009. Tropical and extratropical responses of the North Atlantic atmospheric circulation to a sustained weakening of the MOC. J. Clim. 22, 3146–3155.

Brayshaw, D.J., Hoskins, B., Black, E., 2010. Some physical drivers of changes in the winter storm tracks over the North Atlantic and Mediterranean during the Holocene. Philos. Trans. R. Soc. A 368 (1931), 5185–5223.

Brayshaw, D.J., Rambeau, C.M.R., Smith, S., 2011. Changes in Mediterranean climate during the Holocene: insights from global and regional climate modelling. Holocene 21, 15–31.

Broecker, W.S., Denton, G.H., 1989. The role of ocean–atmosphere reorganizations in glacial cycles. Geochim. Cosmochim. Acta 53, 2465–2501.

van der Burgh, J., Visscher, H., Dilcher, D.L., Kurschner, W.M., 1993. Paleoatmospheric signatures in Neogene fossil leaves. Science 260, 1788–1790.

Burjachs, F., Julià, R., 1994. Abrupt climatic changes during the last glaciation based on pollen analysis of the Abric Romani, Catalonia Spain. Quat. Res. 42, 308–315.

Butler, R., Lickorish, W.H., Grasso, M., Pedley, H.M., Ramberti, L., 1995. Tectonics and sequence stratigraphy in Messinian basins, Sicily: constraints on the initiation and termination of the Mediterranean salinity crisis. Geol. Soc. Am. Bull. 107 (4), 425–439.

Cacho, I., Grimalt, J.O., Pelejero, C., Canals, M., Sierro, F.J., Flores, J.A., et al., 1999. Dansgaard–Oeschger and Heinrich events imprints in Alboran Sea paleotemperatures. Paleoceanography 14 (6), 698–705.

Cacho, I., Grimalt, J.O., Sierro, F.J., Shackleton, N., Canals, M., 2000. Evidence for enhanced Mediterranean thermohaline circulation during rapid climatic coolings. Earth Planet. Sci. Lett. 183, 417–429.

Cacho, I., Grimalt, J.O., Canals, M., Sbaffi, L., Shackleton, N.J., Schoenfeld, J., et al., 2001. Variability of the western Mediterranean Sea surface temperature during the last 25,000 years and its connection with the Northern Hemisphere climatic changes. Paleoceanography 16 (1), 40–52.

Cacho, I., Grimalt, J.O., Canals, M., 2002. Response of the western Mediterranean Sea to the rapid climatic variability that occurred during the last 50,000 years. A molecular biomarker approach. J. Mar. Syst. 33–34, 253–272.

Cacho, I., Shackleton, N.J., Elderfield, H., Sierro, F.J., Grimalt, J.O., 2006. Glacial rapid variability in deep-water temperature and $\delta^{18}O$ from the Western Mediterranean Sea. Quat. Sci. Rev. 25 (23–24), 3294–3311.

Çagatay, M.N., Görür, N., Flecker, R., Sakinc, M., Tunoglu, C., Ellam, R.M., et al., 2006. Paratethyan–Mediterranean connectivity in the Sea of Marmara region (NW Turkey) during the Messinian. Sediment. Geol. 188–189, 171–187.

Calvert, S.E., Nielsen, B., Fontugne, M.R., 1992. Evidence from nitrogen isotope ratios for enhanced productivity during formation of eastern Mediterranean sapropels. Nature 359, 223–225.

Canali, G., Capraro, L., Donnici, S., Rizzetto, F., Serandrei-Barbero, R., Tosi, L., 2007. Vegetational and environmental changes in the eastern Venetian coastal plain (Northern Italy) over the past 80,000 years. Palaeogeogr. Palaeoclimatol. Palaeoecol. 253, 300–316.

Canals-Artiguas, M., 1980. Sedimentos y procesos en el margen continental Sur-Balear: control climatico y oceanografico sobre su distribucion y evolucion durante el Cuaternario Superior. Thesis Licenciatura, Facultad Geologia, Universidade Barcelona, Barcelona, p. 210.

Caralp, M.H., 1988. Late glacial to recent deep-sea Benthic Foraminifera from the Northeastern Atlantic (Cádiz Gulf) and Western Mediterranean (Alboran Sea): paleoceanographic results. Mar. Micropaleontol. 13, 265–289.

Carrión, J.S., 2002. Patterns and processes of Late Quaternary environmental change in a montane region of southwestern Europe. Quat. Sci. Rev. 21, 2047–2066.

Carrión, J.S., 2003. Sobresaltos en el bosque mediterraneo: Incidencia de las perturbaciones observables en una escala paleoecológica. Ecosistemas, 2003-3. <http://www.revistaecosistemas.net>.

Carrión, J.S., Dupré, M., 1996. Late Quaternary vegetational history at Navarrés, eastern Spain. A two core approach. New Phytol. 134, 177–191.

Carrión, J.S., van Geel, B., 1999. Fine-resolution Upper Weichselian and Holocene palynological record from Navarrés (Valencia, Spain) and a discussion about factors of Mediterranean forest succession. Rev. Palaeobot. Palynol. 106 (3–4), 209–236.

Carrión, J.S., Andrade, A., Bennett, K.D., Navarro, C., Munuera, M., 2001. Crossing forest thresholds: inertia and collapse in a Holocene sequence from south-central Spain. Holocene 11 (6), 635–653.

Carrión, J.S., Fuentes, N., Gonzalez-Samperiz, P., Quirante, L.S., Finlayson, J.C., Fernandez, S., et al., 2007. Holocene environmental change in a montane region of southern Europe with a long history of human settlement. Quat. Sci. Rev. 26, 1455.

Casford, J.S.L., Rohling, E.J., Abu-Zied, R., Cooke, S., Fontanier, C., Leng, M., et al., 2002. Circulation changes and nutrient concentrations in the late Quaternary Aegean Sea: a nonsteady state concept for sapropel formation. Paleoceanography 17 (2) doi: 10.1029/2000PA000601.

Castañeda, I.S., Schefuss, E., Paetzold, J., Sinninghe Damste, J.S., Weldeab, S., Schouten, S., 2010. Millennial-scale sea surface temperature changes in the eastern Mediterranean (Nile River Delta region) over the last 27,000 years. Paleoceanography 25, PA1208. doi: 10.1029/2009PA001740.

Cheddadi, R., Rossignol-Strick, M., 1995a. Eastern Mediterranean Quaternary paleoclimates from pollen and isotope records of marine cores in the Nile cone area. Paleoceanography 10 (2), 291–300.
Cheddadi, R., Rossignol-Strick, M., 1995b. Improved preservation of organic matter and pollen in eastern Mediterranean sapropels. Paleoceanography 10 (2), 301–310.
Cheddadi, R., Rossignol-Strick, M., Fontugne, M., 1991. Eastern Mediterranean palaeoclimates from 26 to 5 ka B.P. documented by pollen and isotopic analysis of a core in the anoxic Bannock Basin. Mar. Geol. 100, 53–66.
Cheddadi, R., Lamb, H.F., Guiot, J., van der Kaars, S., 1998. Holocene climatic change in Morocco: a quantitative reconstruction from pollen data. Clim. Dyn. 14, 883–890.
Chondrogianni, C., Ariztegui, D., Rolph, T., Juggins, S., Shemesh, A., Rietti-Shati, M., et al., 2004. Millennial- to interdecadal climate variability in the Mediterranean during the LGM—the Lake Albano record. Quat. Int. 122, 31–41.
Ciampo, G., 2004. Ostracods as palaeoenvironmental indicators in the last 30 ky from the Tyrrhenian continental shelf. Global Planet. Change 40 (1–2), 151–157.
CIESM, 2008. Executive summary. In: Briand, F. (Ed.), CIESM, 2008. The Messinian Salinity Crisis from Mega-Deposits to Microbiology—A Consensus Report. N°33 in CIESM Workshop Monographs, Monaco, pp. 3–28.
Cita, M.B., Wright, R.C., Ryan, W.B.F., Longinelli, A., 1978. Messinian palaeoenvironments. In: Hsü, K.J., Montadert, L. (Eds.), Initial Reports of the Deep Sea Drilling Project. US Government Printing Office, Washington, DC, pp. 1003–1035.
Claussen, M., Fohlmeister, J., Ganopolski, A., Brovkin, V., 2006. Vegetation dynamics amplifies precessional forcing. Geophys. Res. Lett. 33, L09709. doi: 10.1029/2006GL026111.
Clauzon, G., 1973. The eustatic hypothesis and the pre-Pliocene cutting of the Rhône Valley. In: Ryan, W.B.F., Hsü, K.J. (Eds.), Initial Reports of the Deep Sea Drilling Project. US Government Printing Office, Washington, DC, pp. 1251–1256.
Clauzon, G., Suc, J.P., Gautier, F., Berger, A., Loutre, M.F., 1996. Alternate interpretation of the Messinian salinity crisis: controversy resolved? Geology 24 (4), 363–366.
Clauzon, G., Suc, J.P., Popescu, S.M., Marunteanu, M., Rubino, J.L., Marinescu, F., et al., 2005. Influence of Mediterranean sea-level changes on the Dacic Basin (Eastern Paratethys) during the late Neogene: the Mediterranean Lago Mare facies deciphered. Basin Res. 17 (3), 437–462.
Colmenero-Hidalgo, E., Flores, J.-A., Sierro, F.J., Barcena, M.A., Loewemark, L., Schoenfeld, J., et al., 2004. Ocean surface water response to short-term climate changes revealed by coccolithophores from the Gulf of Cadiz (NE Atlantic) and Alboran Sea (W Mediterranean). Palaeogeogr. Palaeoclimatol. Palaeoecol. 205 (3–4), 317–336.
Comas, M.C., Zahn, R., Klaus, A., Shipboard Scientific Party (Eds.), 1996. Sites 974, 975, 976, 979. Proceedings of the Ocean Drilling Program, Initial Reports, 161. Ocean Drilling Program, College Station, TX, pp. 55–297 and 389–426.
Combourieu-Nebout, N., Paterne, M., Turon, J.-L., Siani, G., 1998. A high-resolution record of the last deglaciation in the Central Mediterranean Sea: palaeovegetation and palaeohydrological evolution. Quat. Sci. Rev. 17 (4–5), 303–317.
Combourieu Nebout, N., Londeix, L., Baudin, F., Turon, J.-L., von Grafenstein, R., Zahn, R., 1999. Quaternary marine and continental paleoenvironments in the western Mediterranean (Site 976, Alboran Sea): palynological evidence. In: Zahn, R., Comas, M.C., Klaus, A. (Eds.), Proceedings of the Ocean Drilling Program, Scientific Results. Ocean Drilling Program, College Station, TX, pp. 457–468.

Combourieu-Nebout, N., Fauquette, S., Quezel, P., 2000. What was the late Pliocene Mediterranean climate like; a preliminary quantification from vegetation. Bull. Soc. Geol. Fr. 171 (2), 271–277.

Combourieu-Nebout, N., Turon, J.L., Zahn, R., Capotondi, L., Londeix, L., Pahnke, K., 2002. Enhanced aridity and atmospheric high-pressure stability over the western Mediterranean during the North Atlantic cold events of the past 50 k.y. Geology 30 (10), 863–866.

Combourieu Nebout, N., Peyron, O., Dormoy, I., Desprat, S., Beaudouin, C., Kotthoff, U., et al., 2009. Rapid climatic variability in the west Mediterranean during the last 25 000 years from high resolution pollen data. Clim. Past 5 (3), 503–521.

Copons, R., Bordonau, J., 1994. La Pequeña Edad del Hielo en el Macizo de la Maladeta (alta cuenca del Esera, Pirineos Centrales). In: Bono, C.M., Ruíz, J.G. (Eds.), El Glaciarismo surpirenaico: nuevas aportaciones. Geoforma Ediciones, Logroño, Spain, pp. 111–124.

Cramp, A., O'Sullivan, G., 1999. Neogene sapropels in the Mediterranean: a review. Mar. Geol. 1–4, 11–28.

Dansgaard, W., Johnsen, S.J., Clausen, H.B., Dahl-Jensen, D., Gundestrup, N.S., Hammer, C.U., et al., 1993. Evidence for general instability of past climate from a 250 kyr ice-core record. Nature 264, 218–220.

David, F., 2001. Le tardiglaciaire des Ételles (Alpes françaises du Nord): instabilité climatique et dynamique de végétation. C. R. Acad. Sci. Paris, Sciences de la vie /Life Sciences 324, 373–380.

Davis, B.A.S., Brewer, S., Stevenson, A.C., Guiot, J., 2003. The temperature of Europe during the Holocene reconstructed from pollen data. Quat. Sci. Rev. 22, 1701–1716.

Debret, M., Sebag, D., Crosta, X., Massei, N., Petit, J.-R., Chapron, E., et al., 2009. Evidence from wavelet analysis for a mid-Holocene transition to global climate forcing. Quat. Sci. Rev. 28, 2675–2688.

Decima, A., Wezel, F.C., 1973. Late Miocene evaporites of the Central Sicilian Basin. In: Ryan, W.B.F., Hsü, K.J. (Eds.), Initial Reports of the Deep Sea Drilling Project. US Government Printing Office, Washington, DC, pp. 1234–1240.

DeMenocal, P., Ortiz, J., Guilderson, T., Adkins, J., Sarnthein, M., Baker, L., et al., 2000a. Abrupt onset and termination of the African Humid Period: rapid climate responses to gradual insolation forcing. Quat. Sci. Rev. 19, 347–361.

DeMenocal, P., Ortiz, J., Guilderson, T., Sarnthein, M., 2000b. Coherent high- and low-latitude climate variability during the Holocene warm period. Science 288, 2198–2202.

Desprat, S., Sanchez Goñi, M.F., McManus, J.F., Duprat, J., Cortijo, E., 2009. Millennial-scale climatic variability between 340 000 and 270 000 years ago in SW Europe: evidence from a NW Iberian margin pollen sequence. Clim. Past 5 (1), 53–72.

Diester-Haass, L., Robert, C., Chamley, H., 1998. Paleoproductivity and climate variations during sapropel deposition in the eastern Mediterranean Sea. In: Robertson, A.H.F., Emeis, K.-C., Richter, C., Camerlenghi, A. (Eds.), Proceedings of the Ocean Drilling Program, Scientific Results. Ocean Drilling Program, College Station, TX, pp. 227–248.

Doose, H., 1999. Rekonstruktion hydrographischer Verhaeltnisse im Californienstrom und im Europaeischen Mittelmeer zur Bildungszeit kohlenstoffreicher Sedimente, Geomar, Kiel, Geomar Report, 78, p. 111.

Doose, H., Zahn, R., Bernasconi, S., Pika-Biolzi, M., Murat, A., Pierre, C., et al., 1999. Planktonic $\delta^{18}O$ and $U^{K'}_{37}$ temperature estimates from organic-rich sediments at Sites 974 and 975, Tyrrhenian Sea and Balearic Rise. In: Zahn, R., Comas, M.C., Klaus, A. (Eds.), Proceedings of the Ocean Drilling Program, Scientific Results. Ocean Drilling Program, College Station, TX, pp. 489–503.

Dorale, J.A., Onac, B.P., Fornos, J.J., Gines, J., Gines, A., Tuccimei, P., et al., 2010. Sea-level highstand 81,000 years ago in Mallorca. Science 327 (5967), 860–863.

Dowsett, H.J., Chandler, M.A., Robinson, M.M., 2009. Surface temperatures of the Mid-Pliocene North Atlantic Ocean: implications for future climate. Philos. Trans. R. Soc. A: Math. Phys. Eng. Sci. 367 (1886), 69–84.

Drysdale, R.N., Zanchetta, G., Hellstrom, J.C., Fallick, A.E., Zhao, J.-X., Isola, I., et al., 2004. Palaeoclimatic implications of the growth history and stable isotope ($\delta^{18}O$ and $\delta^{13}C$) geochemistry of a Middle to Late Pleistocene stalagmite from central-western Italy. Earth Planet. Sci. Lett. 227 (3–4), 215–229.

Drysdale, R.N., Zanchetta, G., Hellstrom, J.C., Fallick, A.E., Zhao, J.X., 2005. Stalagmite evidence for the onset of the Last Interglacial in southern Europe at 129 +/− 1 ka. Geophys. Res. Lett. 32 (24), L24708. doi: 10.1029/2005GL024658.

Drysdale, R.N., Hellstrom, J.C., Zanchetta, G., Fallick, A.E., Goni, M.F.S., Couchoud, I., et al., 2009. Evidence for obliquity forcing of glacial termination II. Science 325 (5947), 1527–1531.

Duggen, S., Hoernle, K., van den Bogaard, P., Rupke, L., Morgan, J.P., 2003. Deep roots of the Messinian salinity crisis. Nature 422, 602–606.

Ellison, C.R.W., Chapman, M.R., Hall, I.R., 2006. Surface and deep ocean interactions during the cold climate event 8200 years ago. Science 312 (5782), 1929–1932.

Emeis, K.-C., Robertson, A.H.F., Richter, C., Shipboard Scientific Party (Eds.), 1996. Sites 963, 964, 966, 967, 969. Proceedings of the Ocean Drilling Program, Scientific Results, 160. Ocean Drilling Program, College Station, TX, pp. 55–287 and 335–375.

Emeis, K.-C., Schulz, H.-M., Struck, U., Sakamoto, T., Doose, H., Erlenkeuser, H., et al., 1998. Stable isotope and alkenone temperature records of sapropels from Sites 964 and 967: constraining the physical environment of sapropel formation in the eastern Mediterranean Sea. In: Robertson, A.H.F., Emeis, K.-C., Richter, C., Camerlenghi, A. (Eds.), Proceedings of the Ocean Drilling Program, Scientific Results. Ocean Drilling Program, College Station, TX, pp. 309–331.

Emeis, K.C., Struck, U., Schulz, H.M., Rosenberg, R., Bernasconi, S., Erlenkeuser, H., et al., 2000. Temperature and salinity variations of Mediterranean Sea surface waters over the last 16,000 years from records of planktonic stable oxygen isotopes and alkenone unsaturation ratios. Palaeogeogr. Palaeoclimatol. Palaeoecol. 158 (3–4), 259–280.

Emeis, K.-C., Schulz, H., Struck, U., Rossignol-Strick, M., Erlenkeuser, H., Howell, M.W., et al., 2003. Eastern Mediterranean surface water temperatures and $\delta^{18}O$ composition during deposition of sapropels in the late Quaternary. Paleoceanography 18 (1) doi: 10.1029/2000PA000617.

EPICA members, 2004. Eight glacial cycles from an Antarctic ice core. Nature 429 (6992), 623–628.

Essallami, L., Sicre, M.A., Kallel, N., Labeyrie, L., Siani, G., 2007. Hydrological changes in the Mediterranean Sea over the last 30,000 years. Geochem. Geophys. Geosyst. 8, Q07002. doi: 10.1029/2007GC001587.

Eynaud, F., de Abreu, L., Voelker, A., Schönfeld, J., Salgueiro, E., Turon, J.-L., et al., 2009. Position of the Polar Front along the western Iberian margin during key cold episodes of the last 45 ka. Geochem. Geophys. Geosyst. 10, Q07U05. doi: 10.1029/2009GC002398.

Fairbanks, R.G., 1990. The age and origin of the "Younger Dryas Climate event" in Greeland ice cores. Paleoceanography 5, 937–948.

Fairbanks, R.G., Mortlock, R.A., Chiu, T.-C., Cao, L., Kaplan, A., Guilderson, T.P., et al., 2005. Radiocarbon calibration curve spanning 0 to 50,000 years BP based on paired $^{230}Th/^{234}U/^{238}U$ and ^{14}C dates on pristine corals. Quat. Sci. Rev. 24, 1781–1796.

Fauquette, J.O., Suc, J.P., Guiot, J., 1999. Climate and biomes in the West Mediterranean area during the Pliocene. Palaeogeogr. Palaeoclimatol. Palaeoecol. 152 (1–2), 15–36.

Fauquette, S., Guiot, J., Suc, J.-P., 1998. A method for climatic reconstruction of the Mediterranean Pliocene using pollen data. Palaeogeogr. Palaeoclimatol. Palaeoecol. 144, 183–201.

Favaretto, S., Asioli, A., Miola, A., Piva, A., 2008. Preboreal climatic oscillations recorded by pollen and foraminifera in the southern Adriatic Sea. Quat. Int. 190 (1), 89–102.

Fenton, M., Geiselhart, S., Rohling, E.J., Hemleben, C., 2000. Aplanktonic zones in the Red Sea. Mar. Micropaleontol. 40 (3), 277–294.

Feurdean, A., 2004. Palaeoenvironment in Romania during last 15,000 years. Ph.D. Thesis. Stockholm University, Sweden, p. 44.

Feurdean, A., Mosbrugger, V., Onac, B.P., Polyak, V., Veres, D., 2007. Younger Dryas to mid-Holocene environmental history of the lowlands of NW Transylvania, Romania. Quat. Res. 68 (3), 364–378.

Fischer, G., Wefer, G., 1999. Use of Proxies in Paleoceanography: Examples from the South Atlantic. Springer, Berlin, Heidelberg, New York, p. 735.

Flecker, R., Ellam, R.M., 2006. Identifying Late Miocene episodes of connection and isolation in the Mediterranean–Paratethyan realm using Sr isotopes. Sediment. Geol. 188–189, 189–203.

Fleitmann, D., Burns, S.J., Mudelsee, M., Neff, U., Kramers, J., Mangini, A., et al., 2003. Holocene forcing of the Indian monsoon recorded in a stalagmite from Southern Oman. Science 300, 1737–1739.

Fleitmann, D., Cheng, H., Badertscher, S., Edwards, R.L., Mudelsee, M., Göktürk, O.M., et al., 2009. Timing and climatic impact of Greenland interstadials recorded in stalagmites from northern Turkey. Geophys. Res. Lett. 36, L19707. doi: 10.1029/2009gl040050.

Fletcher, W.J., Sanchez Goñi, M.F., 2008. Orbital- and sub-orbital-scale climate impacts on vegetation of the western Mediterranean basin over the last 48,000 yr. Quat. Res. 70 (3), 451–464.

Fletcher, W.J., Boski, T., Moura, D., 2007. Palynological evidence for environmental and climatic change in the lower Guadiana valley, Portugal, during the last 13 000 years. Holocene 17 (4), 481–494.

Fletcher, W.J., Sanchez Goni, M.F., Allen, J.R.M., Cheddadi, R., Combourieu-Nebout, N., Huntley, B., et al., 2010a. Millennial-scale variability during the last glacial in vegetation records from Europe. Quat. Sci. Rev. 29 (21–22), 2839–2864.

Fletcher, W.J., Sanchez Goñi, M.F., Peyron, O., Dormoy, I., 2010b. Abrupt climate changes of the last deglaciation detected in a western Mediterranean forest record. Clim. Past 5 (1), 203–235.

Florschütz, F., Menéndez Amor, J., Wijmstra, T.A., 1971. Palynology of a thick quaternary succession in southern Spain. Palaeogeogr. Palaeoclimatol. Palaeoecol. 10, 233–264.

Fluteau, F., Ramstein, G., Besse, J., 1999. Simulating the evolution of the Asian and African monsoons during the past 30 Myr using an atmospheric general circulation model. J. Geophys. Res. 104 (D10), 11,995–12,018.

Follieri, M., Magri, D., Sadori, L., 1989. Pollen stratigraphical synthesis from Valle di Castiglione (Roma). Quat. Int. 3/4, 81–84.

Follieri, M., Magri, D., Narcisi, B., 1993. Paleoenvironmental investigations on long sedimentary cores from volcanic lakes of Lazio (Central Italy). In: Negendank, F.W., Zolitschka, B. (Eds.), Lecture Notes in Earth Sciences Paleolimnology of European Maar Lakes. Springer-Verlag, Berlin, pp. 95–107.

Follieri, M., Giardini, M., Magri, D., Sadori, L., 1998. Palynostratigraphy of the last glacial period in the volcanic region of Central Italy. Quat. Int. 47–48, 3–20.

Fontugne, M., Arnold, M., Labeyrie, L., Paterne, M., Calvert, S.E., Duplessy, J.C., 1994. Palaeoenvironment Sapropel chronology and Nile river discharge during the last 20 000 years as indicated by deep sea sediment records in the eastern Mediterranean. In: Bar-Yosef, O., Kra, R.S. (Eds.), Late Quaternary Chronology and Paleoclimate of the Eastern Mediterranean. Radiocarbon, 75–88.

Fortuin, A.R., Krijgsman, W., 2003. The Messinian of the Nijar Basin (SE Spain): sedimentation, depositional environments and paleogeographic evolution. Sediment. Geol. 160, 213–242.

Frigola, J., Moreno, A., Cacho, I., Canals, M., Sierro, F.J., Flores, J.A., et al., 2007. Holocene climate variability in the western Mediterranean region from a deepwater sediment record. Paleoceanography 22 (2), PA2209. doi: 10.1029/2006PA001307.

Frigola, J., Moreno, A., Cacho, I., Canals, M., Sierro, F.J., Flores, J.A., et al., 2008. Evidence of abrupt changes in western Mediterranean deep water circulation during the last 50 kyr: a high-resolution marine record from the Balearic Sea. Quat. Int. 181 (1), 88–104.

Frisia, S., Borsato, A., Mangini, A., Spoetl, C., Madonia, G., Sauro, U., 2006. Holocene climate variability in Sicily from a discontinuous stalagmite record and the Mesolithic to Neolithic transition. Quat. Res. 66 (3), 388–400.

Frogley, M.R., Tzedakis, P.C., Heaton, T.H.E., 1999. Climate variability in Northwest Greece during the last interglacial. Science 285, 1886–1889.

Frumkin, A., Ford, D.C., Schwarcz, H.P., 1999. Continental oxygen isotopic record of the last 170,000 years in Jerusalem. Quat. Res. 51 (3), 317–327.

Frumkin, A., Ford, D.C., Schwarcz, H.P., 2000. Paleoclimate and vegetation of the last glacial cycles in Jerusalem from a speleothem record. Global Biogeochem. Cycles 14 (3), 863–870.

Ganopolski, A., Rahmstorf, S., 2001. Rapid changes of glacial climate simulated in a coupled climate model. Nature 409, 153–158.

Garcia-Castellanos, D., Estrada, F., Jimenez-Munt, J., Gorini, C., Fernandez, M., Vergés, J., et al., 2009. Catastrophic flood of the Mediterranean after the Messinian salinity crisis. Nature 462, 778–782.

Gardien, V., Vernoux, J., Lecuyer, C., Mangini, A., Ariztegui, D., Martineau, F., et al., 2010. Pinpointing rapid climate variability in SouthΘastern France during MIS 5 combining speleothems and mammal teeth. Eos Transactions AGU, Fall Meeting Supplement, 91 (26), Abstract PP21A-09.

Gautier, F., Clauzon, G., Suc, J.P., Cravatte, J., Violanti, D., 1994. Age and duration of the Messinian salinity crisis. C. R.Acad. Sci., Ser. II 318 (8), 1103–1109.

Gennari, G., Tamburini, F., Ariztegui, D., Hajdas, I., Spezzaferri, S., 2009. Geochemical evidence for high-resolution variations during deposition of the Holocene S1 sapropel on the Cretan Ridge, eastern Mediterranean. Palaeogeogr. Palaeoclimatol. Palaeoecol. 273, 239–248.

Gentil, L., 1918. Sur le synchronisme des depots et des movements orogeniques dans les detroits nord-betique et sudrifain. C. R. Acad. Sci. Paris, 167–727.

Genty, D., Blamart, D., Ouahdi, R., Gilmour, M., Baker, A., Jouzel, J., et al., 2003. Precise dating of Dansgaard–Oeschger climate oscillations in western Europe from stalagmite data. Nature 421, 833–837.

Genty, D., Combourieu-Nebout, N., Peyron, O., Blamart, D., Wainer, K., Mansuri, F., et al., 2010. Isotopic characterization of rapid climatic events during OIS3 and OIS4 in Villars Cave stalagmites (SW-France) and correlation with Atlantic and Mediterranean pollen records. Quat. Sci. Rev. 29 (19–20), 2799–2820.

Geraga, M., Tsaila-Monopolis, S., Ioakim, C., Papatheodorou, G., Ferentinos, G., 2005. Short-term climate changes in the southern Aegean Sea over the last 48,000 years. Palaeogeogr. Palaeoclimatol. Palaeoecol. 220 (3–4), 311–332.

Geraga, M., Ioakim, C., Lykousis, V., Tsaila-Monopolis, S., Mylona, G., 2010. The high-resolution palaeoclimatic and palaeoceanographic history of the last 24,000 years in the central Aegean Sea, Greece. Palaeogeogr. Palaeoclimatol. Palaeoecol. 287 (1–4), 101–115.

Gherardi, J.M., Labeyrie, L., McManus, J.F., Francois, R., Skinner, L.C., Cortijo, E., 2005. Evidence from the Northeastern Atlantic basin for variability in the rate of the meridional overturning circulation through the last deglaciation. Earth Planet. Sci. Lett. 240 (3–4), 710–723.

Gil-García, M.J., Dorado-Valiño, M., Valdeolmillos Rodríguez, A., Ruiz-Zapata, M.B., 2002. Late-glacial and Holocene palaeoclimatic record from Sierra de Cebollera (northern Iberian Range, Spain). Quat. Int. 93 (94), 13–18.

Giunta, S., Emeis, K.-C., Negri, A., 2001. Sea-surface temperature reconstruction of the last 16,000 years in the eastern Mediterranean Sea. Riv. Ital. Paleontol. Stratigr. 107, 463–476.

Giunta, S., Negri, A., Morigi, C., Capotondi, L., Combourieu-Nebout, N., Emeis, K.C., et al., 2003. Coccolithophorid ecostratigraphy and multi-proxy paleoceanographic reconstruction in the Southern Adriatic Sea during the last deglacial time (Core AD91-17). Palaeogeogr. Palaeoclimatol. Palaeoecol. 190, 39–59.

Gladstone, R.M., Ross, I., Valdes, P.J., Abe-Ouchi, A., Braconnot, P., Brewer, S., et al., 2005. Mid-Holocene NAO: a PMIP2 model intercomparison. Geophys. Res. Lett. 32, L16707. doi: 10.1029/2005GL023596.

Gogou, A., Bouloubassi, I., Lykousis, V., Arnaboldi, M., Gaitani, P., Meyers, P.A., 2007. Organic geochemical evidence of Late Glacial-Holocene climate instability in the North Aegean Sea. Palaeogeogr. Palaeoclimatol. Palaeoecol. 256 (1–2), 1–20.

Gómez-Orellana, L., Ramil-Rego, P., Muñoz Sobrino, C., 2007. The Würm in NW Iberia, a pollen record from Area Longa (Galicia). Quat. Res. 67, 438–452.

Gonzalez-Mora, B., Sierro, F.J., Schönfeld, J., 2008. Temperature and stable isotope variations in different water masses from the Alboran Sea (Western Mediterranean) between 250 and 150 ka. Geochem. Geophys. Geosyst. 9, Q10016. doi: 10.1029/2007GC001906.

González-Sampériz, P., Valero-Garcés, B.L., Carrion, J.S., Pena-Monne, J.L., Garcia-Ruiz, J.M., Marti-Bono, C., 2005. Glacial and Lateglacial vegetation in northeastern Spain: new data and a review. Quat. Int. 140 (14), 4–20.

Gonzalez-Samperiz, P., Valero-Garces, B.L., Moreno, A., Jalut, G., Garcia-Ruiz, J.M., Marti-Bono, C., et al., 2006. Climate variability in the Spanish Pyrenees during the last 30,000 yr revealed by the El Portalet sequence. Quat. Res. 66 (1), 38–52.

González-Sampériz, P., Valero-Garcés, B.L., Moreno, A., Morellón, M., Navas, A., Machín, J., et al., 2008. Vegetation changes and hydrological fluctuations in the Central Ebro Basin (NE Spain) since the Late Glacial period: saline lake records. Palaeogeogr. Palaeoclimatol. Palaeoecol. 259, 157–181.

Gonzalez-Samperiz, P., Utrilla, P., Mazo, C., Valero-Garces, B., Sopena, M.C., Morellon, M., et al., 2009. Patterns of human occupation during the early Holocene in the Central Ebro Basin (NE Spain) in response to the 8.2 ka climatic event. Quat. Res. 71 (2), 121–132.

Grootes, P.M., Stuiver, M., 1997. $^{18}O/^{16}O$ variability in Greenland snow and ice with 10^{-3} to 10^{5} year time resolution. J. Geophys. Res. 102 (C12), 26,455–26,470.

Guerra-Merchán, A., Serrano, F., Garcés, M., Gofas, S., Esu, D., Gliozzi, E., et al., 2010. Messinian Lago-Mare deposits near the Strait of Gibraltar (Malaga Basin, S Spain). Palaeogeogr. Palaeoclimatol. Palaeoecol. 285 (3–4), 264–276.

Guiter, F., Andrieu-Ponel, V., de Beaulieu, J.L., Cheddadi, R., Calvez, M., Ponel, P., et al., 2003. The last climatic cycles in western Europe: a comparison between long continuous lacustrine sequences from France and other terrestrial records. Quat. Int. 111, 59–74.

Hansen, B., Østerhus, S., 2000. North Atlantic—Nordic seas exchanges. Prog. Oceanogr. 45, 109–208.

Hansen, B., Turrell, W.R., Østerhus, S., 2001. Decreasing overflow from the Nordic seas into the Atlantic Ocean through the Faroe bank channel since 1950. Nature 411, 927–930.

Harrison, S.P., Digerfeldt, G., 1993. European lakes as palaeohydrological and palaeoclimatic indicators. Quat. Sci. Rev. 12 (4), 233–248.

Harzhauser, M., Piller, W.E., 2007. Benchmark data of a changing sea—Palaeogeography, palaeobiogeography and events in the central Paratethys during the Miocene. Palaeogeogr. Palaeoclimatol. Palaeoecol. 253, 8–31.

Haug, G.H., Tiedemann, R., 1998. Effect of the formation of the Isthmus of Panama on Atlantic Ocean thermohaline circulation. Nature 393, 673–676.

Hayes, A., Kucera, M., Kallel, N., Sbaffi, L., Rohling, E.J., 2005. Glacial Mediterranean sea surface temperatures based on planktonic foraminiferal assemblages. Quat. Sci. Rev. 24 (7–9), 999–1016.

Hays, J.D., Imbrie, J., Shackleton, N.J., 1976. Variations in the Earth's orbit: pacemaker of the Ice Ages. Science 194, 1121–1132.

Haywood, A.M., Sellwood, B.W., Valdes, P.J., 2000. Regional warming: Pliocene (3 Ma) paleoclimate of Europe and the Mediterranean. Geology 28 (12), 1063–1066.

Hazan, N., Stein, M., Marco, S., 2004. Lake Kinneret levels and active faulting in the Tiberias area. Isr. J. Earth Sci. 53, 199–205.

Hernandez-Molina, F.J., Llave, E., Stow, D.A.V., Garcia, M., Somoza, L., Vazquez, J.T., et al., 2006. The contourite depositional system of the Gulf of Cadiz: a sedimentary model related to the bottom current activity of the Mediterranean outflow water and its interaction with the continental margin. Deep Sea Res. II 53 (11–13), 1420–1463.

Hilgen, F.J., 1991a. Astronomical calibration of Gaus to Matuyama sapropels in the Mediterranean and implication fo the Gomagnetic Plarity Timescale. Earth Planet. Sci. Lett. 104 (2–4), 226–244.

Hilgen, F.J., 1991b. Extension of the astronomically calibrated (polarity) timescale to the Miocene/Pliocene boundary. Earth Planet. Sci. Lett. 107, 349–368.

Hilgen, F.J., Krijgsman, W., 1999. Cyclostratigraphy and astrochronology of the Tripoli diatomite formation (pre-evaporite Messinian, Sicily, Italy). Terra Nova 11, 16–22.

Hilgen, F.J., Kuiper, K.F., Krijgsman, W., Snel, E., van der Laan, E., 2007. Astronomical tuning as the basis for high resolution chronostratigraphy: the intricate history of the Messinian Salinity Crisis. Stratigraphy 4, 231–238.

Hodell, D.A., Curtis, J.H., Sierro, F.J., Raymo, M.E., 2001. Correlation of late Miocene to early Pliocene sequences between the Mediterranean and North Atlantic. Paleoceanography 16, 164–178.

Hooghiemstra, H., Stalling, H., Agwu, C.O.C., Dupont, L.M., 1992. Vegetational and climatic changes at the northern fringe of the Sahara 250,000–5000 years BP: evidence from 4 marine pollen records located between Portugal and the Canary Islands. Rev. Palaeobot. Palynol. 74, 1–53.

Hsü, K.J., Ryan, W.B.F., Cita, M.B., 1973. Late Miocene desiccation of the Mediterranean. Nature 242, 240–244.

Hsü, K.J., Montadert, L., Bernoulli, D., Cita, M.B., Erickson, A., Garrison, R.E., et al., 1977. History of the Mediterranean salinity crisis. Nature 267, 399–403.

Hughen, K.A., Overpeck, J.T., Peterson, L.C., Trumbore, S., 1996. Rapid climate changes in the tropical Atlantic region during the last deglaciation. Nature 380 (6569), 51–54.

Hunter, S., Wilkinson, D., Louarn, E., McCave, N., Rohling, E.J., Stow, D., et al., 2007. Deep western boundary current dynamics and associated sedimentation on the Eirik Drift, southern Greenland margin. Deep Sea Res. I 54, 2036–2066.

Huntley, B., Prentice, I.C., 1988. July temperatures in Europe from pollen data, 6000 years before present. Science 241, 687–690.

Hüsing, S.K., Zachariasse, W.J., Van Hinsbergen, D.J.J., Krijgsman, W., Inceöz, M., Harzhauser, M., et al., 2009. Oligo-Miocene foreland basin evolution in SE Anatolia: implications for the closure of the eastern Tethys gateway. In: van Hinsbergen, D.J.J., Edwards, M.A., Govers, R. (Eds.), Geodynamics of Collision and Collapse at the Africa–Arabia–Eurasia subduction zone. Geological Society of London Special Publication, London, pp. 107–132.

Iaccarino, S., Bossio, A., 1999. Paleoenvironment of uppermost Messinian sequences in the western Mediterranean (Sites 974, 975, and 978). In: Zahn, R., Comas, M.C., Klaus, A. (Eds.), Proceedings of the Ocean Drilling Program, Scientific Results. Ocean Drilling Program, College Station, TX, pp. 529–541.

Imbrie, J., Imbrie, K.P., 1979. Ice ages. Solving the mystery. Prog. Phys. Geogr. 6, 606–608.

Incarbona, A., Di Stefano, E., Sprovieri, R., Bonomo, S., Censi, P., Dinares-Turell, J., et al., 2008. Variability in the vertical structure of the water column and paleoproductivity reconstruction in the central-western Mediterranean during the Late Pleistocene. Mar. Micropaleontol. 69 (1), 26–41.

Incarbona, A., Di Stefano, E., Sprovieri, R., Bonomo, S., Pelosi, N., Sprovieri, M., 2010. Millennial-scale paleoenvironmental changes in the central Mediterranean during the last interglacial: comparison with European and North Atlantic records. Geobios 43 (1), 111–122.

Iversen, J., 1954. The Late Glacial flora of Denmark and its relations to climate and soil. Danmarks Geologiske Undersøgelser 80, 87–119.

Jacob, D., Goettel, H., Jungclaus, J., Muskulus, M., Podzun, R., Marotzke, J., 2005. Slowdown of the thermohaline circulation causes enhanced maritime climate influence and snow cover over Europe. Geophys. Res. Lett. 32, L21711. doi: 10.1029/2005GL023286.

Jalut, G., Esteban Amat, A., Bonnet, L., Gauquelin, T., Fontugne, M., 2000. Holocene climatic changes in the Western Mediterranean, from south-east France to south-east Spain. Palaeogeogr. Palaeoclimatol. Palaeoecol. 160 (3–4), 255–290.

Jalut, G., Carrion, J., David, F., Gonzalez Samperiz, P., Sanchez Goni, M.F., Tonkov, S., et al., 2005. The vegetation around the Mediterranean basin during the Last Glacial Maximum and the Holocene climatic optimum. In: Petit-Maire, N., Vrielinck, B. (Eds.), The Mediterranean Basin: The Last Two Climatic Extremes. Explanatory Notes of the Maps. Two Maps, Scale 1:5 000 000 N, Agence Nationale pour la Gestión des Déchets Radioactifs, Chátenay-Malabry CEDEX, pp. 37–57.

Jalut, G., Dedoubat, J.J., Fontugne, M., Otto, T., 2009. Holocene circum-Mediterranean vegetation changes: climate forcing and human impact. Quat. Int. 200 (1–2), 4–18.

Jansen, E., Overpeck, J., Briffa, K.R., Duplessy, J.-C., Joos, F., Masson-Delmotte, V., et al., 2007. Palaeoclimate. In: Solomon, S. (Ed.), Climate Change 2007: The Physical Science Basis Contribution of Working Group I to the Fourth Assessment Report of the Intergovernmental Panel on Climate Change. Cambridge University Press, pp. 433–497.

Jimenez-Espejo, F.J., Martinez-Ruiz, F., Sakamoto, T., Iijima, K., Gallego-Torres, D., Harada, N., 2007. Paleoenvironmental changes in the western Mediterranean since the last glacial maximum: high resolution multiproxy record from the Algero-Balearic basin. Palaeogeogr. Palaeoclimatol. Palaeoecol. 246 (2–4), 292–306.

Jimenez-Espejo, F.J., Martinez-Ruiz, F., Rogerson, M., González-Donoso, J.M., Romero, O.E., Linares, D., et al., 2008. Detrital input, productivity fluctuations, and water mass circulation in the westernmost Mediterranean Sea since the Last Glacial Maximum. Geochem. Geophys. Geosyst. 9, Q11U02. doi: 10.1029/2008GC002096.

Jimenez-Moreno, G., Fauquette, S., Suc, J.P., 2010. Miocene to Pliocene vegetation reconstruction and climate estimates in the Iberian Peninsula from pollen data. Rev. Paleobot. Palinol. 162 (3), 403–415.

Johnsen, S.J., Clausen, H.B., Dansgaard, W., Fuhrer, K., Gundestrup, N., Hammer, C.U., et al., 1992. Irregular glacial interstadials recorded in a new Greenland ice core. Nature 359, 311–313.

Johnsen, S.J., Dahl-Jensen, D., Gundestrup, N.S., Steffensen, J.P., Clausen, H.B., Miller, H., et al., 2001. Oxygen isotope and palaeotemperature records from six Greenland ice-core stations: Camp Century, Dye-3, GRIP, GISP, Renland and NorthGRIP. J. Quat. Sci. 16, 299–307.

Jorissen, F.J., Asioli, A., Borsetti, A.M., Capotondi, L., Devisser, J.P., Hilgen, F.J., et al., 1993. Late Quaternary Central Mediterranean Biochronology. Mar. Micropaleontol. 21 (1–3), 169–189.

Jorissen, F.J., 1999. Benthic foraminiferal successions across Late Quaternary Mediterranean sapropels. Mar. Geol. 153, 91–101.

Jost, A., Fauquette, J.A., Kageyama, M., Krinner, S., Ramstein, G., Suc, J.P., et al., 2009. High resolution climate and vegetation simulations of the Late Pliocene, a model-data comparison over western Europe and the Mediterranean region. Clim. Past 5 (4), 585–606.

Jouzel, J., Masson-Delmotte, V., Cattani, O., Dreyfus, G., Falourd, S., Hoffmann, G., et al., 2007. Orbital and millennial Antarctic climate variability over the past 800,000 years. Science 317 (5839), 793–796.

Kallel, N., Paterne, M., Duplessy, J.C., Vergnaud-Grazzini, C., Pujol, C., Labeyrie, L., et al., 1997a. Enhanced rainfall on Mediterranean region during the last sapropel event. Oceanolog. Acta 20, 697–712.

Kallel, N., Paterne, M., Labeyrie, L.D., Duplessy, J.C., Arnold, M., 1997b. Temperature and salinity records of the Tyrrhenian sea during the last 18 000 years. Palaeogeogr. Palaeoclimatol. Palaeoecol. 135, 97–108.

Keigwin, L.D., Lehman, S.J., 1994. Deep circulation change linked to Heinrich Event 1 and Younger Dryas in a middepth North Atlantic core. Paleoceanography 9 (2), 185–194.

Kennett, J., 1982. Marine Geology. Prentice-Hall, Englewood Cliffs, p. 813.

Khelifi, N., Sarnthein, M., Andersen, N., Blanz, T., Frank, M., Garbe-Schönberg, D., et al., 2009. A major and long-term Pliocene intensification of the Mediterranean outflow, 3.5–3.3 Ma ago. Geology 37 (9), 811–814.

Kiage, L.M., Liu, K.-B., 2006. Late Quaternary paleoenvironmental changes in East Africa: a review of multiproxy evidence from palynology, lake sediments, and associated records. Prog. Phys. Geogr. 30 (5), 633–658.

Kim, J.H., Rimbu, N., Lorenz, S.J., Lohmann, G., Nam, S.I., Schouten, S., et al., 2004. North Pacific and North Atlantic sea-surface temperature variability during the Holocene. Quat. Sci. Rev. 23 (20–22), 2141–2154.

Kleiven, H.F., Catherine, K., Laj, C., Ninnemann, U.S., Richter, T.O., Cortijo, E., 2008. Reduced North Atlantic deep water coeval with the glacial Lake Agassiz freshwater outburst. Science 319, 60–64.

Kotthoff, U., Müller, U.C., Pross, J., Schmiedl, G., Lawson, I.T., van de Schootbrugge, B., et al., 2008a. Lateglacial and Holocene vegetation dynamics in the Aegean region: an integrated view based on pollen data from marine and terrestrial archives. Holocene 18, 1019–1032.

Kotthoff, U., Pross, J., Müller, U.C., Peyron, O., Schmiedl, G., Schulz, H., et al., 2008b. Climate dynamics in the borderlands of the Aegean Sea during formation of sapropel S1 deduced from a marine pollen record. Quat. Sci. Rev. 27 (7–8), 832–845.

Kouwenhoven, T.J., Seidenkrantz, M.S., van der Zwaan, G.J., 1999. Deep-water changes: the near-synchronous disappearance of a group of benthic foraminifera from the Late Miocene Mediterranean. Palaeogeogr. Palaeoclimatol. Palaeoecol. 152, 259–281.

Kouwenhoven, T.J., Hilgen, F.J., van der Zwaan, G.J., 2003. Late Tortonian–early Messinian stepwise disruption of the Mediterranean–Atlantic connections: constraints from benthic foraminiferal and geochemical data. Palaeogeogr. Palaeoclimatol. Palaeoecol. 18, 303–319.

Krijgsman, W., Meijer, P.T., 2008. Depositional environments of the Mediterranean "Lower Evaporites" of the Messinian salinity crisis: constraints from quantitative analyses. Mar. Geol. 253, 73–81.

Krijgsman, W., Hilgen, F.J., Raffi, I., Sierro, F.J., Wilson, D.S., 1999. Chronology, causes and progression of the Messinian salinity crisis. Nature 400, 652–655.

Krijgsman, W., Hilgen, F.J., Fortuin, A., Sierro, F.J., 2001. Astrochronology for the Messinian Sorbas Basin (SE Spain) and orbital (precessional) forcing for evaporate cyclicity. Sediment. Geol. 140, 43–60.

Kroon, D., Alexander, I., Little, M., Lourens, L.J., Matthewson, A., Robertson, A.H.F., et al., 1998. Oxygen isotope and sapropel stratigraphy in the eastern Mediterranean during the last 3.2 million years. In: Robertson, A.H.F., Emeis, K.-C., Richter, C., Camerlenghi, A. (Eds.), Proceedings of the Ocean Drilling Program, Scientific Results. Ocean Drilling Program, College Statio, TX, pp. 181–189.

Kuhnt, T., Schmiedl, G., Ehrmann, W., Hamann, Y., Hemleben, C., 2007. Deep-sea ecosystem variability of the Aegean Sea during the past 22 kyr as revealed by Benthic Foraminifera. Mar. Micropaleontol. 64, 141–162.

Kuhnt, T., Schmiedl, G., Ehrmann, W., Hamann, Y., Andersen, N., 2008. Stable isotopic composition of Holocene benthic foraminifers from the eastern Mediterranean Sea: past changes in productivity and deep water oxygenation. Palaeogeogr. Palaeoclimatol. Palaeoecol. 268 (1–2), 106–115.

Kukla, G.J., Bender, M.L., de Beaulieu, J.L., Bond, G., Broecker, W.S., Cleveringa, P., et al., 2002. Last interglacial climates. Quat. Res. 58 (1), 2–13.

van der Laan, E., Gaboardi, S., Hilgen, F.J., Lourens, L.J., 2005. Regional climate and glacial control on high-resolution oxygen isotope records from Ain El Beida (latest Miocene, NW Morocco): a cyclostratigraphic analysis in the depth and time domain. Paleoceanography 20, PA1001. doi: 10.1029/2003PA000995.

van der Laan, E., Snel, E., De Kaenel, E., Hilgen, F.J., Krijgsman, W., 2006. No major deglaciation across the Miocene-Pliocene boundary: integrated stratigraphy and astronomical tuning of the Loulja section (Bou Regreg area, NW Morocco). Paleoceanography 21, PA3011. doi: 10.1029/2005PA001193.

Lamb, H.F., van der Kaars, S., 1995. Vegetational response to Holocene climatic change: pollen and palaeolimnological data from the Middle Atlas, Morocco. Holocene 5, 400–408.

Lamb, H.F., Eicher, U., Switsur, V.R., 1989. An 18,000 year record of vegetation, lake-level and climatic change from the Middle Atlas, Morocco. J. Biogeogr. 16, 65–74.

Lamb, H.F., Gasse, F., Benkaddour, A., El Hamouti, N., van der Kaars, S., Perkins, W.T., et al., 1995. Relation between century-scale Holocene arid intervals in tropical and temperate zones. Nature 373, 134–137.

de Lange, G.J., Krijgsman, W., 2010. Messinian Salinity Crisis: a novel unifying shallow gypsum/deep dolomite formation mechanism. Mar. Geol. 275, 273–277.

de Lange, G.J., Thomson, J., Reitz, A., Slomp, C.P., Principato, M.S., Erba, E., et al., 2008. Synchronous basin-wide formation redox-controlled preservation of Mediterranean sapropel. Nat. Geosci. 1, 606–610.

Laskar, J., Robutel, P., Joutel, F., Gastineau, M., Correia, A.C.M., Levrard, B., 2004. A long-term numerical solution for the insolation quantities of the Earth. Astron. Astrophys. 428, 261–285.

Lawson, I.T., Frogley, M., Bryant, C., Preece, R., Tzedakis, P.C., 2004. The Lateglacial and Holocene environmental history of the Ioannina basin, north-west Greece. Quat. Sci. Rev. 23, 1599–1625.

LeGrande, A.N., Schmidt, G.A., Shindell, D.T., Field, C.V., Miller, R.L., Koch, D.M., et al., 2006. Consistent simulations of multiple proxy responses to an abrupt climate change event. Proc. Nat. Acad. Sci. 103, 837–842.

Leroy, S.A.G., Giralt, S., Francus, P., Seret, G., 1996. The high sensitivity of the palynological record in the Vico Maar Lacustrine sequence (Latium, Italy) highlights the climatic gradient through Italy for the last 90 ka. Quat. Sci. Rev. 15, 189–201.

Lézine, A.-M., Denèfle, M., 1997. Enhanced anticyclonic circulation in the eastern North Atlantic during cold intervals of the last deglaciation inferred from deep-sea pollen records. Geology 25, 119–122.

Lisiecki, L.E., Raymo, M., 2005. A Pliocene-Pleistocene stack of 57 globally distributed benthic $\delta^{18}O$ records. Paleoceanography 20, PA1003. doi: 10.1029/2004PA001071.

Lofi, J., Gorini, C., Berné, S., Clauzon, G., Tadeu Dos Reis, A., Ryan, W.B.F., et al., 2005. Erosional processes and paleo environmental changes in the Western Gulf of Lions (SW France) during the Messinian Salinity Crisis. Mar. Geol. 217 (1–2), 1–30.

Lofi, J., Deverchere, J., Gaullier, J., Gillet, H., Gorini, C., Guennoc, P., et al., 2008. The Messinian Salinity Crisis in the offshore domain: an overview of our knowledge through seismic profile interpretation and multi-site approach. In: Briand, F. (Ed.), CIESM 2008. The Messinian Salinity Crisis from Mega-deposits to Microbiology—A Consensus Report. CIESM Workshop Monographs, Monaco, pp. 83–90.

Loget, N., van den Driessche, J., 2006. On the origin of the Strait of Gibraltar. Sediment. Geol. 1880–189, 341–346.

Loulergue, L., Schilt, A., Spahni, R., Masson-Delmotte, V., Blunier, T., Lemieux, B., et al., 2008. Orbital and millennial-scale features of atmospheric CH_4 over the past 800,000 years. Nature 453 (7193), 383–386.

Lourens, L.J., Antonarakou, A., Hilgen, F.J., Van Hoof, A.A.M., Vergnaud-Grazzini, C., Zachariasse, W.J., 1996. Evaluation of the Plio-Pleistocene astronomical timescale. Paleoceanography 11 (4), 391–413.

Lowe, J.J., Rasmussen, S.O., Bjorck, S., Hoek, W.Z., Steffensen, J.P., Walker, M.J.C., et al., 2008. Synchronisation of palaeoenvironmental events in the North Atlantic region during the last termination: a revised protocol recommended by the INTIMATE group (INTegration of Ice-core, Marine and Terrestrial records (INTIMATE)): refining the record of the Last Glacial–Interglacial Transition. Quat. Sci. Rev. 27 (1–2), 6–17.

Löwemark, L., Lin, Y., Chen, H.-F., Yang, T.-N., Beier, C., Werner, F., et al., 2006. Sapropel burn-down and ichnological response to late Quaternary sapropel formation in two ~400 ky records from the eastern Mediterranean Sea. Palaeogeogr. Palaeoclimatol. Palaeoecol. 239, 406–425.

Lugli, S., Manzi, M., Roveri, M., 2008. New facies interpretation of the Messinian evaporites in the Mediterranean. In: Briand, F. (Ed.), CIESM 2008. The Messinian Salinity Crisis from Mega-Deposits to Microbiology—A Consensus Report, Monaco, pp. 67–72.

Lugli, S., Manzi, V., Roveri, M., Schreiber, C., 2010. The Primary Lower Gypsum in the Mediterranean: a new facies interpretation for the first stage of the Messinian salinity crisis. Palaeogeogr. Palaeoclimatol. Palaeoecol. 297, 83–99.

Lyell, C., 1830. Principles of Geology, Being an Attempt to Explain the Former Changes of the Earth's Surface, by Reference to Causes Now in Operation. John Murray, London, p. 511.

Magny, M., Guiot, J., Schoellammer, P., 2001. Quantitative reconstruction of Younger Dryas to Mid-Holocene Paleoclimates at Le Locle, Swiss Jura, using pollen and lake-level data. Quat. Res. 56, 170–180.

Magny, M., Aalbersberg, G., Bégeot, C., Benoit-Ruffaldi, P., Bossuet, G., Disnar, J.-R., et al., 2006. Environmental and climatic changes in the Jura mountains (eastern France) during the Lateglacial-Holocene transition: a multi-proxy record from Lake Lautrey. Quat. Sci. Rev. 25 (5–6), 414–445.

Magri, D., 1994. Late-Quaternary changes of plant biomass as recorded by pollen-stratigraphical data: a discussion of the problem at Valle di Castiglione, Italy. Rev. Palaeobot. Palynol. 81, 313–325.

Magri, D., 1999. Late Quaternary vegetation history at Lagaccione near Lago di Bolsena (central Italy). Rev. Palaeobot. Palynol. 106, 171–208.

Magri, D., Parra, I., 2002. Late Quaternary western Mediterranean pollen records and African winds. Earth Planet. Sci. Lett. 200 (3–4), 401–408.

Magri, D., Sadori, L., 1999. Late Pleistocene and Holocene pollen stratigraphy at Lago di Vico (central Italy). Veg. Hist. Archaeobot. 8, 247–260.

Malanotte-Rizzoli, P., Manca, B.B., d'Alcala, M.R., Theocharis, A., Brenner, S., Budillon, G., et al., 1999. The eastern Mediterranean in the 80s and in the 90s: the big transition in the intermediate and deep circulations. Dyn. Atmos. Oceans 29, 365–395.

Mangerud, J., Andersen, S.V., Berglund, B.E., Donner, J.J., 1974. Quaternary stratigraphy of Norden, a propossal for terminology and classification. Boreas 3, 109–128.

Manzi, V., Lugli, S., Ricci-Lucchi, F., Roveri, M., 2005. Deep water clastic evaporites deposition in the Messinian Adriatic foredeep (northern Apennines, Italy): did the Mediterranean ever dry out? Sedimentology 52 (4), 875–902.

Manzi, V., Roveri, M., Gennari, R., Bertini, A., Biffi, U., Giunta, S., et al., 2007. The deep-water counterpart of the Messinian lower evaporites in the Apennine foredeep: the Fanantello section (Northern Apennines, Italy). Palaeogeogr. Palaeoclimatol. Palaeoecol. 251 (3–4), 470–499.

Manzi, V., Lugli, S., Roveri, M., Schreiber, B.C., 2009. A new facies model for the Upper Gypsum of Sicily (Italy): chronological and palaeoenvironmental constraints for the Messinian salinity crisis in the Mediterranean. Sedimentology 56 (7), 1937–1960.

Marchal, O., Cacho, I., Stocker, T.F., Grimalt, J.O., Calvo, E., Martrat, B., et al., 2002. Apparent long-term cooling of the sea surface in the northeast Atlantic and Mediterranean during the Holocene. Quat. Sci. Rev. 21 (4–6), 455–483.

Margari, V., Gibbard, P.L., Bryant, C.L., Tzedakis, P.C., 2009. Character of vegetational and environmental changes in southern Europe during the last glacial period; evidence from Lesvos Island, Greece. Quat. Sci. Rev. 28 (13–14), 1317–1339.

Margari, V., Skinner, L.C., Tzedakis, P.C., Ganopolski, A., Vautravers, M., Shackleton, N.J., 2010. The nature of millennial-scale climate variability during the past two glacial periods. Nat. Geosci. 3 (2), 127–131.

Marino, G., Rohling, E.J., Rijpstra, W.I.C., Sangiorgi, F., Schouten, S., Sinninghe Damste, J.S., 2007. Aegean Sea as driver of hydrographic and ecological changes in the eastern Mediterranean. Geology 35 (8), 675–678.

Marino, G., Rohling, E.J., Sangiorgi, F., Hayes, A., Casford, J.L., Lotter, A.F., et al., 2009. Early and middle Holocene in the Aegean Sea: interplay between high and low latitude climate variability. Quat. Sci. Rev. 28, 3246–3262.

Marra, F., Florindo, F., Boschi, E., 2008. History of glacial terminations from the Tiber River, Rome: insights into glacial forcing mechanisms. Paleoceanography 23, PA2205. doi: 10.1029/2007PA001543.

Marret, F., Turon, J.-L., 1994. Paleohydrology and paleoclimatology off Northwest Africa during the last glacial–interglacial transition and the Holocene: palynological evidences. Mar. Geol. 118, 107–117.

Martinez-Ruiz, F., Kastner, M., Paytan, A., Ortega-Huertas, M., Bernasconi, S.M., 2000. Geochemical evidence for enhanced productivity during S1 sapropel deposition in the eastern Mediterranean. Paleoceanography 15 (2), 200–209.

Martrat, B., Grimalt, J.O., Lopez-Martinez, C., Cacho, I., Sierro, F.J., Flores, J.A., et al., 2004. Abrupt temperature changes in the western Mediterranean over the past 250,000 years. Science 306 (5702), 1762–1765.

Martrat, B., Grimalt, J.O., Shackleton, N.J., de Abreu, L., Hutterli, M.A., Stocker, T.F., 2007. Four climate cycls of recurring deep and surface water destabilizations on the Iberian margin. Science 317, 502–507.

Mayewski, P.A., Rohling, E.E., Stager, J.C., Karlen, W., Maasch, K.A., Meeker, L.D., et al., 2004. Holocene climate variability. Quat. Res. 62 (3), 243–255.

McManus, J.F., Francois, R., Gherardi, J.-M., Keigwin, L.D., Brown-Leger, S., 2004. Collapse and rapid resumption of Atlantic meridional circulation linked to deglacial climate changes. Nature 428 (6985), 834–837.

van der Meer, M.T.J., Baas, M., Rijpstra, W.I.C., Marino, G., Rohling, E.J., Sinninghe Damste, J.S., et al., 2007. Hydrogen isotopic compositions of long-chain alkenones record freshwater flooding of the eastern Mediterranean at the onset of sapropel deposition. Earth Planet. Sci. Lett. 262 (3–4), 594–600.

Meijer, P.T., 2006. A box model of the blocked-outflow scenario for the Messinian Salinity Crisis. Earth Planet. Sci. Lett. 248, 471–479.

Meijer, P.T., Krijgsman, W., 2005. A quantitative analysis of the desiccation and re-filling of the Mediterranean during the Messinian Salinity Crisis. Earth Planet. Sci. Lett. 240, 510–520.

Melki, T., Kallel, N., Jorissen, F.J., Guichard, F., Dennielou, B., Berne, S., et al., 2009. Abrupt climate change, sea surface salinity and paleoproductivity in the western Mediterranean Sea (Gulf of Lion) during the last 28 kyr. Palaeogeogr. Palaeoclimatol. Palaeoecol. 279 (1–2), 96–113.

Mercone, D., Thomson, J., Abu-Zied, R.H., Croudace, I.W., Rohling, E.J., 2001. High-resolution geochemical and micropalaeontological profiling of the most recent eastern Mediterranean sapropel. Mar. Geol. 177, 25–44.

Milankovitch, M., 1920. Theorie Mathematique des Phenomenes Thermiques produits par la Radiation Solaire. Gauthier-Villars, Paris.

Montadert, L., Sancho, J., Fail, J.P., Debyser, J., Winnock, E., 1970. De l'âge tertiaire de la série salifère responsable des structures diapiriques en Méditerranée Occidentale (Nord-Est des Baléares). C. R. Acad. Sci. Paris 271, 812–815.

Morellón, M., Valero-Garcés, B., Moreno, A., González-Sampériz, P., Mata, P., Romero, O., et al., 2008. Holocene palaeohydrology and climate variability in northeastern Spain: the sedimentary record of Lake Estanya (Pre-Pyrenean range). Quat. Int. 181, 15–31.

Morellón, M., Valero-Garcés, B., Vegas-Vilarrúbia, T., González-Sampériz, P., Romero, Ó., Delgado-Huertas, A., et al., 2009. Lateglacial and Holocene palaeohydrology in the western Mediterranean region: the Lake Estanya record (NE Spain). Quat. Sci. Rev. 28 (25–26), 2582–2599.

Moreno, A., Cacho, I., Canals, M., Prins, M.A., Sanchez-Goni, M.-F., Grimalt, J.O., et al., 2002. Saharan dust transport and high-latitude glacial climatic variability: the Alboran Sea record. Quat. Res. 58 (3), 318–328.

Moreno, A., Cacho, I., Canals, M., Grimalt, J.O., Sanchez-Vidal, A., 2004. Millennial-scale variability in the productivity signal from the Alboran Sea record, Western Mediterranean Sea. Palaeogeogr. Palaeoclimatol. Palaeoecol. 211 (3–4), 205–219.

Moreno, A., Cacho, I., Canals, M., Grimalt, J.O., Sanchez-Goni, M.F., Shackleton, N., et al., 2005. Links between marine and atmospheric processes oscillating on a millennial time-scale. A multi-proxy study of the last 50,000 yr from the Alboran Sea (Western Mediterranean Sea). Quat. Sci. Rev. 24 (14–15), 1623–1636.

Moreno, A., Stoll, H., Jiménez-Sánchez, M., Cacho, I., Valero-Garcés, B., Ito, E., et al., 2010. A speleothem record of glacial (25–11.6 kyr BP) rapid climatic changes from northern Iberian Peninsula. Global Planet. Change 71, 218–231.

Moreno, A., Gonzalez-Samperiz, P., Morellon, M., Valero-Garces, B.L., Fletcher, W.J., 2012. Northern Iberian abrupt climate change dynamics during the last glacial cycle: a view from lacustrine sediments. Quat. Sci. Rev. 36(0), 139–153. doi: 10.1016/j.quascirev.2010.06.031.

Mudie, P.J., Rochon, A., Aksu, A.E., 2002. Pollen stratigraphy of Late Quaternary cores from Marmara Sea: land–sea correlation and paleoclimatic history. Mar. Geol. 190 (1–2), 233–260.

Muñoz-Sobrino, C., Ramil Rego, P., Rodríguez Guitián, M., 1997. Upland vegetation in the north-west Iberian Peninsula after the last glaciation: forest history and deforestation dynamics. Veg. Hist. Archaeobot. 6, 215–233.

Muñoz-Sobrino, C., Ramil-Rego, P., Rodríguez Guitián, M.A., 2001. Vegetation in the mountains of northwest Iberia during the last glacial–interglacial transition. Veg. Hist. Archaeobot. 10, 7–21.

Muñoz-Sobrino, C., Ramil-Rego, P., Gómez-Orellana, L., 2004. Vegetation of the Lago de Sanabria area (NW Iberia) since the end of the Pleistocene: a palaeoecological reconstruction on the basis of two new pollen sequences. Veg. Hist. Archaeobot. 13, 1–22.

Muñoz-Sobrino, C., Ramil-Rego, P., Gómez-Orellana, L., Díaz Varela, R.A., 2005. Palynological data on major Holocene climatic events in NW Iberia. Boreas 34, 381–400.

Myers, P.G., Rohling, E.J., 2000. Modeling a 200-yr interruption of the Holocene sapropel S1. Quat. Res. 55, 98–104.

Narcisi, B., 2001. Palaeoenvironmental and palaeoclimatic implications of the Late-Quaternary sediment record of Vico volcanic lake (central Italy). J. Quat. Sci. 16, 245–255.

Naughton, F., Bourillet, J.-F., Sanchez Goni, M.F., Turon, J.-L., Jouanneau, J.-M., 2007a. Long-term and millennial-scale climate variability in northwestern France during the last 8850 years. Holocene 17 (7), 939–953.

Naughton, F., Sanchez Goni, M.F., Desprat, S., Turon, J.L., Duprat, J., Malaize, B., et al., 2007b. Present-day and past (last 25 000 years) marine pollen signal off western Iberia. Mar. Micropaleontol. 62 (2), 91–114.

Naughton, F., Sanchez Goñi, M.F., Kageyama, M., Bard, E., Duprat, J., Cortijo, E., et al., 2009. Wet to dry climatic trend in north-western Iberia within Heinrich events. Earth Planet. Sci. Lett. 284 (3–4), 329–342.

NGRIP members, 2004. High-resolution record of Northern Hemisphere climate extending into the last interglacial period. Nature 431 (7005), 147–151.

Niklewski, J., van Zeist, W., 1970. A late quaternary pollen diagram from northwestern Syria. Acta Bot. Neerl. 19, 737–754.

Oppo, D.W., Lehman, S., 1995. Suborbital variability of North Atlantic deep water during the past 200,000 years. Paleoceanography 10, 901–910.

Oppo, D.W., McManus, J.F., Cullen, J.L., 2006. Evolution and demise of the Last Interglacial warmth in the subpolar North Atlantic. Quat. Sci. Rev. 25 (23–24), 3268–3277.

Osborne, A.H., Vance, D., Rohling, E.J., Barton, N., Rogerson, M., Fello, N., 2008. A humid corridor across the Sahara for the migration "Out of Africa" of early modern humans 120,000 years ago. Proc. Nat. Acad. Sci. 105, 16444–16447.

Osborne, A.H., Marino, G., Vance, D., Rohling, E.J., 2010. Eastern Mediterranean surface water Nd during Eemian sapropel S5: monitoring northerly (mid-latitude) versus southerly (sub-tropical) freshwater contributions. Quat. Sci. Rev. 29 (19–20), 2473–2483.

Pailler, D., Bard, E., 2002. High frequency palaeoceanographic changes during the past 140000 yr recorded by the organic matter in sediments of the Iberian Margin. Palaeogeogr. Palaeoclimatol. Palaeoecol. 181 (4), 431–452.

Paterne, M., Kallel, N., Labeyrie, L., Vautravers, M., Duplessy, J.C., Rossignol-Strick, M., et al., 1999. Hydrological relationship between the North Atlantic and the Mediterranean Sea during the past 15–75 kyr. Paleoceanography 14, 626–638.

Peltier, W.R., Fairbanks, R.G., 2006. Global glacial ice volume and Last Glacial Maximum duration from an extended Barbados sea level record. Quat. Sci. Rev. 25, 3322–3337.

Peñalba, C., 1994. The history of the Holocene vegetation in northern Spain from pollen analysis. J. Ecol. 82, 815–832.

Peñalba, M.C., Arnold, M., Guiot, J., Duplessy, J.-C., de Beaulieu, J.-L., 1997. Termination of the Last Glaciation in the Iberian Peninsula inferred from the pollen sequence of Quintanar de la Sierra. Quat. Res. 48, 205–214.

Penaud, A., Eynaud, F., Turon, J.L., Blamart, D., Rossignol, L., Marret, F., et al., 2010. Contrasting paleoceanographic conditions off Morocco during Heinrich events (1 and 2) and the Last Glacial Maximum. Quat. Sci. Rev. 29 (15–16), 1923–1939.

Perez-Obiol, R., Julia, R., 1994. Climatic change on the Iberian Peninsula recorded in a 30,000-yr pollen record from Lake Banyoles. Quat. Res. 41 (1), 91–98.

Petit, J.R., Jouzel, J., Raynaud, D., Barkov, N.I., Barnola, J.M., Basile, I., et al., 1999. Climate and atmospheric history of the past 420,000 years from the Vostok ice core, Antarctica. Nature 399, 429–436.

Pinardi, N., Masetti, E., 2000. Variability of large scale general circulation of the Mediterranean Sea from observations and modelling: a review. Palaeogeogr. Palaeoclimatol. Palaeoecol. 158, 153–174.

Pini, R., Ravazzi, C., Donegana, M., 2009. Pollen stratigraphy, vegetation and climate history of the last 215 ka in the Azzano Decimo core (plain of Friuli, north-eastern Italy). Quat. Sci. Rev. 28, 1268–1290.

Piva, A., Asioli, A., Andersen, N., Grimalt, J.O., Schneider, R.R., Trincardi, F., 2008. Climatic cycles as expressed in sediments of the PROMESS1 borehole PRAD1-2, central Adriatic, for the last 370 ka: 2. Paleoenvironmental evolution. Geochem. Geophys. Geosyst. 9, Q03R02. doi: 10.1029/2007GC001785.

Pla, S., Catalan, J., 2005. Chrysophyte cysts from lake sediments reveal the submillennial winter/spring climate variability in the northwestern Mediterranean region throughout the Holocene. Clim. Dyn. 24 (2–3), 263–278.

Pons, A., Reille, M., 1988. The Holocene- and upper Pleistocene pollen record from Padul (Granada, Spain): a new study. Palaeogeogr. Palaeoclimatol. Palaeoecol. 66 (3–4), 243–249.

Popescu, S.M., Biltekin, D., Winter, H., Suc, J.P., Melinte-Dobrinescu, M.C., Klotz, S.R., et al., 2010. Pliocene and Lower Pleistocene vegetation and climate changes at the European scale: long pollen records and climatostratigraphy. Quat. Int. 219 (1–2), 152–167.

Popov, S.V., Stolyarov, A.S., 1996. Paleogeography and anoxic environments of the Oligocene–Early Miocene Eastern Paratethys. Isr. J. Earth Sci. 45 (3), 161–167.

Popov, S.V., Shcherba, I.G., Ilyina, L.B., Nevesshaya, L.A., Paramonova, N.P., Khondkarian, S.O., et al., 2006. Late Miocene to Pliocene palaeogeography of the Paratethys and its relation to the Mediterranean. Palaeogeogr. Palaeoclimatol. Palaeoecol. 236, 91–106.

Pross, J., Kotthoff, U., Müller, U.C., Peyron, O., Dormoy, I., Schmiedl, G., et al., 2010. Massive perturbation in terrestrial ecosystems of the eastern Mediterranean region associated with the 8.2 kyr B.P. climatic event. Geology 37, 887–890.

Ramstein, G., Fluteau, F., Besse, J., Joussaume, S., 1997. Effect of orogeny, plate motion and land sea distribution on Eurasian climate change over the last 30 million years. Nature 386, 788–795.

Reille, M., Andrieu, V., 1995. The late Pleistocene and Holocene in the Lourdes Basin, Western Pyrénées, France: new pollen analytical and chronological data. Veg. Hist. Archaeobot. 4, 1–21.

Reille, M., Beaulieu, J.L., 1989. The Velay maars (Massif Central, France): key-sites for the Middle and Upper Pleistocene pollen sequences. In: Rose, J., Schlichter, C. (Eds.), Quaternary Type Sections: Imagination or Reality? Balkema, Rotterdam, pp. 79–89.

Reille, M., de Beaulieu, J.L., 1988a. The end of the Eemian and the Prewurm interstadials as evidenced for the 1st time in the French Massif Central from pollen analysis. C. R. Acad. Sci. Ser. II 306 (16), 1205–1210.

Reille, M., de Beaulieu, J.L., 1988b. History of the Wurm and Holocene vegetation in western Velay (Massif Central, France)—a comparison of pollen analysis from 3 corings at Lac-Du-Bouchet. Rev. Palaeobot. Palynol. 54 (3–4), 233–248.

Reille, M., de Beaulieu, J.L., 1990. Pollen analysis of a long Upper Pleistocene continental sequence in a Velay maar (Massif Central, France). Palaeogeogr. Palaeoclimatol. Palaeoecol. 80, 35–48.

Reille, M., Lowe, J.J., 1993. A re-evaluation of the vegetation history of the eastern Pyrenees (France) from the end of the last glacial to the present. Quat. Sci. Rev. 12, 47–77.

Reille, M., Gamisans, J., de Beaulieu, J.-L., Andrieu, V., 1997. The late-glacial at Lac de Creno (Corsica, France): a key site in the western Mediterranean basin. New Phytologist 135, 547–559.

Reille, M., Andrieu, V., de Beaulieu, J.-L., Guenet, P., Goeury, C., 1998. A long pollen record from Lac du Bouchet, Massif Central, France for the period 325 to 100 ka (OIS 9c to OIS 5e). Quat. Sci. Rev. 17, 1107–1123.

Renssen, H., Seppa, H., Heiri, O., Roche, D.M., Goosse, H., Fichefet, T., 2009. The spatial and temporal complexity of the Holocene thermal maximum. Nat. Geosci. 2, 411–414.

Riding, R., Braga, J.C., Martin, J.M., Sanchez-Almazo, I.M., 1998. Mediterranean Messinian salinity crisis: constraints from a coeval marginal basin, Sorbas, southeastern Spain. Mar. Geol. 146 (1–4), 1–20.

de Rijk, S., Hayes, A., Rohling, E.J., 1999. Eastern Mediterranean sapropel S1 interruption: an expression of the onset of climatic deterioration around 7 ka BP. Mar. Geol. 153, 337–343.

Rindsberger, M., Magaritz, M., Carmi, I., Gilad, D., 1983. The relation between air mass trajectories and the water isotope composition of rain in the Mediterranean Sea area. Geophys. Res. Lett. 10, 43–46.

Roberts, N., Jones, M.D., Benkaddour, A., Eastwood, W.J., Filippi, M.L., Frogley, M.R., et al., 2008. Stable isotope records of Late Quaternary climate and hydrology from Mediterranean lakes: the ISOMED synthesis. Quat. Sci. Rev. 27 (25–26), 2426–2441.

Robinson, S.A., Black, S., Sellwood, B.W., Valdes, P.J., 2006. A review of palaeoclimates and palaeoenvironments in the Levant and eastern Mediterranean from 25,000 to 5000 years

BP: setting the environmental background for the evolution of human civilisation. Quat. Sci. Rev. 25, 1517–1541.

Rodrigues, T., Grimalt, J.O., Abrantes, F., Flores, J.A., Lebreiro, S.M., 2009. Holocene interdependences of changes in sea surface temperature, productivity, and fluvial inputs in the Iberian continental shelf (Tagus mud patch). Geochem. Geophys. Geosyst. 10 (7), Q07U06. doi: 10.1029/2008GC002367.

Rodrigues, T., Grimalt, J.O., Abrantes, F., Naughton, F., Flores, J.-A., 2010. The last glacial–interglacial transition (LGIT) in the western mid-latitudes of the North Atlantic: abrupt sea surface temperature change and sea level implications. Quat. Sci. Rev. 29 (15–16), 1853–1862.

Rodrigues, T., Voelker, A.H.L., Grimalt, J.O., Abrantes, F., Naughton, F., 2011. Iberian Margin sea surface temperature during MIS 15 to 9 (580–300 ka): glacial suborbital variability versus interglacial stability. Paleoceanography 26 (1), PA1204. doi: 10.1029/2010pa001927.

Rodwell, M.J., Hoskins, B.J., 1996. Monsoons and the dynamics of deserts. Q. J. R. Meteorol. Soc. 122, 1385–1404.

Roether, W.H., Manca, B.B., Klein, B., Bregant, D., Georgopoulos, D., Beitzel, V., et al., 1996. Recent changes in eastern Mediterranean deep waters. Science 271, 333–335.

Rogerson, M., Rohling, E.J., Weaver, P.P.E., Murray, J.W., 2004. The Azores Front since the Last Glacial Maximum. Earth Planet. Sci. Lett. 222 (3–4), 779–789.

Rogerson, M., Rohling, E.J., Weaver, P.P.E., Murray, J.W., 2005. Glacial to interglacial changes in the settling depth of the Mediterranean Outflow plume. Paleoceanography 20 (3), PA3007. doi: 10.1029/2004PA001106.

Rögl, F., 1998. Palaeogeographic considerations for Mediterranean and Paratethys seaways (Oligocene to Miocene). Ann. Naturhist. Mus. Wien 99A, 279–310.

Rögl, F., 1999. Mediterranean and Paratethys. Facts and hypotheses of an Oligocene to Miocene paleogeography (short overview). Geol. Carpathica 50, 339–349.

Rögl, F., Hansen, H.-J., 2009. *Thyromata nov. gen.*, a benthic foraminifer from the Late Eocene–Early Oligocene of the Paratethys. Ann. Naturhist. Mus. Wien 111A, 15–32.

Rohling, E.J., 1994. Review and new aspects concerning the formation of eastern Mediterranean sapropels. Mar. Geol. 122 (1–2), 1–28.

Rohling, E.J., Gieskes, W.W.C., 1989. Late Quaternary changes in Mediterranean intermediate water density and formation rate. Paleoceanography 4 (5), 531–545.

Rohling, E.J., Pälike, H., 2005. Centennial-scale climate cooling with a sudden cold event around 8,200 years ago. Nature 434, 975–979.

Rohling, E.J., de Rijk, S., 1999. Holocene Climate Optimum and Last Glacial Maximum in the Mediterranean: the marine oxygen isotope record. Mar. Geol. 153, 57–75.

Rohling, E.J., Jorissen, F.J., Grazzini, C.V., Zachariasse, W.J., 1993. Northern Levantine and Adriatic Quaternary planktic foraminifera—reconstruction of paleoenvironmental gradients. Mar. Micropaleontol. 21 (1–3), 191–218.

Rohling, E.J., Jorissen, F.J., De Stigter, H.C., 1997. 200 year interruption of Holocene sapropel formation in the Adriatic Sea. J. Micropalaeontol. 16, 97–108.

Rohling, E.J., Sprovieri, M., Cane, T., Casford, J.S.L., Cooke, S., Bouloubassi, I., et al., 2002a. African monsoon variability during the previous interglacial maximum. Earth Planet. Sci. Lett. 202 (1), 61–75.

Rohling, E.J., Mayewski, P.A., Hayes, A., Abu-Zied, R.H., Casford, J.S.L., 2002b. Holocene atmosphere–ocean interactions: records from Greenland and the Aegean Sea. Clim. Dyn. 18, 587–593.

Rohling, E.J., Sprovieri, M., Cane, T., Casford, J.S.L., Cooke, S., Bouloubassi, I., et al., 2004. Reconstructing past planktic foraminiferal habitats using stable isotope data: a case history for Mediterranean sapropel S5. Mar. Micropaleontol. 50 (1–2), 89–123.

Rohling, E.J., Hopmans, E.C., Sinninghe Damstè, J.S., 2006. Water column dynamics during the last interglacial anoxic event in the Mediterranean (sapropel S5). Paleoceanography 21 (2), PA2018. doi: 10.1029/2005pa001237.

Rohling, E.J., et al., 2008. High rates of sea-level rise during the last interglacial period. Nat. Geosci. 1 (1), 38–42.

Rossignol-Strick, M., 1985. Mediterranean Quaternary sapropels, an immediate response of the African monsoon to variations of insolation. Palaeogeogr. Palaeoclimatol. Palaeoecol. 49, 237–263.

Rossignol-Strick, M., 1996. Sea–land correlation of pollen records in the eastern Mediterranean for the glacial–interglacial transition: biostratigraphy versus radiometric time-scale. Quat. Sci. Rev. 14 (9), 893–915.

Rossignol-Strick, M., Planchais, N., 1989. Climate patterns revealed by pollen and oxygen isotope records of a Tyrrhenian sea core. Nature 342, 413–416.

Rossignol-Strick, M., Nesteroff, V., Olive, P., Vergnaud-Grazzini, C., 1982. After the deluge: Mediterranean stagnation and sapropel formation. Nature 295, 105–110.

Rossignol-Strick, M., Planchais, N., Paterne, M., Duzer, D., 1992. Vegetation dynamics and climate during the deglaciation in the south Adriatic basin from a marine record. Quat. Sci. Rev. 11, 415–423.

Rouchy, J.M., Caruso, A., 2006. The Messinian salinity crisis in the Mediterranean basin: a reassessment of the data and an integrated scenario. Sediment. Geol. 188–189, 35–67.

Rouchy, J.M., Orszag-Sperber, F., Blanc-Valleron, M.M., Pierre, C., Riviere, M., Combourieu-Nebout, N., et al., 2001. Paleoenvironmental changes at the Messinian–Pliocene boundary in the eastern Mediterranean (southern Cyprus basins): significance of the Messinian Lago-Mare. Sediment. Geol. 145 (1–2), 93–117.

Rouchy, J.M., Pierre, C., Et-Touhami, M., Kerzazi, K., Caruso, A., Blanc Valleron, M., 2003. Late Messinian to Early Pliocene paleoenvironment changes in the Melilla Basin (NE Morocco) and their relation to Mediterranean evolution. Sediment. Geol. 163 (1) doi: 10.1016/S0037-0738(03)00157-X.

Rouchy, J.M., Caruso, A., Pierre, C., Blanc-Valleron, M.M., Bassetti, M.A., 2007. The end of the Messinian salinity crisis: evidences from the Chelif Basin (Algeria). Palaeogeogr. Palaeoclimatol. Palaeoecol. 254, 386–417.

Roucoux, K.H., Shackleton, N.J., de Abreu, L., Schönfeld, J., Tzedakis, P.C., 2001. Combined marine proxy and pollen analyses reveal rapid Iberian vegetation response to North Atlantic millennial-scale climate oscillations. Quat. Res. 5, 128–132.

Roucoux, K.H., de Abreu, L., Shackleton, N.J., Tzedakis, P.C., 2005. The response of NW Iberian vegetation to North Atlantic climate oscillations during the last 65 kyr. Quat. Sci. Rev. 24 (14–15), 1637–1653.

Roucoux, K.H., Tzedakis, P.C., de Abreu, L., Shackleton, N.J., 2006. Climate and vegetation changes 180,000 to 345,000 years ago recorded in a deep-sea core off Portugal. Earth Planet. Sci. Lett. 249 (3–4), 307–325.

Rouis-Zargouni, I., Turon, J.L., Londeix, L., Essallami, L., Kallel, N., Sicre, M.A., 2010. Environmental and climatic changes in the central Mediterranean Sea (Siculo-Tunisian Strait) during the last 30 ka based on dinoflagellate cyst and planktonic foraminifera assemblages. Palaeogeogr. Palaeoclimatol. Palaeoecol. 285 (1–2), 17–29.

Roveri, M., Manzi, V., 2006. The Messinian salinity crisis: looking for a new paradygm? Palaeogeogr. Palaeoclimatol. Palaeoecol. 238, 386–398.

Roveri, M., Manzi, V., Bassetti, M.A., Merini, M., Ricci Lucchi, F., 1998. Stratigraphy of the Messinian post-evaporitic stage in eastern Romagna (northern Apennines, Italy). Giorn. Geol. 60, 119–142.

Roveri, M., Bassetti, M.A., Ricci Lucchi, F., 2001. The Mediterranean Messinian salinity crisis: an Apennine foredeep perspective. Sediment. Geol. 140 (3), 201–214.

Roveri, M., Lugli, S., Manzi, V., Schreiber, B.C., 2008. The Messinian Sicilian stratigraphy revisited: new insights for the Messinian salinity crisis. Terra Nova 20 (6), 438–488.

Ruddiman, W.F., 2001. Earth's Climate Past and Future. W.H. Freeman and Co., New York, p. 388.

Sabatier, P., Dezileau, L., Blanchemanche, P., Siani, G., Condomines, M., Bentaleb, I., et al., 2010. Holocene variations of radiocarbon reservoir ages in a Mediterranean lagoonal system. Radiocarbon 52 (1), 91–102.

Sachsenhofer, R.F., Stummer, B., Georgiev, G., 2009. Depositional environment and hydrocarbon source potential of the Oligocene Ruslar Formation (Kamchia Depression; Western Black Sea). Mar. Pet. Geol. 26 (1), 57–84.

Sadori, L., Giardini, M., Chiarini, E., Mattei, M., Papasodaro, F., Porreca, M., 2010. Pollen and macrofossil analyses of Pliocene lacustrine sediments (Salto river valley, Central Italy). Quat. Int. 225 (1), 44–57.

Salgueiro, E., Voelker, A.H.L., de Abreu, L., Abrantes, F., Meggers, H., Wefer, G., 2010. Temperature and productivity changes off the western Iberian margin during the last 150 ky. Quat. Sci. Rev. 29 (5–6), 680–695.

Sanchez-Goñi, M.F., Harrison, S.P., 2010. Millennial-scale climate variability and vegetation changes during the Last Glacial: concepts and terminology. Quat. Sci. Rev. 29 (21–22), 2823–2827.

Sánchez-Goñi, M.F., Eynaud, F., Turon, J.L., Shackleton, N.J., 1999. High resolution palynological record off the Iberian margin: direct land-sea correlation for the Last Interglacial complex. Earth Planet. Sci. Lett. 171 (1), 123–137.

Sánchez-Goñi, M.F., Turon, J.L., Eynaud, F., Glendreau, S., 2000. European climatic response to millennial-scale changes in the atmosphere–ocean system during the last glacial period. Quat. Res. 54, 394–403.

Sánchez-Goñi, M.F., Cacho, I., Turon, J.L., Guiot, J., Sierro, F.J., Peypouquet, J.-P., et al., 2002. Synchroneity between marine and terrestrial responses to millennial scale climatic variability during the last glacial period in the Mediterranean region. Clim. Dyn. 19, 95–105.

Sánchez-Goñi, M.F., Loutre, M.F., Crucifix, M., Peyron, O., Santos, L., Duprat, J., et al., 2005. Increasing vegetation and climate gradient in Western Europe over the Last Glacial Inception (122–110 ka): data-model comparison. Earth Planet. Sci. Lett. 231 (1–2), 111–130.

Sánchez-Goñi, M.F., Landais, A., Fletcher, W.J., Naughton, F., Desprat, S., Duprat, J., 2008. Contrasting impacts of Dansgaard–Oeschger events over a western European latitudinal transect modulated by orbital parameters. Quat. Sci. Rev. 27 (11–12), 1136–1151.

Sánchez-Goñi, M.F., Landais, A., Cacho, I., Duprat, J., Rossignol, L., 2009. Contrasting intrainterstadial climatic evolution between high and middle North Atlantic latitudes: a close-up of Greenland Interstadials 8 and 12. Geochem. Geophys. Geosyst. 10 (4), Q04U04. doi: 10.1029/2008GC002369.

Sangiorgi, F., Capotondi, L., Brinkhuis, H., 2002. A centennial scale organic-walled dinoflagellate cyst record of the last deglaciation in the South Adriatic Sea (Central Mediterranean). Palaeogeogr. Palaeoclimatol. Palaeoecol. 186 (3–4), 199–216.

Sangiorgi, F., Capotondi, L., Nebout, N.C., Vigliotti, L., Brinkhuis, H., Giunta, S., et al., 2003. Holocene seasonal sea-surface temperature variations in the southern Adriatic Sea inferred from a multiproxy approach. J. Quat. Sci. 18 (8), 723–732.

Santos, L., Sanchez-Goni, M.F., 2003. Lateglacial and Holocene environmental changes in Portuguese coastal lagoons 3: vegetation history of the Santo Andre coastal area. Holocene 13, 461–466.

Sbaffi, L., Wezel, F.C., Curzi, G., Zoppi, U., 2004. Millennial- to centennial-scale palaeoclimatic variations during Termination I and the Holocene in the central Mediterranean Sea. Global Planet. Change 40 (1–2), 201–217.

Schmiedl, G., Mitschele, A., Beck, S., Emeis, K.-C., Hemleben, C., Schulz, H., et al., 2003. Benthic foraminiferal record of ecosystem variability in the eastern Mediterranean Sea during times of sapropel S5 and S6 deposition. Palaeogeogr. Palaeoclimatol. Palaeoecol. 190, 139–164.

Schmiedl, G., Kuhnt, T., Ehrmann, W., Emeis, K.-C., Hamann, Y., Kotthoff, U., et al., 2010. Climatic forcing of eastern Mediterranean deep-water formation and benthic ecosystems during the past 22 000 years. Quat. Sci. Rev. 29 (23–24), 3006–3020.

Schönfeld, J., Zahn, R., 2000. Late Glacial to Holocene history of the Meditarranean outflow. Evidence from benthic Foraminiferal assemblages and stable isotopes at the Portuguese margin. Palaeogeogr. Palaeoclimatol. Palaeoecol. 159, 85–111.

Schramm, A., Stein, M., Goldstein, S.L., 2000. Calibration of the ^{14}C timescale to >40 ka by ^{234}U–^{230}Th dating of Lake Lisan sediments (last glacial Dead Sea). Earth Planet. Sci. Lett. 175, 27–40.

Schulz, H.M., Bechtel, A., Sachsenhofer, R.F., 2005. The birth of the Paratethys during the Early Oligocene: from Tethys to an ancient Black Sea analogue? Global Planet. Change 49 (3–4), 163–176.

Scrivner, A.E., Vance, D., Rohling, E.J., 2004. New neodymium isotope data quantify Nile involvement in Mediterranean anoxic episodes. Geology 32 (7), 565–568.

Seidenkrantz, M.S., Kouwenhoven, T.J., Jorissen, F.J., Shackleton, N.J., Van der Zwaan, G.J., 2000. Benthic foraminifera as indicators of changing Mediterranean Atlantic water exchange in the late Miocene. Mar. Geol. 163, 387–407.

Shackleton, N.J., Opdyke, N.D., 1973. Oxygen isotope and paleomagnetic stratigraphy of Equatorial Pacific core V28–238; oxygen isotope temperature and ice volumes on a 10^5 year and 10^6 year scale. Quat. Res. 3, 39–55.

Shackleton, N.J., Hall, M.A., Vincent, E., 2000. Phase relationships between millennial-scale events 64,000–24,000 years ago. Paleoceanography 15 (6), 565–569.

Shackleton, N.J., Sanchez-Goni, M.F., Pailler, D., Lancelot, Y., 2003. Marine isotope substage 5e and the Eemian interglacial. Global Planet. Change 36 (3), 151–155.

Siani, G., Paterne, M., Michel, E., Sulpizio, R., Sbrana, A., Arnold, M., et al., 2001. Mediterranean Sea surface radiocarbon reservoir age changes since the Last Glacial Maximum. Science 294 (5548), 1917–1920.

Siani, G., Paterne, M., Colin, C., 2010. Late glacial to Holocene planktic foraminifera bioevents and climatic record in the South Adriatic Sea. J. Quat. Sci. 25 (5), 808–821.

Siddall, M., Rohling, E.J., Thompson, W.G., Waelbroeck, C., 2008. MIS 3 sea-level fluctuations: data synthesis and new outlook. Rev. Geophys. 46, RG4003. doi: 10.1029/2007RG000226.

Sierro, F.J., Flores, J.A., Zamarreño, I., Vazquez, A., Utrilla, R., Frances, G., et al., 1999. Messinian pre-evaporite sapropels and precession-induced oscillations in western Mediterranean climate. Mar. Geol. 153, 137–146.

Sierro, F.J., Krijgsman, W., Hilgen, F.J., Flores, J.A., 2001. The Abad composite (SE Spain): a Mediterranean reference section for the Messinian and the Astronomical Polarity Timescale (APTS). Palaeogeogr. Palaeoclimatol. Palaeoecol. 168 (1–2), 143–172.

Sierro, F.J., Flores, J.A., Francés, G., Vazquez, A., Utrilla, R., Zamarreño, I., et al., 2003. Orbitally controlled oscillations in planktic communities and cyclic changes in western Mediterranean hydrography during the Messinian. Palaeogeogr. Palaeoclimatol. Palaeoecol. 190, 289–316.

Sierro, F.J., Hodell, D.A., Curtis, J.H., Flores, J.A., Reguera, I., Colmenero-Hidalgo, E., et al., 2005. Impact of iceberg melting on Mediterranean thermohaline circulation during Heinrich events. Paleoceanography 20 (2), PA2019. doi: 10.1029/2004PA001051.

Sierro, F.J., Ledesma, S., Flores, J.A., 2008. Astrobiochronology of Late Neogene deposits near the Strait of Gibraltar (SW Spain). Implications for the tectonic control of the Messinian Salinity Crisis, 45-49. In: Briand, F. (ed.). CIESM, 2008. The Messinian Salinity Crisis from mega-deposits to microbiology - A consensus report. Nº 33 in CIESM Workshop Monographs pp 45-49, Monaco.

Sierro, F.J., Andersen, N., Bassetti, M.A., Berne, S., Canals, M., Curtis, J.H., et al., 2009. Phase relationship between sea level and abrupt climate change. Quat. Sci. Rev. 28 (25–26), 2867–2881.

Skinner, L.C., Elderfield, H., 2007. Rapid fluctuations in the deep North Atlantic heat budget during the last glaciation. Paleoceanography 22 (1), PA1205. doi: 10.1029/2006PA001338.

Solomon, S. (Ed.), 2007. Contribution of Working Group I to the Fourth Assessment Report of the Intergovernmental Panel on Climate Change, 2007. Cambridge University Press, Cambridge, UK and New York, NY. p. 996.

Sperling, M., Schmiedl, G., Hemleben, C., Emeis, K.C., Erlenkeuser, H., Grootes, P.M., 2003. Black Sea impact on the formation of eastern Mediterranean sapropel S1? Evidence from the Marmara Sea. Palaeogeogr. Palaeoclimatol. Palaeoecol. 190, 9–21.

Sprovieri, R., Di Stefano, E., Incarbona, A., Gargano, M.E., 2003. A high-resolution record of the last deglaciation in the Sicily Channel based on foraminifera and calcareous nannofossil quantitative distribution. Palaeogeogr. Palaeoclimatol. Palaeoecol. 202 (1–2), 119–142.

Sprovieri, R., Di Stefano, E., Incarbona, A., Oppo, D.W., 2006a. Suborbital climate variability during Marine Isotopic Stage 5 in the central Mediterranean basin: evidence from calcareous plankton record. Quat. Sci. Rev. 25 (17–18), 2332–2342.

Sprovieri, R., Sprovieri, M., Caruso, A., Pelosi, N., Bonono, S., Ferraro, L., 2006b. Astronomic forcing on the planktonic foraminifera assemblage in the Piacenzian Punta Piccola section (southern Italy). Paleoceanography 21, PA4204. doi: 10.1029/2006PA001268.

Stanford, J.D., Rohling, E.J., Hunter, S.E., Roberts, A.P., Rasmussen, S.O., Bard, E., et al., 2006. Timing of meltwater pulse 1a and climate responses to meltwater injections. Paleoceanography 21, PA4103. doi: 10.1029/2006PA001340.

Stein, M., Torfstein, A., Gavrieli, I., Yechieli, Y., 2010. Abrupt aridities and salt deposition in the post-glacial Dead Sea and their North Atlantic connection. Quat. Sci. Rev. 29 (3–4), 567–575.

Struck, U., Emeis, K.-C., Voß, M., Krom, M.D., Rau, G.H., 2001. Biological productivity during sapropel S5 formation in the eastern Mediterranean Sea: evidence from stable isotopes of nitrogen and carbon. Geochim. Cosmochim. Acta 65 (19), 3249–3266.

Suc, J.-P., 1984. Origin and evolution of the Mediterranean vegetation and climate in Europe. Nature 307, 429–432.

Tantau, I., Reille, M., de Beaulieu, J.-L., Farcas, S., 2006. Late Glacial and Holocene vegetation history in the southern part of Transylvania (Romania): pollen analysis of two sequences from Avrig. J. Quat. Sci. 21 (1), 49–61.

Targarona, J., 1997. Climatic and oceanographic evolution of the Mediterranean region over the last Glacial–Interglacial transition. A palynological approach. Ph.D. Thesis. Utrecht University, Utrecht, The Netherlands, p. 155.

Teller, J.T., Leverington, D.W., Mann, J.D., 2002. Freshwater outbursts to the ocean from glacial Lake Agassiz and their role in climate change during the last deglaciation. Quat. Sci. Rev. 21, 879–887.

Theocharis, A., Georgopoulos, D., 1993. Dense water formation over the Samothraki and Limnos Plateaux in the north Aegean Sea (eastern Mediterranean Sea). Cont. Shelf Res. 13, 919–939.

Thompson, W.G., Goldstein, S.L., 2005. Open-system coral ages reveal persistent suborbital sea-level cycles. Science 308 (5720), 401–404.

Thouveny, N., de Beaulieu, J.L., Bonifay, E., Creer, M.K., Guiot, J., Icole, M., et al., 1994. Climate variations in Europe over the past 140 kyr deduced from rock magnetism. Nature 371, 503–506.

Thunell, R.C., Williams, D.F., Belyea, P.R., 1984. Anoxic events in the Mediterranean Sea in relation to the evolution of late Neogene climates. Mar. Geol. 59, 105–134.

Tinner, W., Lotter, A.F., 2001. Central European vegetation response to abrupt climate change at 8.2 ka. Geology 29, 551–554.

Tinner, W., van Leeuwen, J.F.N., Colombaroli, D., Vescovi, E., van der Knaap, W.O., Henne, P.D., et al., 2009. Holocene environmental and climatic changes at Gorgo Basso, a coastal lake in southern Sicily, Italy. Quat. Sci. Rev. 28 (15–16), 1498–1510.

Tonkov, S., Possnert, G., Bozilova, E.D., 2006. The lateglacial vegetation and radiocarbon dating of Lake Trilistnika, Rila Mountains (Bulgaria). Veg. Hist. Archaeobot. 16 (1), 15–22.

Toucanne, S., Mulder, T., Schönfeld, J., Hanquiez, V., Gonthier, E., Duprat, J., et al., 2007. Contourites of the Gulf of Cadiz: a high-resolution record of the paleocirculation of the Mediterranean outflow water during the last 50,000 years. Palaeogeogr. Palaeoclimatol. Palaeoecol. 246 (2–4), 354–366.

Toucanne, S., Jouet, G.l., Ducassou, E., Bassetti, M.-A., Dennielou, B., Angue Minto'o, C.M., et al., 2012. A 130,000-year record of Levantine Intermediate Water flow variability in the Corsica Trough, western Mediterranean Sea. Quat. Sci. Rev. 33, 55–73.

Tripati, A.K., Roberts, C.D., Eagle, R.A., 2009. Coupling of CO_2 and ice sheet stability over major climate transitions of the last 20 million years. Science 326, 1394–1397.

Tsimplis, M.N., Josey, S.A., 2001. Forcing of the Mediterranean Sea by atmospheric oscillations over the North Atlantic. Geophys. Res. Lett. 28, 803–806.

Turon, J.L., Lézine, A.-M., Denèfle, M., 2003. Land-sea correlations for the last glaciation inferred from a pollen and dinocyst record from the Portuguese Margin. Quat. Res. 59, 88–96.

Tzedakis, P.C., 1994. Vegetation change through glacial–interglacial cycles: a long pollen sequence perspective. Philos. Trans. R. Soc. London B 345, 403–432.

Tzedakis, P.C., 1999. The last climatic cycle at Kopais, central Greece. J. Geol. Soc. 156, 425–434.

Tzedakis, P.C., Andrieu, V., de Beaulieu, J.L., Crowhurst, S., Follieri, M., Hooghiemstra, H., et al., 1997. Comparison of terrestrial and marine records of changing climate of the last 500,000 years. Earth Planet. Sci. Lett. 150 (1–2), 171–176.

Tzedakis, P.C., Lawson, I.T., Frogley, M.R., Hewitt, G.M., Preece, R.C., 2002. Buffered tree population changes in a quaternary refugium: evolutionary implications. Science 297, 2044–2047.

Tzedakis, P.C., Frogley, M.R., Heaton, T.H.E., 2003a. Last Interglacial conditions in southern Europe: evidence from Ioannina, northwest Greece. Global Planet. Change 36 (3), 157–170.

Tzedakis, P.C., McManus, J.F., Hooghiemstra, H., Oppo, D.W., Wijmstra, T.A., 2003b. Comparison of changes in vegetation in northeast Greece with records of climate variability on orbital and suborbital frequencies over the last 450 000 years. Earth Planet. Sci. Lett. 212 (1–2), 197–212.

Tzedakis, P.C., Roucoux, K.H., de Abreu, L., Shackleton, N.J., 2004. The duration of forest stages in southern Europe and interglacial climate variability. Science 306 (5705), 2231–2235.

Tzedakis, P.C., Raynaud, D., McManus, J.F., Berger, A., Brovkin, V., Kiefer, T., 2009. Interglacial diversity. Nat. Geosci. 2 (11), 751–755.

Vaks, A., Bar-Matthews, M., Ayalon, A., Schilman, B., Gilmour, M., Hawkesworth, C.J., et al., 2003. Paleoclimate reconstruction based on the timing of speleothem growth and oxygen and carbon isotope composition in a cave located in the rain shadow in Israel. Quat. Res. 59 (2), 182–193.

Vaks, A., Bar-Matthews, M., Ayalon, A., Matthews, A., Frumkin, A., Dayan, U., et al., 2006. Paleoclimate and location of the border between Mediterranean climate region and the Saharo-Arabian Desert as revealed by speleothems from the northern Negev Desert, Israel. Earth Planet. Sci. Lett. 249 (3–4), 384–399.

Valero-Garcés, B.L., Zeroual, E., Kelts, K., 1998. Arid phases in the western Mediterranean region during the last glacial cycle reconstructed from lacustrine records. In: Benito, G., Baker, V.R., Gregory, K.J. (Eds.), Paleohydrology and Environmental Change. Wiley, London, pp. 67–80.

Vallve, M.B., Martin-Vide, J., 1998. Secular climatic oscillations as indicated by catastrophic floods in the Spanish Mediterranean coastal area (14th–19th centuries). Clim. Change 38 (4), 473–491.

Vautravers, M., Shackleton, N.J., 2006. Centennial scale surface hydrology off Portugal during Marine Isotope Stage 3: insights from planktonic foraminiferal fauna variability. Paleoceanography 21 (3), PA3004. doi: 10.1029/2005PA001144.

Vegas, J., Ruiz-Zapata, B., Ortiz, J.E., Galán, L., Torres, T., García-Cortés, Á., et al., 2010. Identification of arid phases during the last 50 cal. ka BP from the Fuentillejo maar-lacustrine record (Campo de Calatrava Volcanic Field, Spain). J. Quat. Sci. 25, 1051–1062.

Vellinga, M., Wood, R.A., 2002. Global climatic impacts of a collapse of the Atlantic thermohaline circulation. Clim. Change 54, 251–267.

Vergnaud-Grazzini, C., Pierre, C., 1991. High fertility in the Alboran Sea since the Last Glacial Maximum. Paleoceanography 6, 519–536.

Vergnaud-Grazzini, C., Caralp, M., Faugères, J.-C., Gonthier, E., Grousset, F., Pujol, C., et al., 1989. Mediterranean outflow through the Strait of Gibraltar since 18 000 years BP. Oceanolog. Acta 12 (4), 305–324.

Vidal, L., Labeyrie, L., Cortijo, E., Arnold, M., Duplessy, J.C., Michel, E., et al., 1997. Evidence for changes in the North Atlantic Deep Water linked to meltwater surges during the Heinrich events. Earth Planet. Sci. Lett. 146, 13–27.

Vidal, L., Menot, G., Joly, C., Bruneton, H., Rostek, F., Çagatay, M.N., et al., 2010. Hydrology in the Sea of Marmara during the last 23 ka: implications for timing of Black Sea connections and sapropel deposition. Paleoceanography 25, PA1205. doi: 10.1029/2009pa001735.

Voelker, A.H.L., 2002. Global distribuition of centennial-scale records for Marine Isotope Stage (MIS) 3: a database. Quat. Sci. Rev. 21, 1185–1212.

Voelker, A.H.L., de Abreu, L., 2011. A review of abrupt climate change events in the northeastern Atlantic Ocean (Iberian Margin): latitudinal, longitudinal and vertical gradients. In: Rashid, H., Polyak, L., Mosley-Thompson, E. (Eds.), Abrupt Climate Change: Mechanisms, Patterns, and Impacts. Geophysical Monograph Series. AGU, Washington, DC, vol. 193, 15–37. doi: 10.1029/2010GM001021.

Voelker, A.H.L., Lebreiro, S.M., Schönfeld, J., Cacho, I., Erlenkeuser, H., Abrantes, F., 2006. Mediterranean outflow strengthening during northern hemisphere coolings: a salt source for the glacial Atlantic? Earth Planet. Sci. Lett. 245 (1–2), 39–55.

Voelker, A.H.L., de Abreu, L., Schönfeld, J., Erlenkeuser, H., Abrantes, F., 2009. Hydrographic conditions along the western Iberian margin during marine isotope stage 2. Geochem. Geophys. Geosyst. 10, Q12U08. doi: 10.1029/2009GC002605.

Waldmann, N., Stein, M., Ariztegui, D., Starinsky, A., 2009. Stratigraphy, depositional environments and level reconstruction of the last interglacial Lake Samra in the Dead Sea basin. Quat. Res. 72, 1–15.

Waldmann, N., Torfstein, A., Stein, M., 2010. Northward intrusions of low- and mid-latitude storms across the Saharo-Arabian belt during past interglacials. Geology 38, 567–570.

Walker, M., Johnsen, S.J., Rasmussen, S.O., Popp, T., Steffensen, J.P., Gibbard, P., et al., 2009. Formal definition and dating of the GSSP (Global Stratotype Section and Point) for the base of the Holocene using the Greenland NGRIP ice core, and selected auxiliary records. J. Quat. Sci. 24, 3–17.

Watts, W.A., Allen, J.R.M., Huntley, B., 2000. Palaeoecology of three interstadial events during oxygen-isotope Stage 3 and 4: a lacustrine record from Lago Grande di Monticchio, southern Italy. Palaeogeogr. Palaeoclimatol. Palaeoecol. 155, 83–93.

Weaver, P.P.E., Pujol, C., 1988. History of the last deglaciation in the Alboran Sea (Western Mediterranean) and adjacent North Atlantic as revealed by coccolith floras. Palaeogeogr. Palaeoclimatol. Palaeoecol. 64, 35–42.

Webb, R.S., 1997. Influence of ocean heat transport on the climate of the Last Glacial Maximum. Nature 385, 695–699.

Wehausen, R., Brumsack, H.-J., 1998. The formation of Pliocene Mediterranean sapropels: constraints from high-resolution major and minor element studies. In: Robertson, A.H.F., Emeis, K.-C., Richter, C., Camerlenghi, A. (Eds.), Proceedings of the Ocean Drilling Program, Scientific Results. Ocean Drilling Program, College Station, TX, pp. 207–217.

Weldeab, S., Siebel, W., Wehausen, R., Emeis, K.-C., Schmiedl, G., Hemleben, C., 2003. Late Pleistocene sedimentation in the Western Mediterranean Sea: implications for productivity changes and climatic conditions in the catchment areas. Palaeogeogr. Palaeoclimatol. Palaeoecol. 190, 121–137.

Wiersma, A.P., Renssen, H., 2006. Model–data comparison for the 8.2 ka BP event: confirmation of a forcing mechanism by catastrophic drainage of Laurentide Lakes. Quat. Sci. Rev. 25, 63–88.

Wijmstra, T.A., 1969. Palynology of the first 30 metres of a 120 m deep section in northern Greece. Acta Bot. Neerl. 18, 511–527.

Wijmstra, T.A., Smit, A., 1976. Palynology of the middle part (30–78 metres) of the 120 m deep section in Northern Greece (Macedonia). Acta Bot. Neerl. 25, 297–312.

Wohlfarth, B., Hannon, G., Feurdean, A., Ghergari, L., Onac, B.P., Possnert, G., 2001. Reconstruction of climatic and environmental changes in NW Romania during the early part of the last deglaciation (15,000–13,600 cal years BP). Quat. Sci. Rev. 20, 1897–1914.

Zachos, J., Pagani, M., Sloan, L., Thomas, E., Billups, K., 2001. Trends, rhythms, and aberrations in global climate 65 Ma to present. Science 292, 686–693.

Zervakis, V., Krasakopoulou, E., Georgopoulos, D., Souvermezoglou, E., 2003. Vertical diffusion and oxygen consumption during stagnation periods in the deep North Aegean. Deep Sea Res. I 50, 53–71.

Zhao, Y., Braconnot, P., Marti, O., Harrison, S.P., Hewitt, C., Kitoh, A., et al., 2005. A multimodel analysis of the role of the ocean on the African and Indian monsoon during the mid-Holocene. Clim. Dyn. 25, 777–800.